University of Wollongong
Research Online

University of Wollongong Thesis Collection

University of Wollongong Thesis Collections

1995

Multifrequency signal enhancement and estimation using IIR filter bank structures

Mehdi Tavassoli Kilani
University of Wollongong

Recommended Citation

Kilani, Mehdi Tavassoli, Multifrequency signal enhancement and estimation using IIR filter bank structures, Doctor of Philosophy thesis, Department of Electrical and Computer Engineering, University of Wollongong, 1995. http://ro.uow.edu.au/theses/1346

Research Online is the open access institutional repository for the University of Wollongong. For further information contact the UOW Library: research-pubs@uow.edu.au

NOTE

This online version of the thesis may have different page formatting and pagination from the paper copy held in the University of Wollongong Library.

UNIVERSITY OF WOLLONGONG

COPYRIGHT WARNING

You may print or download ONE copy of this document for the purpose of your own research or study. The University does not authorise you to copy, communicate or otherwise make available electronically to any other person any copyright material contained on this site. You are reminded of the following:

Copyright owners are entitled to take legal action against persons who infringe their copyright. A reproduction of material that is protected by copyright may be a copyright infringement. A court may impose penalties and award damages in relation to offences and infringements relating to copyright material. Higher penalties may apply, and higher damages may be awarded, for offences and infringements involving the conversion of material into digital or electronic form.

In the name of God, the Beneficent, the Merciful

Multifrequency Signal Enhancement and Estimation Using IIR Filter Bank Structures

Mehdi Tavassoli Kilani

B.Sc (Hons. 1), MSc.

A thesis submitted in fulfilment of the requirements for the award of the degree of

DOCTOR OF PHILOSOPHY

from

The University of Wollongong

Department of Electrical and Computer Engineering

1995

Dedicated to my family

Declaration

This is to certify that the work reported in this thesis was done by the author, unless specified otherwise, and that no part of it has been submitted in a thesis to any other university or similar institution.

Mehdi Tavassoli Kilani

Acknowledgments

First of all, I would like to express my special thanks to Associate Professor Joe F. Chicharo, my supervisor, for his invaluable academic supervision. He has been very generous with his time in helping me with various aspects of my thesis.

I wish to sincerely thank my wife, Tahereh, and my children for their continued encouragement and patient understanding during this research. I also express my thanks to both my mother and father.

I thankfully acknowledge the financial support provided by the government of the Islamic Republic of IRAN. Finally, I appreciate the assistance and friendship of Jiangtao Xi, Ali Yazdian and Mansour Esmaili.

Abstract

This thesis deals with the accurate estimation of phase, amplitude and frequency of sinusoids buried in noise. Several algorithms are proposed to determine these parameters.

A Constrained Notch Fourier Transform (CNFT) is proposed for estimating the Fourier coefficients of noise corrupted harmonic signals given *a priori* knowledge of the signal frequencies. The proposed method provides bandwidth controlled bandpass filters in contrast to the conventional Notch Fourier Transform (NFT) [Tadokoro and Abe (1987)] and its equivalent real valued Frequency Sampling (FS) structures which utilise fixed bandwidth bandpass filters. New sliding algorithms have been derived for both the NFT and CNFT for the purpose of estimating the Fourier coefficients of the sinusoidal components. A similar algorithm to the CNFT is also proposed for estimating the coefficients of sinusoids at arbitrary known frequencies. The main feature of the modified CNFT is that it uses a second order IIR bandpass filter whose centre frequency parameter is decoupled from the bandwidth parameter. In these techniques, the bandwidth control aspect provides the user with an efficient means of achieving the required resolution as well as reducing spectral leakage. In general, the proposed approach leads to considerable reduction in terms of acquisition time and memory storage.

The sliding CNFT algorithm is extended to the Generalised Frequency Sampling (GFS) filter bank whose parametisation is derived based on the Least Means Square (LMS) spectrum analyser. The GFS filter bank possesses the desired characteristics that its resonant frequencies and nulls are arbitrarily set. This feature is used to effectively reduce the leakage problem. The use of GFS filter bank together with the CNFT algorithm provides faster acquisition time when

compared with the conventional FS filter bank. Further, it is computationally more efficient than the direct use of the LMS spectrum analyser.

The merits and demerits of the conventional Goertzel algorithm are evaluated when it is applied for the task of estimating sinusoidal parameters. A sliding Goertzel algorithm is then developed based on parallel second order digital resonators that are tuned at the input spectral lines. This approach exhibits good performance in low Signal to Noise Ratio (SNR) as verified by extensive simulation tests. Further, unlike the modified and conventional Goertzel algorithms which require a complete signal period to accurately compute the phase and amplitude of the input sinusoids, it computes Fourier coefficients in less than one signal period.

The conventional FS structure was modified to obtain a new modular IIR FS filter bank with reduced spectral overlap as well as minimal spectral hole between adjacent bandpass filters. The IIR FS structure together with the self-orthogonalising LMS algorithm is employed for Adaptive Line Enhancer (ALE) applications. The proposed method provides faster convergence than the conventional adaptive FS methods. The Performance characteristics such as the minimum Mean-Squared-Error (MSE), steady-state excess MSE and convergence conditions of the adaptive FS filter bank is analysed. A performance comparison of three adaptive techniques (the IIR FS structure, conventional FS structure and the Tapped Delay Line (TDL)) is carried out to establish the merits of each algorithm.

Finally, the conventional IIR Parallel Adaptive Line Enhancer (PALE) which is comprised of a parallel second order IIR bandpass filter is modified such that the convergence to local minima or saddle points is avoided. Error surface analysis

is carried out to establish the convergence behaviour of the proposed technique. It is shown that the convergence speed of the proposed structure is the same as the serial configuration. However, it provides superior performance in terms of reduced distortion in amplitude and phase associated with each of the enhanced sinusoids.

Author's Publications

Journal Papers:

Mehdi T. Kilani and Joe F. Chicharo, "A constrained notch Fourier transform," *IEEE Trans. Signal Processing,* Accepted for publication [full paper].

Mehdi T. Kilani and Joe F. Chicharo, "A novel parallel IIR adaptive line enhancer model structure," *International Journal of Electronics*, Vol. 77, No. 3, pp. 269-281, 1994.

Mehdi T. Kilani and Joe F. Chicharo, "A sliding Goertzel algorithm," *Signal Processing: An International Journal*, Accepted for publication subject to minor revision, [full paper].

Mehdi T. Kilani and Joe F. Chicharo, "Relationship between the LMS and Goertzel algorithms for Fourier coefficients estimation at arbitrary frequencies," Submitted to *IEEE Trans. Circuits and Systems.*

Mehdi T. Kilani and Joe F. Chicharo, "A new adaptive IIR frequency sampling structure," Submitted to *Journal of Electrical and Electronics Engineering, Australia.*

Conference Papers:

Mehdi T. Kilani and Joe F. Chicharo, "Sliding Fourier coefficient estimation at arbitrary frequencies using equivalent filter bank for LMS spectrum analyser," *ISITA, International Symposium on Information theory and Its Applications*, Sydney, Australia, Vol. 2, pp. 1345-1350, November 1994.

Mehdi T. Kilani and Joe F. Chicharo, "Adaptive frequency sampling filter bank using a constrained IIR comb filter," *ISITA, International Symposium on Information theory and Its Applications*, Sydney, Australia, Vol. 2, pp. 733-738, November 1994.

Mehdi T. Kilani and Joe F. Chicharo, "A constrained notch Fourier transform," *ISSPA, 3rd International symposium on Signal Processing and Its Application*, Gold Coast, Australia, Vol. 2, pp. 348-351, August 1992.

Mehdi T. Kilani and Joe F. Chicharo, "MFSK demodulation using parallel IIR ALE with a time varying step size factor," *IEEE Singapore International Conference on Communication Systems*, Singapore, Vol. 2, pp. 639-643, November 1994.

Contents

List of Symbols

a_k, $\hat{a}_k$	sine term coefficient of k th input sinusoid and its estimate
b_k, $\hat{b}_k$	cosine term coefficient of k th input sinusoid and its estimate
C_k, $\hat{C}_k$	amplitude of k th sinusoid and its estimate
ϕ_k, $\hat{\phi}_k$	phase of the k th sinusoid and its estimate
f_k, $\hat{f}_k$	frequency of k th sinusoid and its estimate
α, β	comb filter parameters
g, h	second order IIR bandpass filter parameters
μ, μ_f, μ_t	step size factors
$\mathbf{P}_x$, $\mathbf{P}_x^*$	cross correlation matrix between input and desired signal and its complex conjugate transpose
k_p, k_q	indices of DFT coefficients
M_p, M_q	integer numbers
w_{1k}, w_{2k}	coefficients of adaptive filter at the output of the k th bandpass filter
p_k, q_k	adaptive coefficients of LMS spectrum analyser
$\mathbf{X}(n)$, $\overline{\mathbf{X}}(n)$	input vector sequence and its complex conjugate
$X(k)$	k th DFT coefficient
λ_k	k th eigenvalue of input autocorrelation function
$r_j(m)$	(j,m) th element of matrix $\mathbf{R}$
t_{acq}	acquisition time
N_{acq}	acquisition sample number
$\mathbf{W}$	adaptive weight vector of TDL filter
ω	angular frequency

$\mathbf{R}_X$	autocorrelation matrix of input signal
$H_{BP}(z^{-1})$	bandpass filter transfer function
$H_c(z^{-1})$	comb filter transfer function
$d(n)$	desired signal
$\delta(.)$	Dirac delta function
$e(n)$	error signal
ε_{Δ}^{f}	excess mean square error of adaptive FS filter bank
ε_{Δ}	excess mean square error of adaptive TDL filter
$E(e^2)$	expected error
γ	forgetting factor
$f_{sampler}$	frequency of sampler
Δf	greatest common factor of input frequencies
$\varepsilon_{\min}^{f}$	minimum of mean square error of adaptive FS filter bank
$\varepsilon_{\min}$	minimum of mean square error of adaptive TDL filter
$\nu(n)$	noise sequence
BW	normalised bandwidth
$\Gamma(n)$	normalising factor
$H_N(z^{-1})$	notch filter transfer function
m	number of input sinusoids
$y_k(n)$	output of k th bandpass filter
∂	partial derivative
∇_h	partial derivative of error squared
f_p	peak frequency of second order IIR bandpass filter
σ_x^2	power of signal $x(n)$
$\Phi_{xx}(\omega)$	power spectrum of signal $x(t)$
$H_r(z^{-1})$	resonator transfer function
f_s	sampling frequency
$x(n)$	noise corrupted sinusoidal signal

τ	time constant
$Tr(\mathbf{R})$	trace of matrix $\mathbf{R}$
z^{-1}	unit backward shift operator
$\mathbf{W}_{opt}$	Wiener optimal solution of adaptive TDL filter
$\mathbf{W}_{opt}^{f}$	Wiener optimal solution of adaptive FS filter bank
$X(z)$	z-transform of $x(n)$

CHAPTER 1:

Preliminaries

1.1 Introduction

This thesis deals with the use of digital signal processing techniques for the task of enhancement and characterisation of Multifrequency (MF) signals buried in broadband noise. The MF signals refer to a particular class of signals which consist of sinusoidal components whose frequencies are either uniformly distributed (harmonic) or arbitrarily located (non harmonic) in the frequency domain spectrum. The objectives are to enhance the individual sinusoidal components as well as to estimate their characteristic parameters such as frequency, phase and amplitude.

The application of MF signal characterisation is found in many areas of engineering. For example, the transmission of signals consisting of sets or combs of frequencies is commonly used in communication systems. In conventional telephone networks several types of Multifrequency Code (MFC) are used to transmit dialling and signalling information. For instance, Dual Tone Multifrequency (DTMF) signals are widely used in modern day telephone networks [Braun (1975), Koval and Gara (1973), Gay *et al.* (1989), Tadokoro and Abe (1987), Wong and Seng (1990)]. Another example is the M-ary Frequency Shift Keying (MFSK) signalling technique where information is carried by the frequency of the signal. The transmitted MFSK signal consists of

a sinusoid whose frequency changes rapidly within the successive sequences. As an extension of the MFSK, a bandwidth efficient code division multiple access scheme called Frequency Comb Multiple Access (FCMA) technique has been proposed [Stevenson and Yates (1989)]. In FCMA, each symbol contains a set or comb of frequencies spread across the information bandwidth which is currently used in a Very Small Aperture Terminal (VSAT) satellite communication systems [Simington and Percival (1991)]. In all the above applications the sinusoidal signals are often corrupted by interfering signals or noise. At the receiver, it is of critical importance to detect individual sinusoids and to estimate their parameters fast and accurately. The application of enhancement and estimation of noise corrupted sinusoidal signals are also found in other engineering areas such as radar, sonar, biomedical, control and power systems engineering.

Our approach in this thesis is firstly to consider the case where the input frequency locations are known *a priori*. Accurate coefficient estimation of noise corrupted sinusoids is performed by using specially constrained tuneable bandpass filters whose resonant frequencies are set at the known input frequency locations. Secondly, adaptive Infinite Impulse Response (IIR) filter banks are developed for the situations where no *a priori* information regarding the locations of input spectral lines is available.

This chapter is organised as follows: Section 1.2 describes the background to the thesis and reviews the current state of the art in relevant published literature. Attention has been paid mainly to the contributions which are most related to the work presented in this thesis. Section 1.3 discusses the approach taken and the resulting contributions. Finally, Section 1.4 provides an outline for the rest of the thesis.

1.2 Background to the Thesis

In this section a brief review of those techniques which are commonly used for the estimation of sinusoidal parameters is given. The use of Discrete Fourier Transform (DFT) is the central part of most techniques in this area. Much of this interest is motivated by the availability of the fast computational techniques such as Fast Fourier Transform (FFT). The DFT simply means that the input sequence is projected on to a set of complex sinusoidal functions whose frequencies are evenly distributed in the frequency spectrum. When applying the DFT technique to the estimation of the phase and amplitude of MF signals, two important issues must be considered including: the accuracy of the estimates and the required acquisition time.

The accuracy of the estimates is affected by the leakage which is an inherent property of the DFT technique. The problem of the leakage can be examined from two different points of view. One approach is that the signal in the observation window has frequencies other than those of the basis functions. Therefore, the input data will have non zero projection on the other basis functions [Harris (1978)]. This problem is due to the truncation of the input signal; that is, the periodic extension of the signal does not match with its natural frequency. Based on this approach, widowing techniques which apply multiplicative weighting functions to the data have been proposed. The objective of windowing functions is to bring the data smoothly to zero at the boundaries of the observation sequence thus reducing the effect of truncation. A comprehensive and concise review on the use of windows and their performance is found in [Rife and Vincent (1970), Harris (1978)].

The second approach which provides additional insight into the leakage problem is through the use of an equivalent filter bank for the DFT. In this approach, the

DFT is performed by passing data through parallel Finite Impulse Response (FIR) bandpass filters whose centre frequencies are equally distributed in the frequency domain. The equivalent filter bank associated with the DFT is composed of an FIR comb filter followed by parallel digital resonators, as depicted in Figure 1.1, and is commonly referred to as a Frequency Sampling (FS) structure [Rabiner and Gold (1975)].

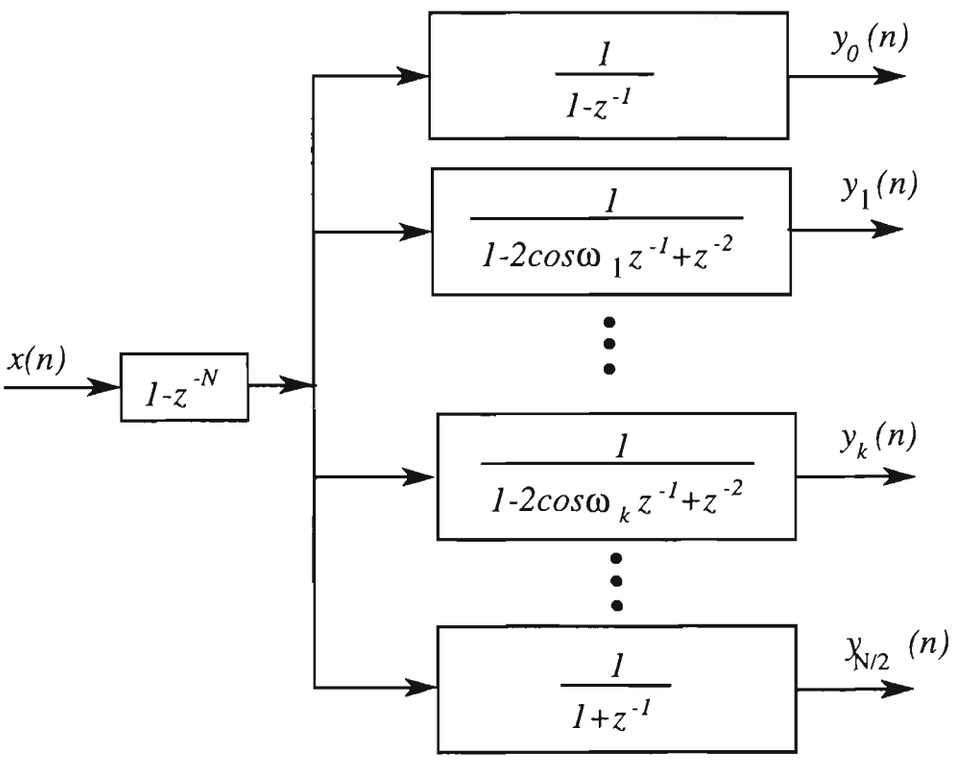

Figure 1.1: DFT implementation using FS filter bank.

The comb filter (Figure 1.1) possesses N zeros that are equally spaced around the unit circle. The poles of resonators are also evenly spaced on the unit circle at the same frequencies as the zeros of the comb filter. At each branch, the pole of resonator cancels the corresponding zero of the comb filter thus resulting in an FIR bandpass filter. The resonant frequencies of the bandpass filters are equally spaced over the entire frequency domain. The magnitude response of two adjacent bandpass filters is shown in Figure 1.2. From this point of view, the leakage can be interpreted as the amount of overlap amongst the bandpass filters which results in spreading the sinusoid energy into the other bandpass filters

[Harris (1978)]. Although the structure shown in Figure 1.1 is an equivalent representation of the sliding DFT, special care must be taken when it is to be practically implemented. In fact, because the pole of the FS filter lies exactly on the unit circle, this realisation becomes marginally stable so that any round off errors could result in filter instability. To overcome this problem, the poles and zeros are placed slightly within the unite circle [Shynk (1992, 1989a), Kuo and Rodrigues (1986)].

The filter bank approach has a similar computational burden as the direct DFT method. However, in situations where the input sinusoidal parameters are time varying and Fourier coefficients are to be computed for each successive sample update (sliding measurement), the filter bank approach becomes computationally efficient when compared to the direct DFT and FFT techniques [Rabiner and Gold (1975)]. This sliding implementation of the DFT is also called a recursive DFT [Clark *et al.* (1985)].

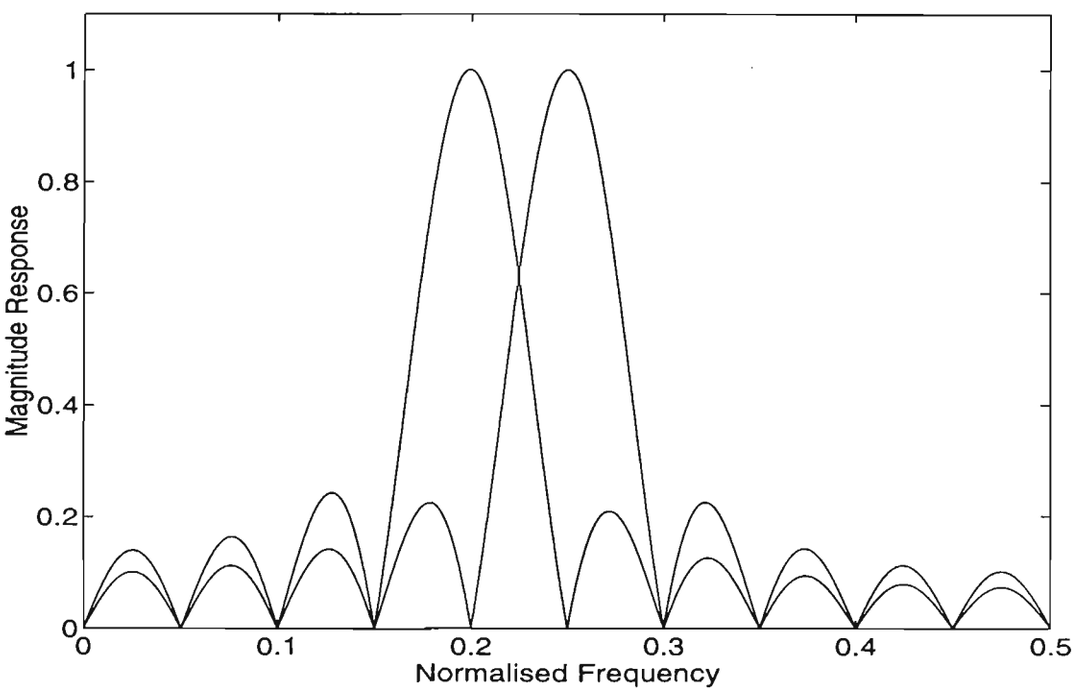

Figure 1.2: Magnitude Response of two adjacent bandpass filters for the FS filter bank.

Using the DFT technique to compute the parameters of the sinusoids, the required acquisition time depends on the length of the input data. Assuming that the data are N evenly spaced samples of the input signal, the DFT provides N uniformly spaced samples of the associated signal spectrum. Clearly for situations where high resolution is required the acquisition time will necessarily increase. Also, in order to obtain an accurate estimate for the phase and amplitude of each sinusoid, the input data must cover exactly one period of the signal. The period of the signal containing sinusoidal components depends on the input constituent frequencies. If the input frequencies are mutually prime factor, the period of the signal is equal to 1Hz. Under such circumstances a large number of samples will be required which also increase the acquisition time.

From a filter bank point of view, accurate phase and amplitude estimates are obtained when the input spectral lines lie exactly in the middle of the bandpass filters where the nulls of other spectral bins are located (see Figure 1.2). When the input frequencies are mutually prime factor or closely spaced a higher resolution is needed to accurately estimate the sinusoids coefficients. The desired frequency resolution can be achieved by reducing the bandwidth of the bandpass filters. This requires a higher order FIR bandpass filter thus resulting in an increased acquisition time. In other words, by using the DFT to estimate the input signal parameters there is a trade off between accuracy and acquisition time.

The DFT is restricted in the sense that the Fourier coefficients of the input signal are given at equally spaced points in the frequency domain. This is a major disadvantage of the DFT approach particularly when the spectrum of the signal must be evaluated at arbitrary locations. When dealing with noise corrupted sinusoids at known frequencies, the information of input frequencies can be used.

Therefore, instead of looking at the spectrum of the signal at the entire frequency spectrum, we confide ourselves to a particular frequency region.

An efficient algorithm which is suitable for computing only few DFT points is known as the Goertzel algorithm [Goertzel (1958)]. The Goertzel algorithm requires $2(N+2)$ real multiplications and $4(N+1)$ real additions for each value of Fourier coefficient, about half the number of multiplications required with the direct DFT method. In situations where the Fourier coefficients at (M) frequency points are of interest, the complex computation in the Goertzel algorithm is proportional to MN, where N is the number of input data samples [Oppenheim and Schafer (1989)]. In the FFT case the required complex computation is proportional to $N \log N$ (assuming N is a power of 2). Clearly, when M is less than $N \log N$, the Goertzel algorithm provides better performance in terms of computational complexity than the FFT technique. Although the Goertzel algorithm is a computationally efficient method when the number of the DFT points is small, its frequency resolution and acquisition time remain the same as the DFT.

A modified Goertzel algorithm was proposed by Gay *et al.* (1989) to evaluate the Fourier coefficients of sinusoids at arbitrary frequencies. This algorithm uses the information of the input frequencies and evaluates the transfer function of the Goertzel filter at the exact frequency of interest. This method provides higher frequency resolution and estimates the amplitudes of the sinusoids faster when compared with the conventional Goertzel algorithm. However, when both amplitude and phase estimates are required the same acquisition time as the conventional approach is needed.

Another method called Interpolated FFT (IFFT) was developed [Jain *et al.* (1979)] for accurately measuring of periodic signal parameters. The IFFT algorithm uses the information of the input sinusoids for the general multitone case and achieves more accurate estimates when compared with the DFT technique. Since, the IFFT employs interpolation to reduce the effects of the leakage, it requires more calculations after performing the DFT. Unfortunately, this algorithm also does not provide insight into the transient behaviour and its effect on the coefficient estimates.

A Recursive DFT (RDFT) algorithm was presented by Hostetter (1980) based on using a homogeneous differential equation whose general solution is in the form of a sum of sinusoidal functions. This method employs observer theory to estimate the states of a hypothetical system of resonators that model the input signal. The main advantage of RDFT method is that if *a priori* information regarding the input frequencies exists, it is computationally more efficient than the DFT method.

Recently, Tadokoro and Abe (1987) suggested a Notch Fourier Transform (NFT) which utilises second order FIR notch filters whose notch frequencies are exactly tuned at the input spectral lines except the one of the interest. Thus, individual components are easily separated from each other. This method provides faster detection time when compared to the DFT. Although this method is computationally efficient and provides an interesting physical interpretation when compared to the RDFT method, it requires a high Signal to Noise Ratio (SNR) conditions to accurately estimate the phase and amplitude.

Adaptive algorithms are also widely used for the estimation of phase and amplitude of sinusoids buried in noise. These algorithms match the weighted

sum of sinusoidal functions (reference signal) to the input signal using the Least Mean Squared (LMS) [Widrow *et al.* (1975)] and the Recursive Least Square (RLS) [Nehorai and Porat (1986), Chicharo and Ng (1990c)] algorithms. The relationship between the LMS algorithm and the DFT transform was established by Widrow *et al.* (1987), who showed that the LMS algorithm can be used to determine the Fourier coefficients in a sliding fashion. For situations where the input sequence is composed of sinusoids with known frequencies, the reference signals are set in the form of sinusoidal functions with known frequencies, as shown in Figure 1.3. Once convergence takes place the phase and amplitude of individual components are obtained from the adaptive weights. This structure is known as an adaptive spectrum analyser [Widrow *et al.* (1987) and Ogunfunmi and Peterson (1987)].

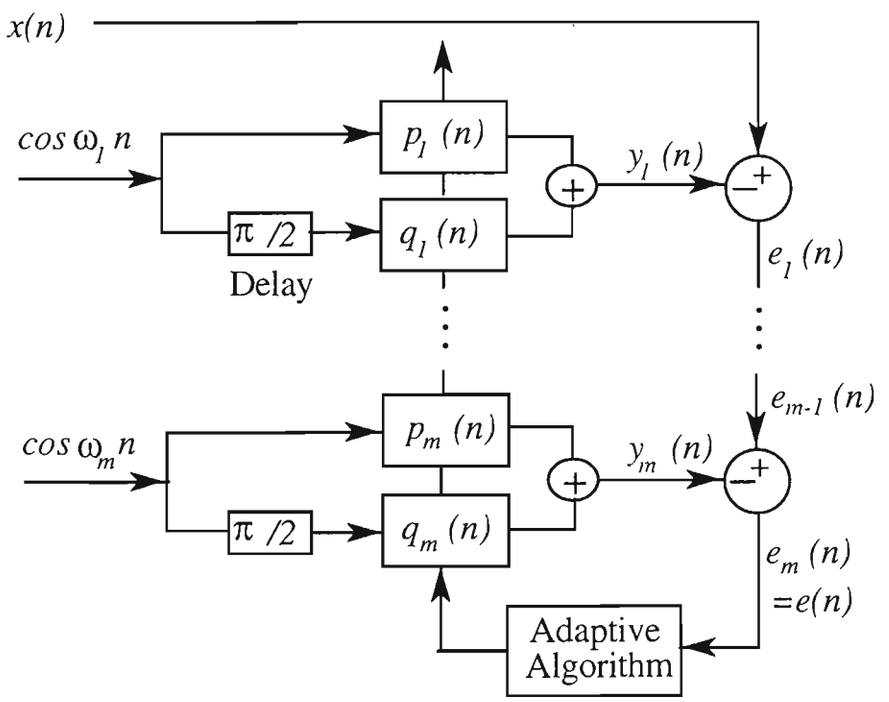

Figure 1.3: Adaptive spectrum analyser.

It has been shown by McGee (1989a, 1989b) that the transfer function from input to the output of each adaptive weight is equal to an IIR bandpass filter. McGee (1989) examined this structure using sinusoidal steady state analysis. His approach is similar to that used by Glover (1977) whereby an equivalent filter

bank was obtained for adaptive noise cancellation scheme applied to sinusoidal interferences. The resonant frequency of the bandpass filter is equal to the frequency of the corresponding reference sinusoid. The bandpass filter also possesses nulls at frequencies determined by other reference sinusoids. This means that by setting the frequencies of the reference sinusoids arbitrarily, a bandpass filter can be realised with resonant frequencies and nulls at any desired locations. Therefore, this structure can be considered as a Generalised Frequency Sampling (GFS) structure which is in contrast with the conventional FS filter bank whose resonant frequencies and nulls are equally spaced over the entire frequency spectrum.

The parametisation of the GFS filter bank structure has been derived independently using different approaches such as observer theory [Peceli (1989)] and an active RC realisation of the singly terminated ladder filter [Padmanabhan and Martin (1991)]. It has been shown that this filter bank consists of parallel digital resonators in a common feedback loop and is therefore sometimes referred to as a resonator-based filter bank. Such a filter bank is very suitable for the enhancement and characterisation of MF signals. This is due to the fact that the nulls of the bandpass filter can be placed exactly at the unwanted frequencies and consequently the effect of leakage can be significantly minimised.

For the case where little or no *a priori* information is available, adaptive filters are employed since they can adjust their parameters according to the input signal automatically. A Tapped Delay Line (TDL) Adaptive Line Enhancer (ALE) using the LMS algorithm was introduced for both enhancement and frequency estimation of sinusoidal signal corrupted by noise [Widrow *et al.* (1975)]. The performance of the TDL ALE was later studied extensively by Zeidler *et al.* (1978), Rickard and Zeidler (1979), Treichler (1979) and Yoganadam *et al.*

(1988). The popularity of TDL ALE over the conventional DFT-based spectral analysis for sinusoidal enhancement is due to its computational efficiency, robustness and better performance in low SNR conditions [Widrow *et al.* (1975)]. Because of the potential savings in computational complexity, adaptive IIR filtering has also been proposed for ALE application [Friedlander (1982, 1984), David *et al.* (1983), Rao and Kung (1984), Ahmed *et al.* (1984), Hush and Ahmed (1984), Nehorai (1985), Ng (1987), Kwan and Martin (1989), Chicharo and Ng (1990a, 1990b, 1992), Chicharo (1992), Padmanabhan and Martin (1991)]. ALE's based on FS filter banks have also been developed which provide faster convergence than the TDL ALE's [Narayan and Peterson (1981), Narayan *et al.* (1983), Kuo and Rodrigues (1985), Rodrigues and Kuo (1985), Kuo and Rodrigues (1986)].

1.2.1 Adaptive Frequency Sampling Structures

Frequency Domain Block Adaptive Filtering (FDBAF) was suggested mainly for the purpose of reducing the computational complexity associated with FIR-based adaptive algorithms [Dentino *et al.* (1978), Ferrera (1980), Clark *et al.* (1983)]. In this method a transformation is firstly applied to the input and the desired signal after a large block of data has been accumulated. Then the filter convolution and the gradient correlation are performed by using computationally efficient techniques such as the FFT. The nett result is that the computational burden is substantially reduced particularly in situations where the adaptive filter is characterised by a long impulse response.

Another class of frequency domain techniques commonly referred to as transform domain LMS algorithms were proposed which only apply a transformation on the input and the desired sequences in a sliding fashion [Narayan and Peterson (1981), Narayan *et al.* (1983), Bitmead and Anderson (1981)]. This approach

transforms the input signal into a set of sequences which are less correlated with one another before performing the adaptive process. Although this does not possess the computational efficiency of the FDBAF, it has the following main advantages. Firstly, the convergence speed dramatically increases when compared with the time domain approach. This is due to the fact that a self-orthogonalising LMS algorithm [Narayan *et al.* (1983), Lee and Un Kwan (1986)] can be used which compensates for the power variation of input signal spectrum. It is well known that a large dynamic range of the input signal spectrum tends to spread the eigenvalues of the input correlation function thus resulting in slow convergence speed [Makhoul (1975)]. In general, it has been shown that for a stationary input, the speed of convergence of the LMS algorithm is dependent on the eigenvalue spread or the ratio of the maximum to minimum eigenvalues of the input correlation matrix [Widrow *et al.* (1976)]. Secondly, it provides a uniform convergence speed for all the adaptive weights [Narayan *et al.* (1983), Lee and Un (1986)].

An efficient realisation of sliding transforms such as DFT and Discrete Cosine Transforms (DCT) can be performed by using equivalent FS filter banks [Rabiner and Gold (1975), Narayan *et al.* (1983)]. Viewed in this way, the transform domain technique is implemented by applying the input signal to a set of parallel bandpass filters whose centre frequencies are uniformly distributed in the frequency domain. The output of each bandpass filter is then multiplied by an adaptive weight which is updated by using a self-orthogonalising LMS algorithm as depicted in Figure 1.4. The algorithm is similar to the LMS algorithm except that it uses a time-varying step size factor which is inversely proportional to the power of the signal at output of each bin. This technique is also referred to as an adaptive FS filter bank [Bitmead and Anderson (1981)].

The Adaptive FS filter bank structure is very suitable for ALE application particularly when the powers of the sinusoidal components are widely spread [Narayan *et al.* (1983)]. A parallel architecture ALE scheme based on FS structure was proposed [Kuo and Rodrigues (1985), Rodrigues and Kuo (1985)] and later implemented [Kuo and Rodrigues (1986)]. In the proposed technique a corresponding set of two-weight LMS adaptive filter was used to gate sinusoidal signals to the output. The weights associated with those bands which contain only noise are set equal to zero. The proposed scheme resulted in a reduction in excess error and improvement in convergence. However, the problem of large spectral overlap amongst the bandpass filter modules is one of the inherent difficulties associated with the conventional FS structure. This spectral overlap reduces the orthogonalisation characteristics of the FS filter bank.

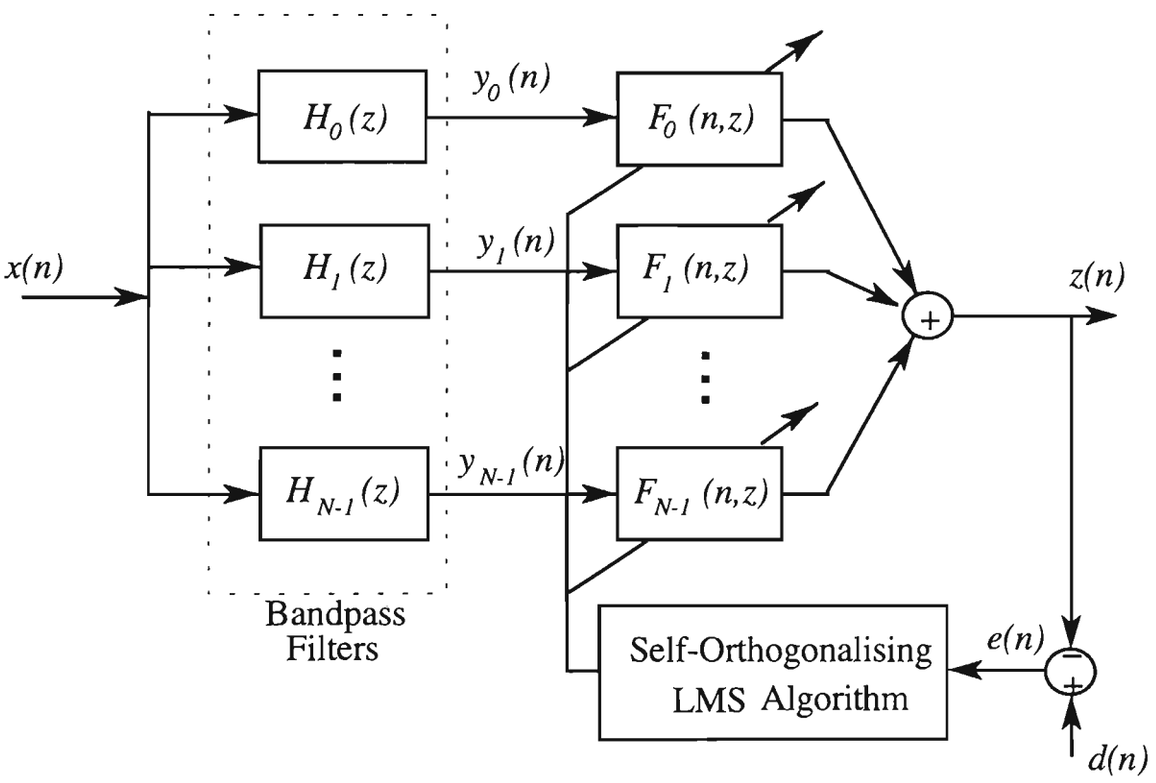

Figure 1.4: Adaptive FS filter bank.

1.2.2 Adaptive IIR Filtering

For ALE applications, an adaptive IIR filtering approach can provide substantial computational savings particularly when higher resolution is required. The IIR

ALE is usually implemented by using a specially constrained IIR bandpass or bandstop (notch) filter. Those techniques which employ an IIR notch filter parametisation are sometimes called Adaptive Notch filtering (ANF) [Friedlander (1984), Rao and Kung (1984), Nehorai (1985), Ng (1987), Chicharo and Ng (1990a)].

An adaptive IIR line enhancer was developed using an Autoregressive Moving Average (ARMA) model together with a Recursive Maximum Likelihood (RML) algorithm [Friedlander (1982)]. It was shown [Friedlander (1982)] that this approach was capable of providing improved performance in low SNR conditions. The next interesting contribution occurred when an IIR notch filter which required only half the number of parameters was proposed by Rao and Kung (1984). In other words, Rao and Kung's solution (1984) required $2n$ adaptive filter coefficients for implementing n notches. The filter parameters were updated using the Stochastic Gauss-Newton (SGN) algorithm. The reduced number of parameters resulted in decreased adaptation error. In addition, the proposed notch filter parametisation enabled simplification of the gradient which could be easily implemented in both cascade and parallel forms. However, as pointed out by Nehorai (1985), the approach suffers from high nonlinearity in the minimisation process, which complicates the algorithm and degrades its performance particularly as the number of input sinusoids increases.

An adaptive IIR notch filter based on the general prediction error framework [Ljung and Soderstrom (1983), Ljung (1981)] was developed by Friedlander (1984). The IIR notch filter was designed with zeros on the unit circle and soft-constrained poles. This algorithm was also characterised by $2n$ parameters for n notches plus pole-zero pair or notch at the Nyquist frequency. It was suggested by Nehorai (1985) that the use of soft-constrained poles may cause numerical

problems due to near pole-zero cancellation on the unit circle. The proposed algorithm also required stability monitoring as convergence was not guaranteed.

A minimal IIR notch filter parametisation together with the use of RML algorithm was proposed by Nehorai [Nehorai (1985), Nehorai and Porat (1986)]. Statistical analysis was later presented to provide insight into the performance of the algorithm [Stoica and Nehorai (1988)]. The proposed notch filter [Nehorai (1985)] has a minimal parametisation; that is, n notches can be implemented using n parameters. This is in contrast with previous techniques which required $2n$ parameters. The proposed algorithm resulted in reduced computational burden, improved convergence rate and ensured numerical robustness. However, it presents convergence problems and requires a complicated procedure for checking the stability of the filter during the adaptation process [Ng (1987)]. A range for the minimal IIR notch filter parameters was derived for stability monitoring purposes [Ng (1987)]. The simulation studies presented by Ng (1987) showed that under certain conditions the RML algorithm did not converge. As an alternative solution, Ng (1987) proposed the use of an Approximate Maximum Likelihood (AML) algorithm which yields improved performance in terms of convergence.

The use of gradient search techniques together with a second order IIR bandpass filter was presented for the ALE applications [David *et al.* (1983)]. This method was applied for the task of enhancing a single sinusoid buried in white noise. It was shown that the proposed technique provides considerable computational savings for the same SNR enhancement when compared with FIR ALE. Further, gradient-based algorithms were found to possess the desirable advantages of simplicity and robustness.

A gradient-based ALE was later developed for multiple sinusoid case using second order IIR bandpass filter modules in cascaded [Ahmed *et al.* (1984)] and parallel [Hush and Ahmed (1984)] structures. The advantage of a cascaded structure is that it provides guaranteed convergence [Ahmed *et al.* (1984)]. In other words, assuming that the number of modules are equal to the number of input sinusoids, each module in the cascaded structure is expected to converge to each sinusoid. This is not the case for parallel structures since the parameter estimates may converge to the local minima or saddle points in the error surface [Hush and Ahmed (1984), Rao and Kung (1984), Padmanabhan and Martin (1991)]. Therefore when using a parallel structure, a judicious choice for the initial values of the adaptive parameters is required.

The gradient-based technique was applied to a modified notch filter parametisation for the purpose of estimating the frequencies of multiple sinusoids buried in noise [Chicharo and Ng (1990a)]. The advantage of the proposed modified notch filter is that it can be easily converted to a bandpass filter by swapping the positions of poles and the zeros of the notch filter [Chicharo and Ng (1990b)]. Error surface analysis was used to demonstrate the convergence behaviour of the gradient based technique. It was shown that for single sinusoid buried in white noise, the algorithm provides guaranteed convergence. For the multiple sinusoids in noise case, a cascaded structure was suggested as being the preferred option.

A constrained adaptive IIR filter consisting of a cascade of biquadratic notch sections was used to track multiple sinusoids [Kwan and Martin (1989)]. The proposed adaptive algorithm approximates the Gauss-Newton method but without the associated computational burden. It was shown that the technique can enhance the input sinusoids with minimum phase shift distortion. The structure

provides reduced bias in frequency estimates when compared with the conventional cascaded structure and is especially good at isolating small amplitude sinusoids which are in the proximity of much higher amplitude sinusoids. However, the complexity of this method increases quadratically with the number of sinusoids. The algorithm is felt to be impractical for tracking more than five sinusoids [Martin (1990)].

1.3 Approach and Contribution of the Thesis

As mentioned earlier, the DFT can be implemented in a sliding form by using FS filter bank whose resonant frequencies are equally distributed from dc to half the sampling frequency (see Figure 1.1). Consequently, individual sinusoidal components are separated and the associated coefficients are obtained at the outputs of the bandpass filters after the Nth sampling time. In the NFT method, the input sinusoids are separated by placing the nulls of FIR notch filter modules at all other frequencies other than the sinusoid of interest. The NFT method has been generalised for the case of DFT where the input frequencies are assumed equally spaced [Tadokoro and Abe (1987)]. In this case, the DFT and NFT methods are in fact equivalent. In other words, the comb filter in the FS structure can be considered as N complex notch filter whose notch frequencies are equally distributed around the unit circle. The pole of each resonator cancels the corresponding zero of the notch filter. As a result, the structure becomes identical to $N-1$ second order complex notch filters whose notch frequencies are tuned at all the frequencies except the one of interest (see Figure 1.5(a)). Assuming that one is dealing with real signals, it is desirable to use real operations. One way to achieve this is through the use of a real valued FS structure as shown in Figure 1.5(b) [Bitmead and Anderson (1981)]. The comb filter consists of $N/2$ second order notch filters that are equally spaced around

the unit circle. Each notch is then cancelled by a corresponding second order digital resonator.

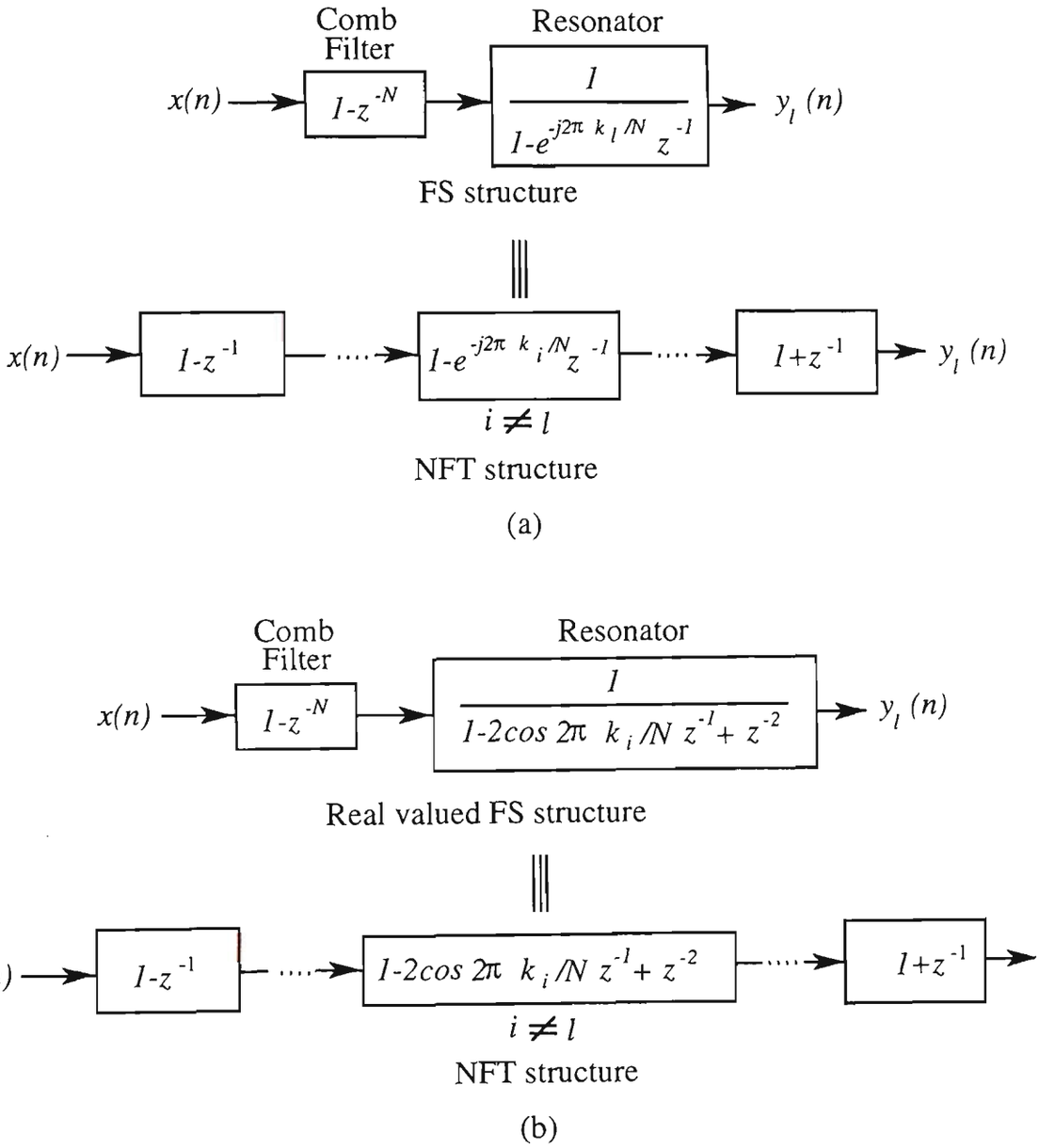

Figure 1.5: Relationship between FS and NFT structures.

The previous section noted that the sinusoidal coefficients can be accurately computed provided the input frequencies lie exactly at the resonant frequencies of the FS filter bank. Otherwise, distortion in Fourier coefficient estimation will occur because of the overlap amongst the bandpass filters (spectral leakage). In order to satisfy the above condition, the resolution must be increased. This is particularly necessary when the input frequencies have a small common factor or are closely spaced. The required resolution in the FS filter bank can be achieved

by increasing the order of the FIR comb filter which also unfortunately results in increased memory storage and acquisition time.

Since the DFT computation at a particular frequency is equivalent to a tuned bandpass filter, other bandpass filter parametisations can be used as an alternative solution. A new filter bank is proposed for the enhancement of noise corrupted harmonic signals. The proposed method is similar in principle to the Notch Fourier Transform (NFT) technique [Tadokoro and Abe (1987)] except that it employs an IIR rather than an FIR notch filter parametisation. In addition, the proposed IIR parametisation provides simple bandwidth controlled bandpass filters. Note that the DFT and NFT both have fixed bandwidth bandpass filter characteristics. In this sense the proposed technique can be regarded as a Constrained Notch Fourier Transform (CNFT). The filter bank is also modified such that the phase characteristic of each bandpass filter is equal to zero at the centre frequency. The bandpass filters are tuned exactly at the input frequency locations which are assumed to be known *a priori*. By evaluating the phase and gain characteristics of the bandpass filters at centre frequencies, the output signal associated with each bandpass filter is presented in the time domain. Using the resulting output signals, a sliding algorithm for CNFT filter bank is proposed to accurately estimate the phase and amplitude of each component.

One of the advantages of the proposed CNFT method is the availability of the bandwidth control parameter which can be used to obtain a comb of bandpass filters with variable bandwidth without increasing the order of the filter. This is in direct contrast with existing DFT and NFT techniques. In order to compare the acquisition time associated with each technique (i.e., the NFT and CNFT), the NFT algorithm has also been developed in a sliding form; that is, the coefficients are updated at every sample time. The sliding NFT algorithm has a

similar parametisation to the conventional Goertzel algorithm and hence can be referred to as the Sliding Goertzel (SG) algorithm.

The CNFT algorithm is generalised for computing the amplitude and phase of the Fourier coefficients of sinusoids at arbitrary known frequencies. The generalised CNFT algorithm uses a second order IIR bandpass filter whose bandwidth and centre frequency can be adjusted independently. The bandwidth control aspect of the proposed approach provides the user with an efficient means of achieving the required resolution as well as reducing spectral leakage. The main advantage of this approach is that it provides faster acquisition time when the input frequencies are mutually prime factor or closely spaced. Further, it leads to a considerable reduction in memory storage requirements when compared with the NFT method.

The proposed sliding algorithms for the CNFT and NFT techniques can be used to estimate the Fourier coefficients of sinusoids at any desired sample time. Accurate estimates are obtained once transient effects of the filters have elapsed. This approach provides an interesting interpretation for the relationship between acquisition time and frequency resolution. It is shown that for higher resolution in frequency, narrower bandwidth is required which increases the transient time of the filter. This means that one can trade the acquisition time for frequency resolution and *vice versa.*

The relationship between the LMS and the SG as well as CNFT algorithms for coefficient estimation of sinusoidal components is established from the point of view that these methods can be considered as narrow bandpass filters tuned to the exact input frequencies. A new derivation for the equivalent filter bank of the LMS spectrum analyser is presented which has similar parametisation as the

resonator-based filter bank recently proposed [Padmanabhan and Martin (1991)]. Our approach is similar to that used by Widrow *et al.* (1975) whereby an equivalent notch filter was obtained for the adaptive noise cancellation scheme applied to single sinusoidal interference. The GFS filter bank is used for the enhancement and coefficient estimation of noise corrupted sinusoids. Since the phase and gain characteristics of each bandpass filter at the resonant frequency are equal to zero and unity; respectively, the enhanced output sinusoid is undistorted in phase and amplitude. Hence, the generalised CNFT algorithm can be used to effectively estimate the phase and amplitude coefficients associated with each sinusoid. This approach also provides more accurate estimates since the nulls of the GFS filter bank are placed at the other unwanted frequencies which may be present. In other words, the effect of leakage is minimised. Further, the GFS filter bank yields significant computational savings when compared with the direct use of the LMS algorithm under the same accuracy and acquisition time conditions.

For comparison purposes, the merits and demerits of the DFT technique are evaluated for estimating sinusoidal parameters. Using the DFT, the required minimum block length is inversely proportional to the greatest common factor of the input frequencies. In situations where the common factor between the input frequencies is small, a large number of samples are required thus resulting in increased acquisition time. The same problem exists for the conventional Goertzel algorithm as it is merely an efficient realisation of the DFT. Further, a SG algorithm is developed based on setting the resonance frequency of a second order digital resonator exactly at the input frequency location. Hence, the proposed technique is referred to as the resonator-based SG algorithm. The resonator based SG algorithm is particularly suitable when the input components are heavily corrupted by noise. This is expected since a digital resonator can be

considered as an ideal matched filter for sinusoidal signal buried in noise. The proposed technique significantly reduces the acquisition time when compared with the conventional Goertzel method particularly when the common factor of the input frequencies is small. As a result, the proposed approach seems promising for the situations where the input sinusoid parameters change rapidly. We consider the performance of the proposed techniques for the task of DTMF signal detection under adverse SNR conditions.

The issue of large spectral overlap amongst bandpass filters in the FS structures is examined. This problem leads to slow convergence speed when FS structures are employed for adaptive filtering. A new IIR FS filter bank is proposed which yields less spectral overlap while preserving the modularity of the conventional FS structures. The proposed structure is composed of a constrained IIR comb filter followed by two successive digital resonators. The IIR comb filter consists of zeros equally spaced on the unit circle together with zeros and poles evenly distributed on the circle with radius less than unity. The positions of the poles and zeros within the unit circle are controllable thus enabling bandpass filters with variable transition band as well as bandwidth. The frequency response characteristics of each bandpass filter is obtained in terms of the position of poles and zeros which are located inside the unit circle.

The additional feature of the proposed IIR FS structure is its reduced spectral gap between two adjacent channels. Using a self-orthogonalising LMS algorithm, it is shown that this technique provides faster convergence when compared to the conventional adaptive TDL and FS structures. This is expected since the spectral overlap amongst the bandpass filters has been considerably reduced. Performance characteristics including convergence speed, minimum Mean Squared Error (MSE), excess (MSE) and convergence condition are presented. The proposed adaptive IIR FS structure is employed for the task of ALE and the

results are compared with those of the conventional FS structure and TDL adaptive filtering. The improvement in convergence speed is quite significant and is particularly evident when the input eigenvalues are widely spread.

FS structures orthogonalises the input signal by passing the signal through parallel bandpass filters which cover the entire frequency domain. This provides an effective means for the compensation of the input power variation thus resulting in faster convergence speed. Note that the slow convergence speed associated with the TDL method is due to the large spectral dynamic range of the input signal. The resolution of transform domain techniques; however, is the same as the TDL technique. An alternative method can be considered by using parallel IIR ALE. This structure, as shown in Figure 1.6, is composed of parallel second order IIR bandpass filters whose centre frequencies are allowed to vary adaptively. Although this structure provides less computational complexity when compared with adaptive FS structure, it may converge to local minima or saddle points [Hush and Ahmed (1985)]. Note that the existence of local minima is one of the inherent problems associated with IIR adaptive filtering [Widrow and Stearns (1985)].

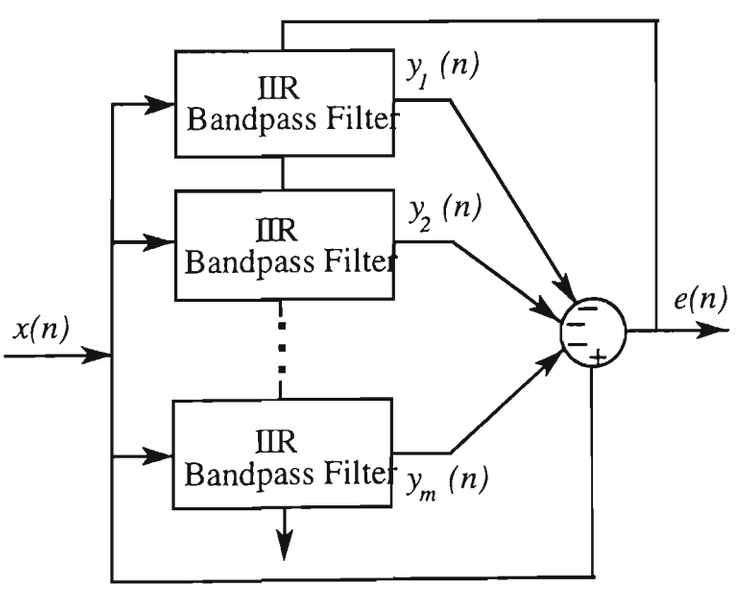

Figure 1.6: Conventional parallel adaptive line enhancer.

To overcome this problem, the conventional parallel ALE is modified. The proposed structure is shown in Figure 1.7 in which the error signal is established separately for each module. The modified structure effectively retrieves all the input sinusoidal components without converging to local minima or saddle points. Therefore, it is attractive for the situations where there is no *a priori* information regarding the locations of the frequencies. Gradient-based algorithms such as RPE and Pseudolinear Regression (PLR) algorithms for the proposed structure are given. The convergence behaviour of the modified parallel ALE structure is studied by using error surface analysis.

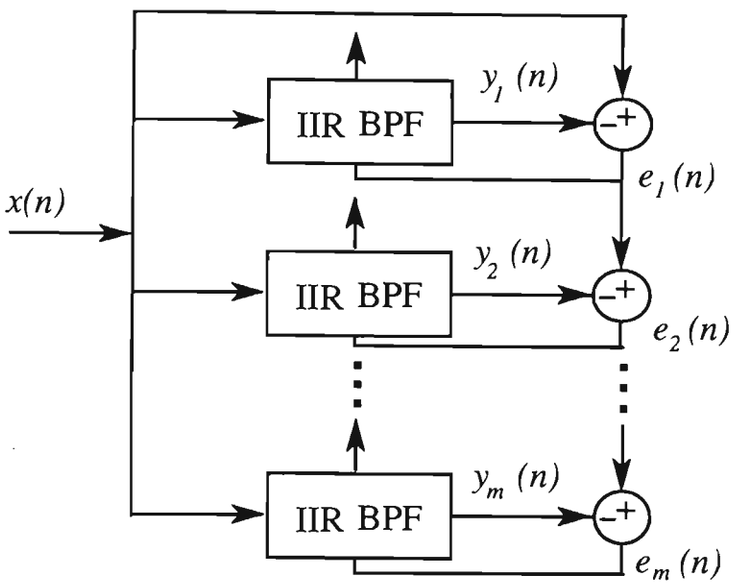

Figure 1.7: Modified Parallel Adaptive IIR line enhancer.

Modular structures have some unique features when compared with the direct implementation. Firstly, they offer simple stability monitoring. Secondly, the input frequencies can be easily determined from bandpass filter coefficients. Thirdly, individual sinusoids are available in the time domain for further processing.

The advantage of the parallel structure over the serial configuration is that it introduces less distortion in phase and amplitude. This is due to the fact that each sinusoid only passes through one module rather than successive modules as

in the case of cascaded structures. It also provides less degradation due to quantisation noise and round off accumulation error when compared with direct or cascaded configuration [Rabiner and Gold (1975), Liu and Kaneko (1969)]. Simulation results are performed to demonstrate the convergence of the given structure and the results are compared with those of conventional parallel [David (1984), Hush and Ahmed (1984)] and cascaded [Ahmed *et al.* (1984), Chicharo and Ng (1990a)] structures.

1.3.1 Point Summary of Contributions

- A new sliding algorithm is developed for the Notch Fourier Transform (NFT) filter bank to accurately compute the phase and amplitude of sinusoidal signals.

- A new Constrained Notch Fourier Transform (CNFT) which provides a bandwidth controlled filter bank is proposed for the enhancement and accurate estimation of Fourier coefficients of harmonic signals. The bandwidth control parameter is used to obtain the required enhancement without necessarily increasing the order of the filter.

- The CNFT algorithm is generalised for coefficient estimation of sinusoidal signals at arbitrary frequencies by using a tuneable second order IIR bandpass filter. This approach provides faster acquisition time and less memory storage when compared with the NFT method.

- The acquisition time versus frequency resolution of the CNFT and NFT algorithms is established.

- A new derivation for the Generalised Frequency Sampling (GFS) filter bank based on a Least Mean Square (LMS) spectrum analyser is presented.

- The GFS filter bank together with the generalised CNFT algorithm is proposed for the task of Fourier coefficient estimation of sinusoidal signals. This technique effectively minimises the leakage problem. Further, it is computationally more efficient when compared with the direct use of the LMS algorithm.

- A sliding Goertzel algorithm is developed based on a digital resonator which is tuned at the input spectral lines to increase the slow acquisition time associated with the conventional Goertzel algorithm.

- A new IIR frequency sampling filter bank is developed for Adaptive Line Enhancer (ALE) applications which provides increased convergence speed when compared to the conventional Frequency Sampling (FS) structures.

- A simple design procedure using a graphical technique is presented to select appropriate ripple and transition band for the bandpass filters of the proposed IIR FS filter bank.
- The conventional parallel IIR ALE is modified such that the convergence to local minima or saddle points is avoided. Convergence behaviour has been established based on error surface analysis.

- The Recursive Prediction Error (RPE) and Pseudolinear Regression (PLR) algorithms have been derived for the proposed parallel IIR ALE.

1.4 Outline of the Thesis

The NFT and CNFT filter bank parametisations for harmonic retrieval together with the associated sliding algorithms for phase and amplitude estimation of individual components are given in Chapter 2. This chapter also includes the use of the sliding CNFT algorithm for the estimation of Fourier coefficients of sinusoidal components with arbitrary known frequencies using a constrained second order IIR bandpass filter. Further, the issues of acquisition time and frequency resolution are discussed. Simulation tests are conducted for harmonic and nonharmonic signals to evaluate the relative performance of both NFT and CNFT methods. For the nonharmonic signal, a typical DTMF signal corrupted by noise is simulated.

Chapter 3 derives the GFS filter bank based on the conventional LMS spectrum analyser. Further, the stability of the structure is analysed. The sliding CNFT algorithm is generalised to the GFS filter bank. It is shown that under the same accuracy and acquisition time the proposed CNFT algorithm provides less computational burden when compared with the direct use of the LMS algorithm. Simulation results for the estimation of Fourier coefficients of typical DTMF signal are conducted to evaluated the performance of both CNFT and LMS algorithms.

In Chapter 4, the individual sinusoids of the input signal are separated using digital resonators whose resonance frequencies are tuned at the input frequency locations. Using the z-transform technique, the output of the resonator is derived and an algorithm similar to the sliding Goertzel algorithm is proposed which can be used to accurately estimate the phase and amplitude of each sinusoid. The proposed technique provides faster detection time when compared with the conventional and modified Goertzel algorithms and this is verified by simulation tests. It is also shown that the given approach is appropriate for the situations

where the input sinusoidal parameters change rapidly within the successive sequences.

The parametisation of IIR FS structure is given in Chapter 5. The proposed filter bank provides faster convergence when compared with TDL and FS adaptive filters. Performance analysis in terms of minimum MSE, excess MSE and convergence condition using the self orthogonalising LMS algorithm are given. Simulation tests for the task of ALE are performed and the results are compared with those obtained by using TDL and FS structure adaptive filters.

A novel parallel IIR ALE using second order IIR bandpass filter modules is described in Chapter 6. We show that the proposed structure together with the gradient based algorithms provides an efficient means of retrieving all sinusoids while the conventional parallel structure may converge to local minima or saddle points. This is justified by using error surface analysis. Extensive simulation results for the enhancement of multiple sinusoids buried in noise is carried out to evaluate the performance of the given structure. The results are compared with those of the conventional cascaded and parallel structures. Finally, Chapter 7 concludes the thesis and outlines some suggestions for further research.

CHAPTER 2:

A Constrained Notch Fourier Transform

2.1 Introduction

This chapter presents a new technique for estimating the coefficients of sinusoidal components buried in noise. The proposed technique utilises *a priori* information regarding the locations of the input frequencies and estimates the phase and amplitude of each sinusoid for every sample update. The proposed algorithm is obtained by examining the output of the bandpass filters which are tuned at the desired frequencies. Important issues such as spectral leakage, desired resolution and required acquisition time are discussed.

An efficient method for performing the sliding spectral analysis at a few frequency bins is by using the DFT filter bank implementation which is often referred to as Frequency Sampling (FS) structure. This structure consists of an FIR comb filter followed by a bank of digital resonators [Rabiner and Gold (1975)] and is equivalent to parallel bandpass filters whose centre frequencies are equally distributed in the frequency domain. Due to the leakage problem, if the input frequencies do not fall exactly in the middle of the bandpass filters then distortion in Fourier coefficient estimation will occur [Koval and Gara (1973), Harris (1978)]. In order to reduce the effect of leakage, the number of bandpass filters must be increased. This can be achieved by increasing the order of the FIR comb filter which results in increased memory storage and acquisition time.

The Notch Fourier Transform (NFT) approach proposed by Tadokoro and Abe (1987) provides an efficient method for computing the Fourier coefficients when the signal is composed of arbitrary frequencies. This method utilises *a priori* information regarding the location of the frequencies and provides reduced computational burden and faster detection time when compared with the DFT approach. The NFT method uses a second order FIR notch filter parametisation as follows:

$$H_k(z^{-1}) = 1 - 2\cos\omega_k z^{-1} + z^{-2} \qquad (2.1)$$

Effectively Equation (2.1) places a null at frequency ω_k while allowing the rest of the input signal through. Assuming that the signal is composed of m sinusoids, this method uses $(m-1)$ FIR notch filters in a cascaded structure whose notch frequencies are equivalent to all the signal frequencies except the frequency of interest. As a result, individual components can easily be separated from each other. The NFT algorithm in the general case, can also perform the same task as the DFT where frequencies of the input signal are evenly arranged in the range of $0 \le f \le f_s/2$ [Tadokoro and Abe (1987), Liu and Lin (1992)]. The input signal in this case is composed of $m+1$ equally spaced frequencies and is written by:

$$x(n) = a_0 + \sum_{k=1}^{m-1}(a_k \cos\omega_k n + b_k \sin\omega_k n) + a_{N/2}\cos\pi n \qquad (2.2)$$

where $N = 2m$ and $\omega_k = 2\pi k / N$. Using the NFT method to find the Fourier coefficients means that $((N/2)-1)$ serially connected second order FIR notch filter modules are required. An efficient realisation of this approach consists of a structure composed of an FIR comb filter of order N followed by a second order digital resonator as depicted in Figure 2.1. Note that N is an even number and the zeros of the comb filter appear in complex conjugate form on the unit circle. The pole of each digital resonator module cancels the corresponding zero of the FIR comb filter. The overall structure can also be considered as an $(N-2)$ order

FIR bandpass filter. The comb filter also consists of two first order zeros, $H_0(z^{-1}) = 1 - z^{-1}$ at frequency f_0 (direct component) and $H_{N/2}(z^{-1}) = 1 + z^{-1}$, at $f_{N/2}$. Therefore, in order to compute a_0 and $a_{N/2}$, resonators are replaced by $1/(1-z^{-1})$ and $1/(1+z^{-1})$, respectively (see Figure 2.1). It is interesting to note that the NFT filter bank structure is an alternative form of implementing the real valued FS structures [Bitmead and Anderson (1981)]. Obviously for high resolution applications the NFT method requires a higher order FIR comb filter as well.

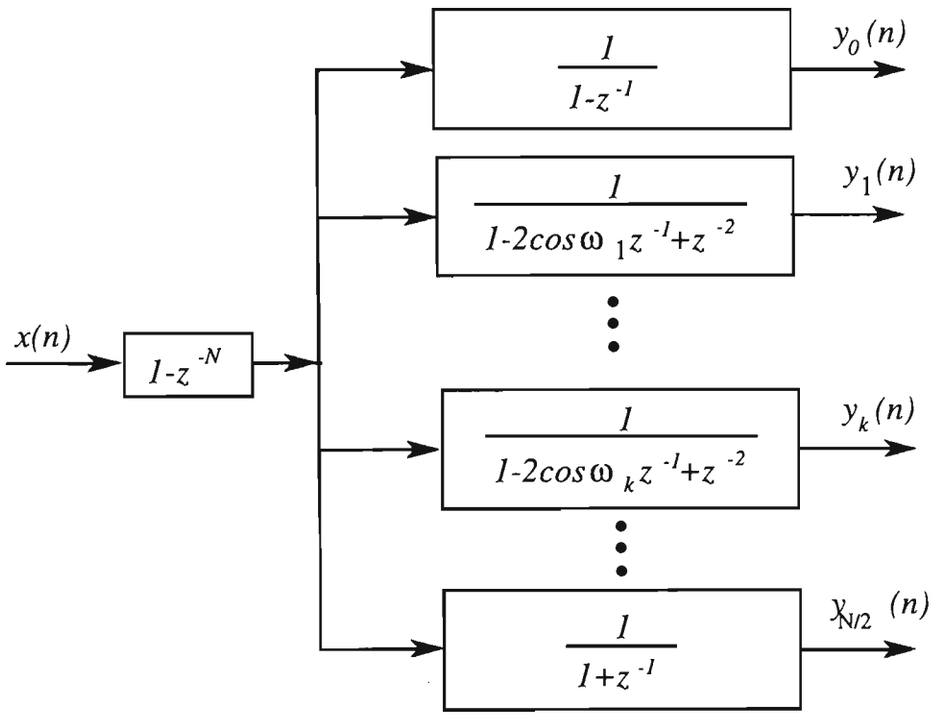

Figure 2.1: Block diagram of the NFT filter bank.

The individual FIR notch filter modules within the comb filter structure are replaced by a constrained IIR parametisation. The resulting structure provides a bandwidth control parameter for each of the parallel bandpass filters. Hence, the proposed structure is referred to as a Constrained Notch Fourier Transform (CNFT). This approach is most appropriate for estimating the amplitude and phase of harmonic signals. By examining the magnitude and phase characteristics of the CNFT filter bank at the centre frequency of each bandpass filter, a sliding computational algorithm for Fourier coefficient estimation is

developed. The bandwidth parameter in the CNFT filter bank is used to obtain the required enhancement without necessarily increasing the order of the comb filter.

For the situation where the spectral components of interest are not distributed uniformly, a constrained second order IIR notch filter is proposed for the realisation of a bandpass filter at arbitrary frequencies. Bandwidth and centre frequency of each individual bandpass filter can be adjusted independently. It is shown that a similar algorithm to the CNFT algorithm can be applied for the second order IIR bandpass filter. This approach provides the following advantages. Firstly, the required spectral bin is easily realised by setting the resonant frequency of the bandpass filter at the desired frequency. The bandwidth control parameter can also be used to achieve the required resolution and to reduce the leakage problem. In other words, we can effectively control the filter bandwidth to minimise spectral leakage without increasing the order of the comb filter. These features will reduce the memory requirements when compared to the NFT method which utilises an FIR parametisation. Secondly, for estimating the coefficients of the sinusoids whose frequencies are mutually prime factors, the proposed approach provides faster acquisition time than the NFT method. In such cases, the NFT filter bank requires $1\,Hz$ resolution to provide an accurate (leakage free) estimate. This can be realised by using a high order FIR bandpass filter which results in increased acquisition time.

Simulation tests have been carried out to evaluate the performance of the proposed method for both uniform and arbitrary spectral frequency distributions. For the former situation, a harmonic signal is used while for the latter case a typical DTMF signal is simulated. In both instances, it is assumed that the signal is corrupted by noise. Sliding algorithms are employed to estimate the Fourier

coefficients of the sinusoidal components. The results are compared with those obtained by the NFT method.

This chapter is organised as follows: In Sections 2.2 and 2.3, the parametisation of IIR bandwidth controlled comb and bandpass filters are presented, respectively. The sliding computational algorithms for estimation of Fourier coefficients are derived in Section 2.4. Performance evaluation using simulation tests is included in Section 2.5. Finally, Section 2.6 concludes the chapter.

2.2 Comb Filter Parametisation

Suppose the sliding DFT is to be computed using the NFT bandpass filter depicted in Figure 2.1. As mentioned before, the FIR comb filter can be considered as N serial FIR notch filters with notch frequencies uniformly spaced on the unit circle. The FIR comb filter is defined as follows:

$$H_c(z^{-1}) = 1 - z^{-N} = (1 - z^{-2}) \prod_{k=1}^{N/2-1} H_k(z^{-1}) \qquad (2.3)$$

where $H_k(z^{-1})$ is a second order FIR notch filter as described by Equation (2.1). In this case, ω_k, is equal to $2\pi k / N$ where N is an even number. Note that the zeros of the FIR comb filter are equally spaced on the unit circle. Notches are also placed at $\omega = 0$ and $\omega = \pi$ using the $(1 - z^{-2})$ term. The poles of the resonator at the kth branch eliminate the zeros of the comb filter at frequency ω_k thus resulting in an FIR bandpass filter. The FIR notch filter can be replaced by a constrained second order IIR notch filter of the following form:

$$H_k(z^{-1}) = \frac{1 - 2\cos\omega_k z^{-1} + z^{-2}}{1 - 2\alpha\cos\omega_k z^{-1} + \alpha^2 z^{-2}} \qquad (2.4)$$

where the positions of the zeros of the notch filter are placed on the unit circle, while the poles are constrained to be within the unit circle by the coefficient α. In order to obtain variable notch bandwidth characteristics and guaranteed

stability, α is chosen to satisfy the inequality; $(0 \leq \alpha < 1)$, as discussed in [Chicharo and Ng (1990a)]. Further, replacing the $(1-z^{-2})$ term in Equation (2.3) with $(1-z^{-2})/(1-(\alpha^{-1}z)^{-2})$ leads to the following transfer function:

$$H_c(z^{-1}) = \frac{1-z^{-N}}{1-\beta z^{-N}} \tag{2.5}$$

where

$$\beta = \alpha^N \tag{2.6}$$

From Equation (2.5), it is evident that the zeros of the IIR comb filter are also equally spaced on the unit circle while the poles are at the same frequencies but constrained to be within the unit circle. The IIR comb filter can be implemented in Direct Form II which means that it only requires N delay registers [Oppenheim and Schafer (1989)]. A block diagram of the proposed filter bank using an IIR comb filter parametisation is shown in Figure 2.2.

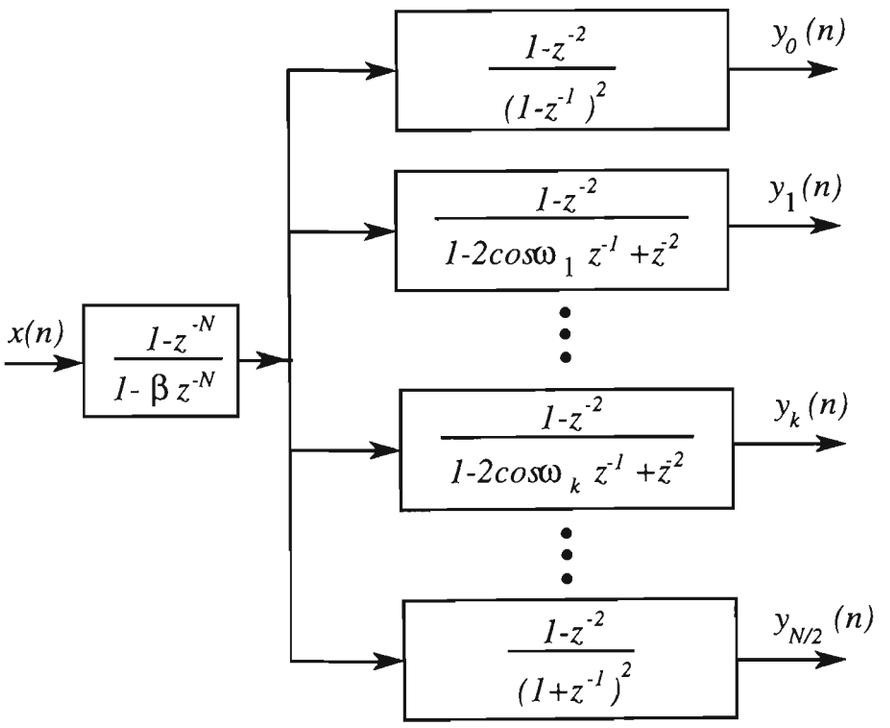

Figure 2.2: Block diagram of the CNFT filter bank.

The $(1-z^{-2})$ term is added to provide a zero phase shift at the centre frequency of each bandpass filter. This means that the components are obtained in the time domain with zero phase shift. Note that only two multiplications are needed per output sample at each branch. Further, the parameter N represents the number of

bandpass filters which are equally distributed over the entire frequency band while β is used to control the bandwidth. Figures 2.3(a) and 2.3(b) compare the gain versus frequency response of the proposed bandpass filter ($N = 16$, $\beta = 0.7$) with the conventional NFT structure ($N = 128$) at normalised centre frequencies of $f = 0.25$ and $f = 0.125$, respectively. It is evident from Figure 2.3 that by choosing an appropriate β, the same bandwidth can be realised but with considerable reduction in N. For the NFT structure, the normalised bandwidth of the bandpass filter depends on the order of the comb filter and is equal to $1/N$. However, in the CNFT approach, the bandwidth also depends on the distance of the poles from the origin. The normalised $-3dB$ bandwidth is obtained geometrically by finding the two points around ω_k on the unit circle which are $\sqrt{2}$ times the distance between the kth pole and the unit circle. For α very close to one, these points are considered to be approximately at the same distance from the pole at ω_i as they are from the zero at ω_i (for all i , where $i \neq k$). The normalised $-3dB$ bandwidth is then given by [Chicharo (1990)]:

$$BW \approx \frac{1}{\pi}(1-\sqrt[N]{\beta}) = \frac{1}{\pi}(1-\alpha) \qquad (2.7)$$

Figure 2.4 shows the magnitude response of the resulting filter bank for different values of β ($\beta = 0$, $\beta = 0.5$ and $\beta = 0.7$) for two adjacent spectral bins.

2.3 A Constrained Second Order IIR Bandpass Filter

The centre frequencies of the above bandpass filters are constrained to be equally spaced over the entire frequency band. In order to realise the spectral bins at arbitrary frequencies, the following constrained second order IIR bandpass filter is proposed:

$$H_{BP}(z^{-1}) = (1-g)\frac{1-z^{-2}}{1+ghz^{-1}+(2g-1)z^{-2}} \qquad (2.8)$$

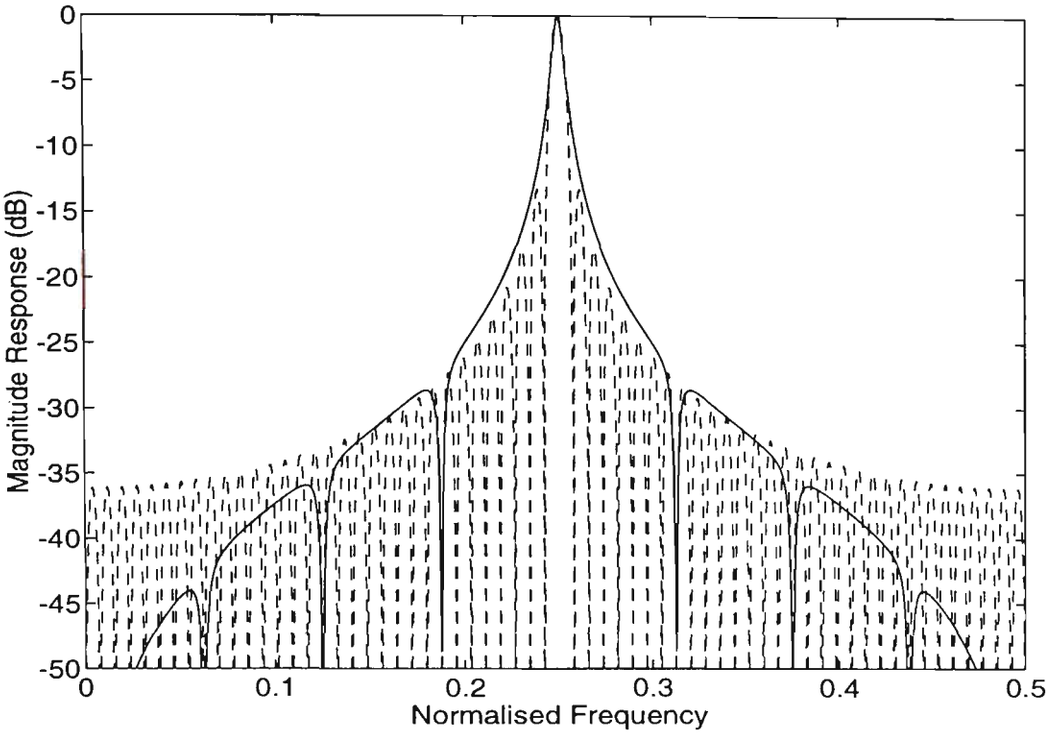

(a)

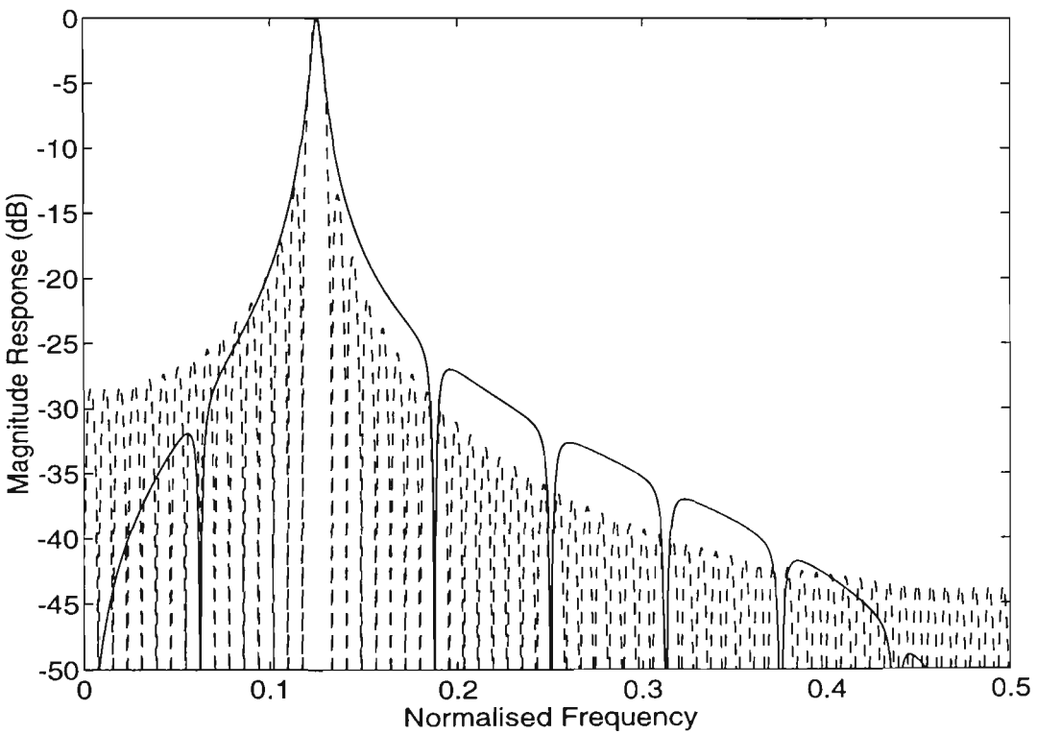

(b)

Figure 2.3: The gain response of the NFT bandpass filter (dashed line $N = 128$) and CNFT bandpass filter (solid line $N = 16$, $\beta = 0.7$) at centre frequencies (a) $f = 0.25$, (b) $f = 0.125$.

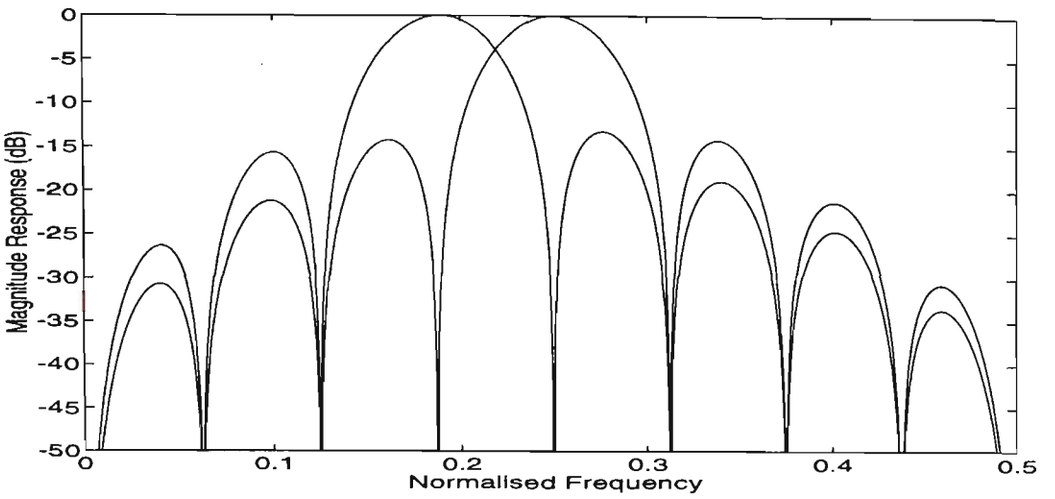

(a)

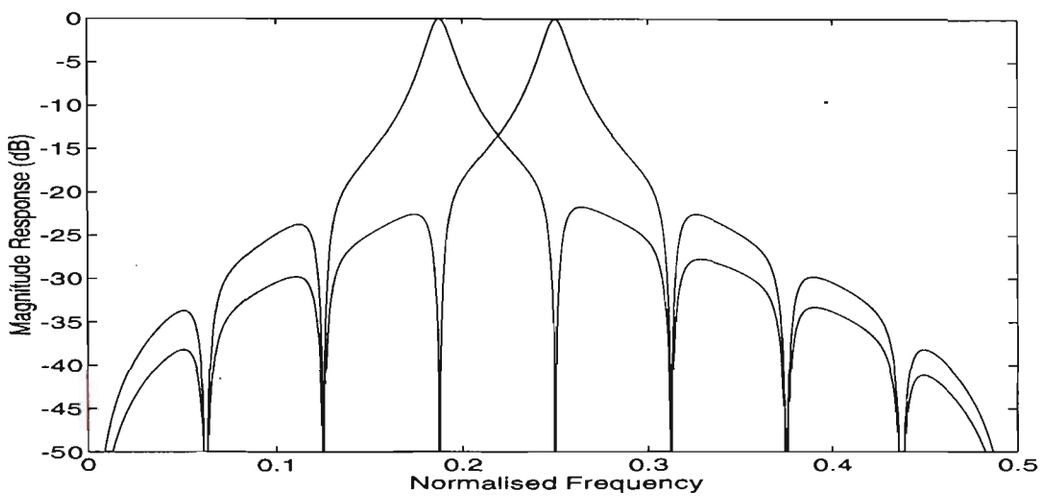

(b)

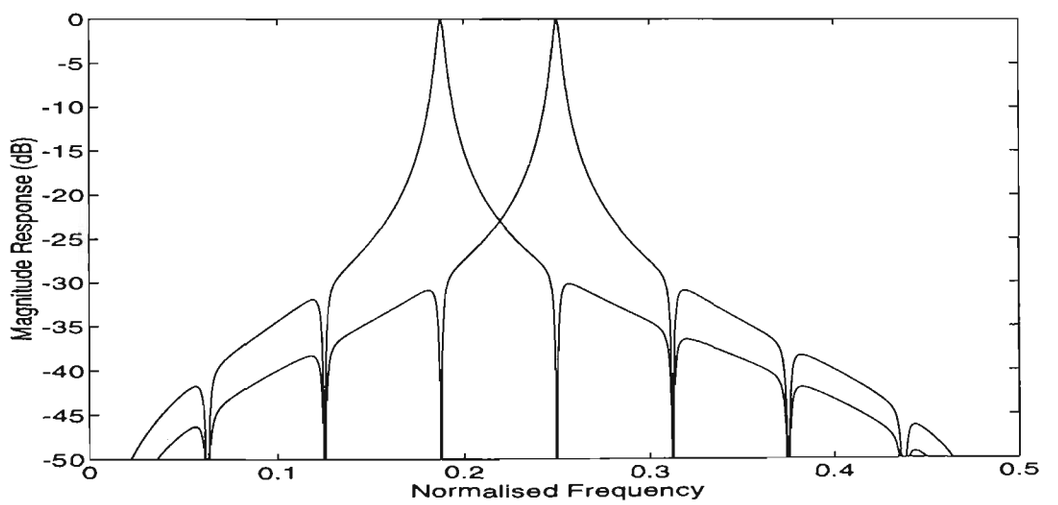

(c)

Figure 2.4: The magnitude response of the CNFT bandpass filter for different values of β (a) $\beta = 0$, (b) $\beta = 0.5$ and (c) $\beta = 0.7$.

where g controls the bandwidth of the filter and should be in the range of $0.5 \leq g < 1$ to ensure that the filter is stable. The derivation for the proposed bandpass filter is detailed in Appendix (A). $H_{BP}(z^{-1})$ has a maximum gain of unity at the frequency given by:

$$f_p = \frac{1}{2\pi}\cos^{-1}\left(\frac{-h}{2}\right) \tag{2.9}$$

where $-2 < h < 2$. Equation (2.9) can be verified by considering the fact that the following second order IIR notch filter is realised by subtracting the output of the bandpass filter from the input signal:

$$H_N(z^{-1}) = 1 - H_{BP}(z^{-1}) = g\frac{1 + hz^{-1} + z^{-2}}{1 + ghz^{-1} + (2g-1)z^{-2}} \tag{2.10}$$

This implies that the gain and phase values for the bandpass filter are unity and zero, respectively at the centre frequency. The centre frequency also occurs at the zero transmission of the notch filter transfer function. Thus, by letting the numerator of the notch filter transfer function equal zero, Equation (2.9) is easily derived.

It is interesting that the two parameters h and g, provide effective means of independently setting the required centre frequency and bandwidth. The gain versus frequency response of the proposed bandpass filter for different values of g (i.e., $g = 0.9$, $g = 0.96$ and $g = 0.99$) is depicted in Figure 2.5 and this is compared with the NFT structure ($N = 20$). The normalised bandwidth (BW) of the proposed bandpass filter can be determined geometrically (for values of g close to one) by the following approximate relationship:

$$BW \approx \frac{1-g}{\pi} \tag{2.11}$$

The bandwidth control parameter (g) is useful from the point of view of reducing the spectral leakage due to other components in the input signal. Further, it can

be used to obtain the required resolution when spectral components are closely spaced.

It must be emphasised that in order to use the proposed approach to resolve the input frequency components, *a priori* knowledge regarding the location of these frequencies is required. In many applications such as Dual-Tone Multifrequency (DTMF) signals [Tadokoro and Abe (1987), Braun (1975)], digital Multifrequency (MF) receivers [Koval and Gara (1973)] and in very small aperture terminal (VSAT) satellite communication systems [Simington and Percival (1991)], this information is available *a priori*.

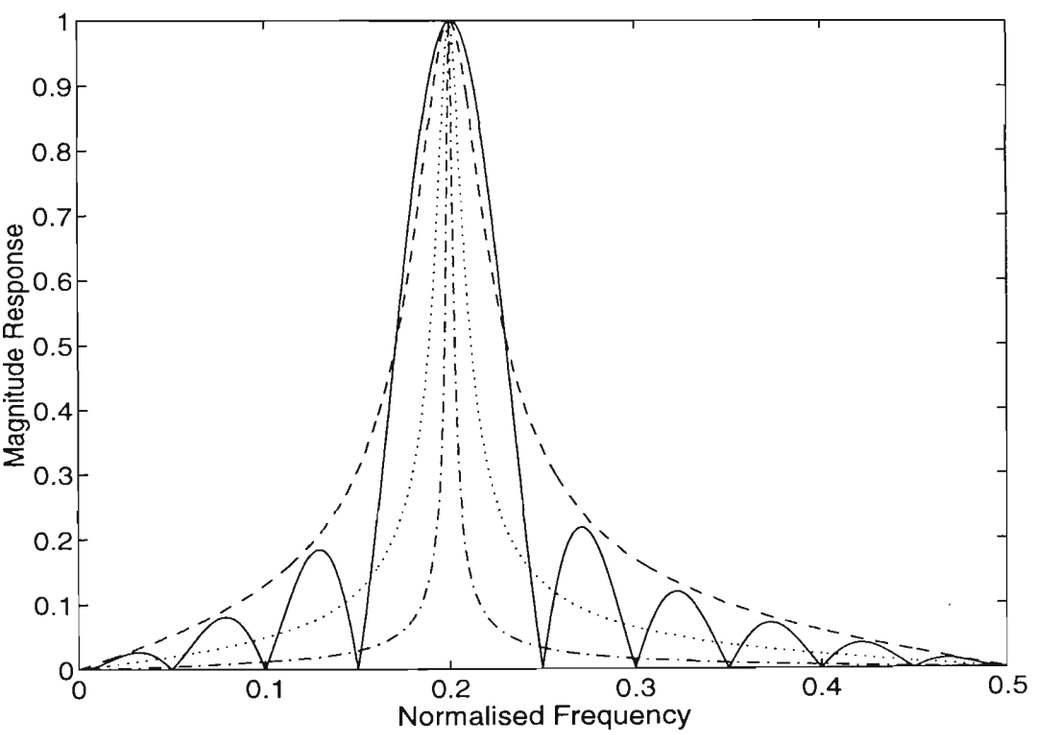

Figure 2.5: Magnitude response of the NFT bandpass filter $N = 20$ (solid line) and the second order IIR bandpass filter for different values of g ($g = 0.9$ (dashed line), $g = 0.96$ (dotted line) and $g = 0.99$ (dashdot line)).

2.4 Derivation of Sliding Algorithms for Computing the Fourier Coefficients

This section presents the derivations of the sliding NFT and CNFT algorithm for determining the Fourier coefficients. Consider the following cases:

a) *The NFT case.*

In order to establish the sliding algorithm, the transfer function of each bandpass filter is evaluated at its centre frequency. Assuming that each bandpass filter enhances only one component, the output can easily be derived in the time domain. The transfer function for each bandpass filter in the NFT case is as follows (refer to Figure 2.1):

$$H_{BP}^{k}(z^{-1}) = G_{1k}(z^{-1}) = \frac{1-z^{-N}}{1-2\cos\omega_k z^{-1}+z^{-2}} \qquad (2.12)$$

where $k = 1,\cdots,N/2-1$

Evaluation of the above transfer function (Equation (2.12)) at frequency ω_k results in [Tadokoro and Abe (1987), Liu and Lin (1992)]:

$$G_{1k}(e^{j\omega_k}) = \frac{N(-1)^{k+1}}{2\sin\omega_k} e^{-j\omega_k(\frac{N}{2}-1)+j\frac{\pi}{2}} \qquad (2.13)$$

Letting ω_k equal $2\pi k/N$, Equation (2.13) reduces to:

$$G_{1k}(e^{j\omega_k}) = \frac{-N}{2\sin\omega_k} e^{j(\omega_k+\frac{\pi}{2})} \qquad (2.14)$$

The kth component of the input signal given by Equation (2.2) can be expressed as:

$$x_k(n) = a_k\cos\omega_k n + b_k\sin\omega_k n \qquad (2.15)$$

Using Equation (2.14), the output of the kth branch, $y_k(n)$, is:

$$\begin{aligned} y_k(n) &= \frac{N}{2\sin\omega_k}\{a_k \sin\omega_k(n+1) - b_k \cos\omega_k(n+1)\} \\ &= \frac{N}{2\sin\omega_k}(a_k \sin\omega_k n\cos\omega_k + a_k \cos\omega_k n\sin\omega_k \\ &\qquad - b_k \cos\omega_k n\cos\omega_k + b_k \sin\omega_k n\sin\omega_k) \end{aligned} \tag{2.16}$$

Evaluating Equation (2.16) at $(n-1)$th sampling time we have:

$$y_k(n-1) = \frac{N}{2\sin\omega_k}(a_k \sin\omega_k n - b_k \cos\omega_k n) \tag{2.17}$$

From Equations (2.16) and (2.17), the following Equations are obtained:

$$A_k(n) = \frac{2}{N}\{y_k(n) - \cos\omega_k y_k(n-1)\} = a_k \cos\omega_k n + b_k \sin\omega_k n \tag{2.18}$$

$$B_k(n) = \frac{-2\sin\omega_k}{N} y_k(n-1) = b_k \cos\omega_k n - a_k \sin\omega_k n \tag{2.19}$$

The algorithm given by Equations (2.18) and (2.19) is similar to the Goertzel algorithm. In other words, since ω_k is equal $2\pi k / N$, the sine and cosine terms are equal to zero and one at every N sampling time, respectively. Hence, $A_k(N) = a_k$ and $B_k(N) = b_k$. However, it is interesting to note that by solving the resulting linear Equations (2.18) and (2.19), a sliding algorithm for accurate computation of Fourier coefficients is obtained as follows:

$$\begin{bmatrix} a_k(n) \\ b_k(n) \end{bmatrix} = \begin{bmatrix} \cos\omega_k n & -\sin\omega_k n \\ \sin\omega_k n & \cos\omega_k n \end{bmatrix} \begin{bmatrix} A_k(n) \\ B_k(n) \end{bmatrix} \tag{2.20}$$

Note that Equations (2.18), (2.19) and (2.20) can be used at any desired sample time to evaluate the Fourier coefficients (a_k, b_k). At this point, it is important to address the issue of the transient behaviour associated with the bandpass filter. In the NFT case, the overall bandpass filter is an FIR filter with the order of $(N-2)$. Hence accurate results will be achieved after $(N-2)$ samples. Increasing the order of the bandpass filter leads to a narrower bandwidth bandpass filter and consequently leads to an increase in resolution. However, this means that the transient time will also increase. As expected, accurate

results are obtained when the transient time of the filter has elapsed. From the block diagram of the NFT (see Figure 2.1), for $k = 0$ we have:

$$G_{10}(z^{-1}) = \frac{1 - z^{-N}}{1 - z^{-1}} \tag{2.21}$$

Given that the value of the above transfer function at zero frequency is equal to N, the sliding algorithm for amplitude of direct component (f_0) is:

$$A_0(n) = \frac{1}{N} y_0(n) \tag{2.22}$$

For $f_{N/2}$, the filter transfer function becomes (refer to Figure 2.1):

$$G_{1\frac{N}{2}}(z^{-1}) = \frac{1 - z^{-N}}{1 + z^{-1}} \tag{2.23}$$

Appendix (B) derives and shows that the sliding algorithm for amplitude of $f_{N/2}$ component is given by:

$$A_{N/2}(n) = \frac{(-1)^n}{N} y_{N/2}(n) \tag{2.24}$$

Since the order of the FIR filters given by Equations (2.21) and (2.23) is equal to $(N-1)$, then a_0 and $a_{N/2}$ are given by $A_0(N-1)$ and $A_{N/2}(N-1)$, respectively. Manipulating Equations (2.18) and (2.19) leads to the following expression:

$$A_k^2(n) + B_k^2(n) = a_k^2 + b_k^2 \tag{2.25}$$

This means that the amplitude can be updated at every sampling time without computing Equation (2.20). We now show that when the input frequency is not exactly in the middle of the spectral bins, Equation (2.25) is still approximately valid provided the deviation is small. Consider the case where the kth input sinusoidal frequency is $\omega_k + \Delta\omega$, where $\Delta\omega$ is a small deviation from the bandpass filter centre frequency. In this case $x_k(n)$ is given by:

$$x_k(n) = a_k \cos(\omega_k + \Delta\omega)n + b_k \sin(\omega_k + \Delta\omega)n \tag{2.26}$$

Expanding the above equation results in:

$$x_k(n) = a_k' \cos\omega_k n + b_k' \sin\omega_k n \tag{2.27}$$

where

$$a'_k = a_k \cos\Delta\omega n + b_k \sin\Delta\omega n \tag{2.28}$$

$$b'_k = b_k \cos\Delta\omega n - a_k \sin\Delta\omega n \tag{2.29}$$

Hence, the sliding algorithm will compute a'_k and b'_k. Clearly from Equations (2.28) and (2.29), it is seen that:

$$a'^2_k + b'^2_k = a^2_k + b^2_k \tag{2.30}$$

Note that the amplitude will be reduced due to the deviation of the sinusoid from the centre of the bandpass filter where the gain is maximum. Therefore the deviation in frequency must be small to ensure that the sinusoid is located within the passband of the bandpass filter.

b) *The CNFT case.*

Using the same approach as employed for the NFT case, a sliding algorithm for the proposed bandpass filters will be derived. The transfer function of each bandpass filter in the CNFT structure is given by (see Figure 2.2):

$$H^k_{BP}(z^{-1}) = G_{1k}(z^{-1})G_2(z^{-1}) = \frac{1-z^{-N}}{1-2\cos\omega_k z^{-1}+z^{-2}} \frac{1-z^{-2}}{1-\beta z^{-N}} \tag{2.31}$$

where $k = 1,\cdots, N/2-1$

The frequency response for $G_2(z^{-1})$ at ω_k is expressed as:

$$G_2(e^{j\omega_k}) = \frac{2\sin\omega_k}{1-\beta} e^{-j(\omega_k - \frac{\pi}{2})} \tag{2.32}$$

Using Equation (2.14), the total response of each bandpass filter at ω_k will be:

$$H^k_{BP}(e^{j\omega_k}) = \rho N \tag{2.33}$$

where

$$\rho = \frac{1}{1-\beta} \tag{2.34}$$

As stated previously the zero phase shift characteristics (at the centre frequency) in Equation (2.33) is achieved by adding the $(1-z^{-2})$ block. Consider the kth

component of the real input signal given by Equation (2.15), using Equation (2.33), the output of the kth branch is given by:

$$y_k(n) = \rho N(a_k \cos \omega_k n + b_k \sin \omega_k n) \tag{2.35}$$

In order to derive the sliding algorithm for computing the Fourier coefficients, we evaluate $y_k(n)$ at nth and $(n-1)$th samples. Solving the resulting equations simultaneously, we obtain:

$$A_k(n) = \frac{1}{\rho N} y_k(n) = a_k \cos \omega_k n + b_k \sin \omega_k n \tag{2.36}$$

$$B_k(n) = \frac{-1}{\rho N \sin \omega_k} \{y_k(n-1) - \cos \omega_k y_k(n)\} = b_k \cos \omega_k n - a_k \sin \omega_k n \tag{2.37}$$

where $k = 1, \cdots, N/2 - 1$

From Equations (2.36) and (2.37) it is evident that Equation (2.20) can be used, as in the case of NFT, to update the Fourier coefficients (a_k, b_k) at every sample time. Further, Equation (2.25) is also valid even with a small deviation of input frequency from the middle of the spectral bin. Note that because of the additional bandwidth control parameter β, the proposed technique provides an extra degree of flexibility when compared to the NFT approach. For the special case when β is equal to zero the proposed CNFT is equivalent to the NFT method. Referring to the block diagram shown in Figure 2.2 the filter transfer function for $(k = 0)$ is as follows:

$$H_{BP}^0(z^{-1}) = \frac{1 - z^{-N}}{1 - z^{-1}} \frac{1 + z^{-1}}{1 - \beta z^{-N}} \tag{2.38}$$

It is straight forward to show that the frequency response of the first and the second terms of Equation (2.38) at $\omega = 0$ are equal to N and $2/(1-\beta)$, respectively. Therefore, $A_0(n)$ is given by:

$$A_0(n) = \frac{1}{2\rho N} y_0(n) \tag{2.39}$$

For the case when $k = N/2$, $A_{N/2}(n)$ can be expressed as (see Appendix (B)):

$$A_{N/2}(n) = \frac{(-1)^n}{2\rho N} y_{N/2}(n) \tag{2.40}$$

The phase shift of the proposed second order IIR bandpass filter is also equal to zero at the peak frequency. This means that the corresponding component appears without phase shift at the output. Therefore, Equations (2.20), (2.36) and (2.37) can be employed to compute the Fourier coefficients of the sinusoidal component provided that ρN is replaced by 1 in Equations (2.36) and (2.37). Note that the second order IIR bandpass filter has unity gain at the centre frequency while the gain of the CNFT filter bank is equal to ρN. The required acquisition time for obtaining the Fourier coefficients depends on the bandwidth of the bandpass filter. In other words, for situations where a narrow bandwidth is required, the transient time will necessarily increase. This is the same situation as in the NFT case when a higher order comb filter is required which also increases the acquisition time. Clearly the same detection time will be achieved with both methods if the bandwidth of the NFT and CNFT bandpass filters are equal. The number of samples required (N_{acq}) to obtain accurate Fourier coefficient estimates for the proposed IIR bandpass filters is approximately given by:

$$N_{acq} \approx \frac{1}{BW} \tag{2.41}$$

where the normalised bandwidth (BW) is given by Equations (2.7) and (2.11). Hence, Equation (2.20) must be evaluated at N_{acq}th sample time as follows:

$$\begin{bmatrix} a_k \\ b_k \end{bmatrix} = \begin{bmatrix} \cos\omega_k N_{acq} & -\sin\omega_k N_{acq} \\ \sin\omega_k N_{acq} & \cos\omega_k N_{acq} \end{bmatrix} \begin{bmatrix} A_k(N_{acq}) \\ B_k(N_{acq}) \end{bmatrix} \tag{2.42}$$

The complete sliding NFT and CNFT algorithms are summarised in Table 2.1. Note that Equations (2.20), (2.36) and (2.37) are evaluated at the time instant when the transient response of the filter has elapsed. However, in situations where the sinusoidal parameters (phase and amplitude) are time varying, Equations (2.20), (2.36) and (2.37) can be computed at any sample time to update

the estimates. For such cases, the rate of parameter variation must be slower than the required acquisition time of the filter. In other words, if the sinusoidal coefficients change, we must wait until N_{acq} samples to obtain accurate results. The performance of the two approaches from this point of view is evaluated by simulation tests in the next section.

NFT Method :	CNFT Method :
$for \quad k = 1, \cdots, \frac{N}{2} - 1$	$for \quad k = 1, \cdots, \frac{N}{2} - 1$
$A_k(n) = \frac{2}{N}\{y_k(n) - \cos\omega_k y_k(n-1)\}$	$A_k(n) = \frac{1}{\rho N} y_k(n)$
$B_k(n) = \frac{-2\sin\omega_k}{N} y_k(n-1)$	$B_k(n) = \frac{-1}{\rho N \sin\omega_k}\{y_k(n-1) - \cos\omega_k y_k(n)\}$
$a_k = A_k(N)$	$N_{acq} \approx \frac{1}{BW}$
$b_k = B_k(N)$	$\begin{bmatrix} a_k \\ b_k \end{bmatrix} = \begin{bmatrix} \cos\omega_k N_{acq} & -\sin\omega_k N_{acq} \\ \sin\omega_k N_{acq} & \cos\omega_k N_{acq} \end{bmatrix} \begin{bmatrix} A_k(N_{acq}) \\ B_k(N_{acq}) \end{bmatrix}$
$A_0(n) = \frac{1}{N} y_0(n), \; a_0 = A_0(N)$	$A_0(n) = \frac{1}{2\rho N} y_0(n), \; a_0 = A_0(N_{acq})$
$A_{N/2}(n) = \frac{(-1)^n}{N} y_{N/2}(n), \; a_{N/2} = A_{N/2}(N)$	$A_{N/2}(n) = \frac{(-1)^n}{2\rho N} y_{N/2}(n), \; a_{N/2} = A_{N/2}(N_{acq})$

Table 2.1: NFT and CNFT sliding algorithms.

2.5 Simulation Results

Two cases are considered to evaluate the performance of the proposed bandpass filters together with their sliding algorithms. The first is where the input signal is a harmonic series and secondly, where the input signal is composed of arbitrary frequencies. In both cases the signals are buried in noise and an estimate of amplitude and phase will be computed. The results are compared with those obtained from the NFT algorithm.

Example 1. Harmonic signal. Consider a noise corrupted input harmonic signal as follows:

$$x(n) = \sum_{k=1}^{3} C_k \sin(\frac{2\pi k f_0}{f_s} n - \phi_k) + \nu(n) \qquad (2.43)$$

where $\nu(n)$ is a unit variance, zero mean white noise sequence. The coefficients C_1, C_2 and C_3 are chosen to be 4, 2 and 1 respectively and $\phi_1 = \phi_2 = \phi_3 = 1$ (rad) while the fundamental and sampling frequencies are $50Hz$ and $400Hz$, respectively. In this case the frequencies are distributed uniformly. The bandpass filters are realised by using a comb filter of order $N = 16$ followed by parallel resonators. Note that the frequency components are also placed on the centre of the spectral bins. The amplitude and phase of the fundamental frequency is computed at every sample for two different values of β (i.e., 0.7 and 0.9). The results are depicted in Figure 2.6 and as can be seen the accuracy improves as β increases. It is interesting to note that slower acquisition time is obtained as β approaches unity for the amplitude coefficient estimate but not for the phase coefficient. In other words, β only affects the accuracy of the phase estimate. This phenomenon was also observed for the NFT case and can be interpreted as follows. Consider a sinusoidal component defined by:

$$x_k(n) = C_k \sin(\omega_k n - \phi_k) \qquad (2.44)$$

where

$$C_k = \frac{a_k}{\sin(\phi_k)} \quad ; \quad \phi_k = -\tan^{-1}(\frac{a_k}{b_k}) \qquad (2.45)$$

Since the transient behaviour of the bandpass filter has similar effect on $a_k(n)$ and $b_k(n)$, therefore the ratio in the argument of $\tan^{-1}(.)$ will not be affected significantly. Figure 2.7 compares the amplitude and phase estimates obtained for both the NFT ($N = 128$) and CNFT ($N = 16$, $\beta = 0.7$) approaches. As expected, since the bandwidth of the two methods are nearly equal (see Figure 2.3), the acquisition times are also equal. However, N has been reduced from 128 for the case of the NFT to 16 in the case of CNFT.

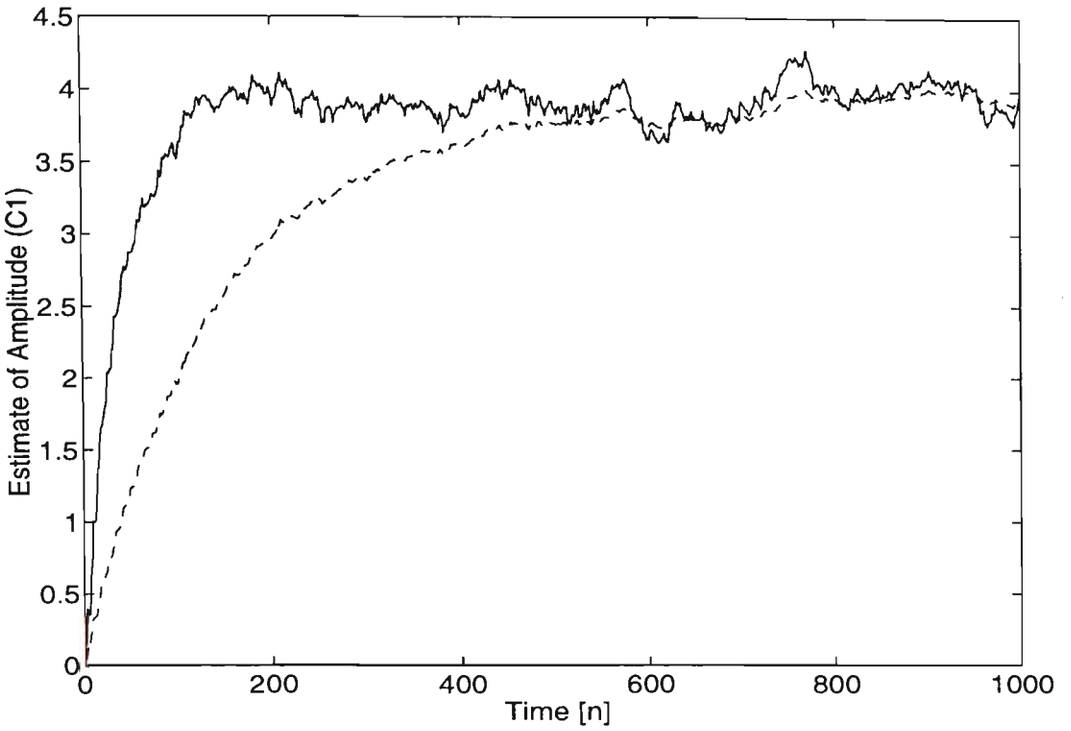

(a)

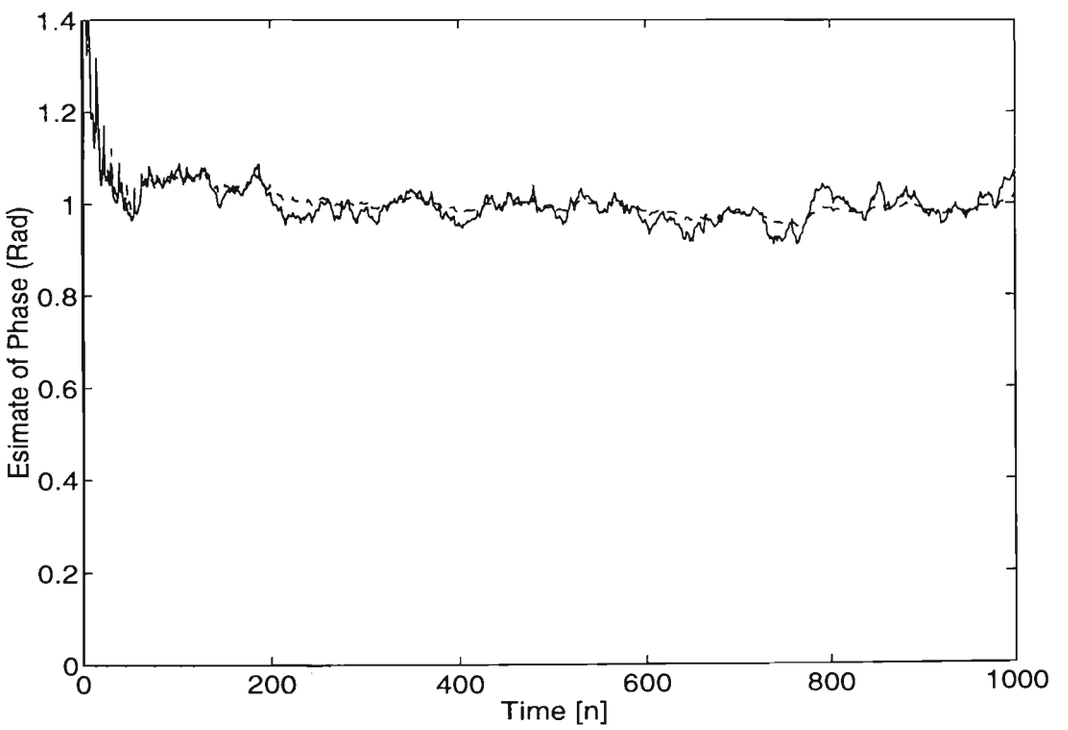

(b)

Figure 2.6: Sliding computation of the (a) amplitude and (b) phase of the fundamental frequency corrupted by zero mean, unit variance white noise for $\beta = 0.7$ (solid lines) and $\beta = 0.9$ (dashed lines) using CNFT algorithm.

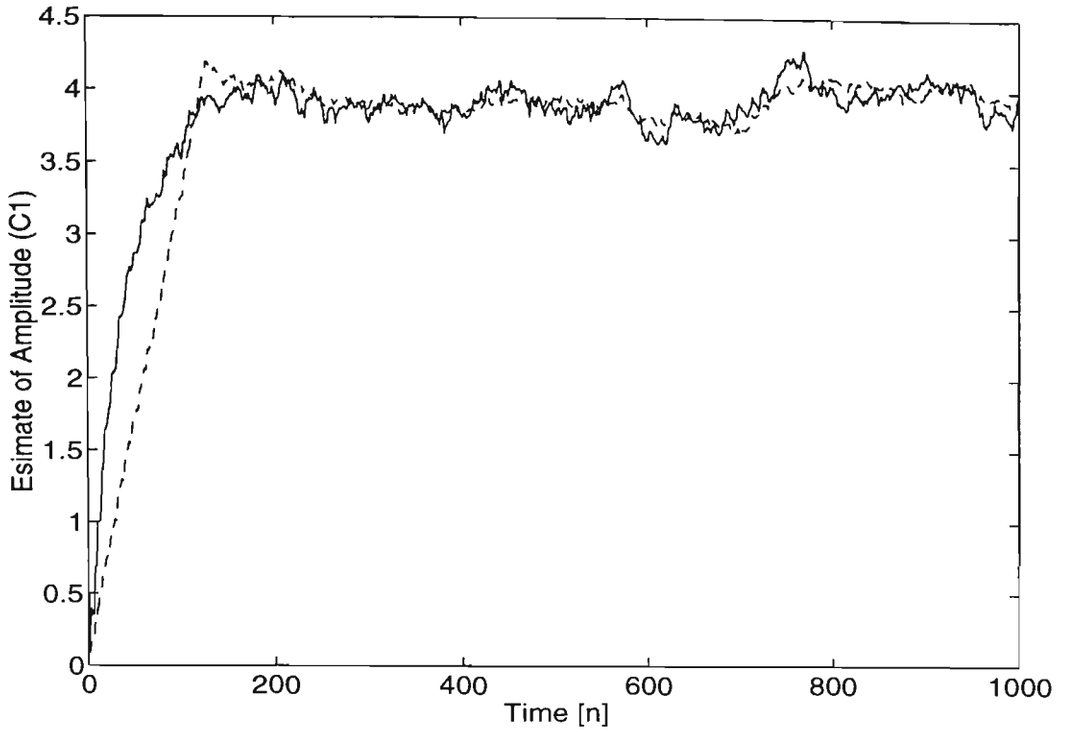

(a)

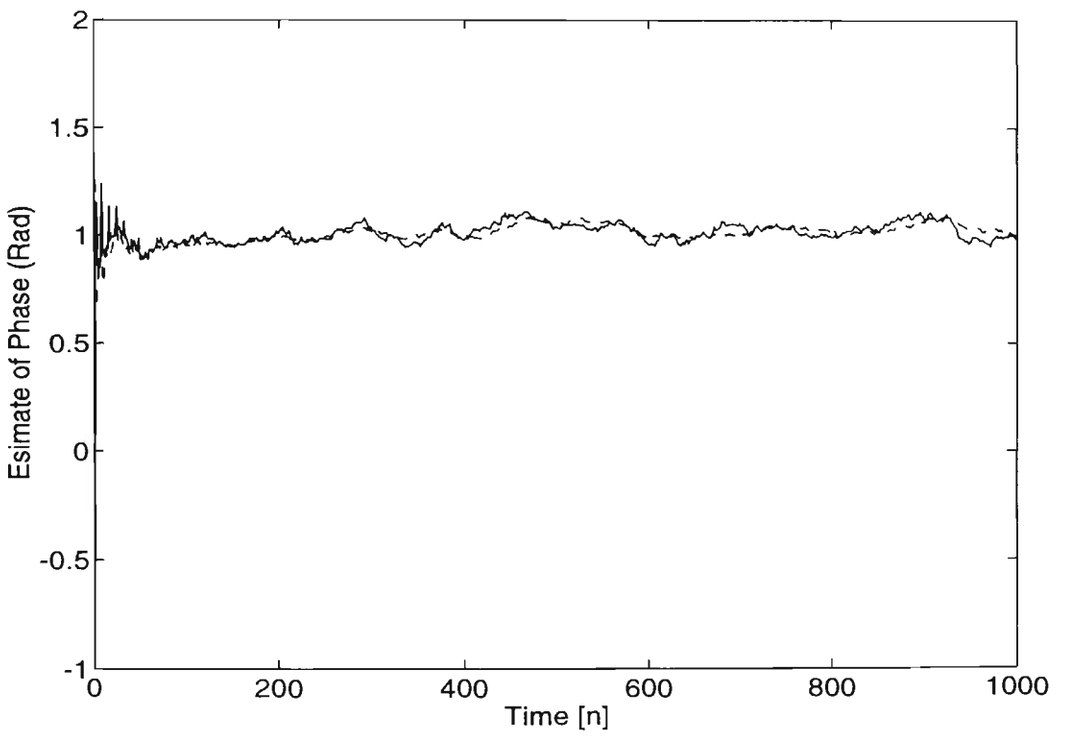

(b)

Figure 2.7: Sliding computation of the (a) amplitude and (b) phase of the fundamental component corrupted by zero mean, unit variance white noise using NFT (dashed lines, $N = 128$) and CNFT (solid lines, $N = 16$ and $\beta = 0.7$).

Based on 50 independent experiments, the average and the standard deviation of the estimated amplitudes and phases of the fundamental and subharmonics were obtained. In the NFT case, the estimates were computed after the 256th output sample. For the CNFT approach, the 256th and 1024th output samples were chosen for β equal to 0.7 and 0.9, respectively. The amplitude and phase estimate results are given in Tables 2.2 and 2.3.

		CNFT $N=16$		NFT
		β =0.7	β =0.9	$N=128$
Amplitude (Average)	$\hat{C}_1$	4.0156	3.9889	4.0174
	$\hat{C}_2$	1.9901	1.9826	1.9946
	$\hat{C}_3$	1.0168	0.9987	1.0389
Amplitude (STD)	$\hat{C}_1$	0.1145	0.0512	0.1250
	$\hat{C}_2$	0.1054	0.0622	0.1311
	$\hat{C}_3$	0.1325	0.0567	0.1461

Table 2.2: The average and standard deviation of the amplitude estimates of the fundamental and subharmonics components.

		CNFT $N=16$		NFT
		β =0.7	β =0.9	$N=128$
Phase (Average)	$\hat{\phi}_1$	1.0010	0.9988	1.0016
	$\hat{\phi}_2$	0.9884	1.0020	0.9748
	$\hat{\phi}_3$	1.0176	0.9868	1.0192
Phase (STD)	$\hat{\phi}_1$	0.0280	0.0151	0.0308
	$\hat{\phi}_2$	0.0567	0.0205	0.0639
	$\hat{\phi}_3$	0.1193	0.0700	0.1292

Table 2.3: The average and standard deviation of the phase estimates of the fundamental and subharmonics components.

From these tables, it is evident that as the bandwidth decreases (β increases), the accuracy of the estimates improves. Clearly the proposed method provides the necessary bandwidth control (β) to reduce output noise effectively without increasing the order of the FIR comb filter. Since the kth component appears with zero phase shift at the output of the kth branch, by adding all the outputs, the harmonic signal will be retrieved in time domain if so desired.

Example 2. Nonharmonic signal. As an example we will apply the proposed approach for the task of computing the coefficients of a noise corrupted DTMF signal. The DTMF signals are composed of two frequencies which are selected from four low frequencies (f_l) and four high frequencies (f_h). In this case, f_l and f_h were chosen to be equal to $941\,Hz$ and $1209\,Hz$, respectively and the sampling frequency was selected as $4000\,Hz$. The amplitudes of components, f_l and f_h were both set to a magnitude of 3 while the corresponding phases were assumed to be 0.4 (*rad*), and 1.2 (*rad*), respectively. The given DTMF tones were buried in a zero mean unit variance white noise sequence. In this example the input frequencies are mutually prime factors. In other words, the greatest common measure frequency of two frequencies is equal to $1\,Hz$. Therefore, if the NFT bandpass filter is used for estimation and retrieval purposes a $1\,Hz$ resolution is needed which means that a comb filter with an order of 4000 is required. As a result a large amount of memory storage and computational burden would be required. Such a situation also applies to the conventional Goertzel algorithm which is equivalent to the NFT algorithm. The proposed constrained second order IIR bandpass filter given in Section 2.3 was used and g was chosen to be equal to 0.995 in order to achieve the required resolution. Using Equation (2.9), the centre frequencies of the second order IIR bandpass filter (h_1 and h_2) were set equal to -0.185 and 0.645, respectively. The results of the amplitude and phase estimates are depicted in Figure 2.8.

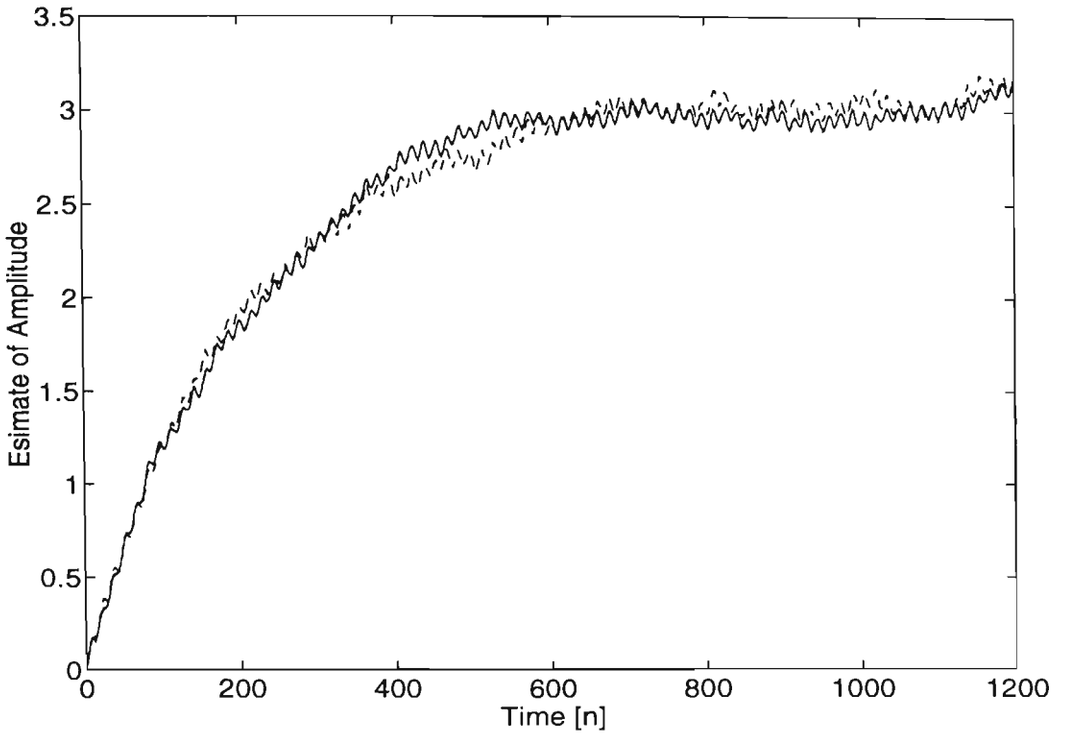

(a)

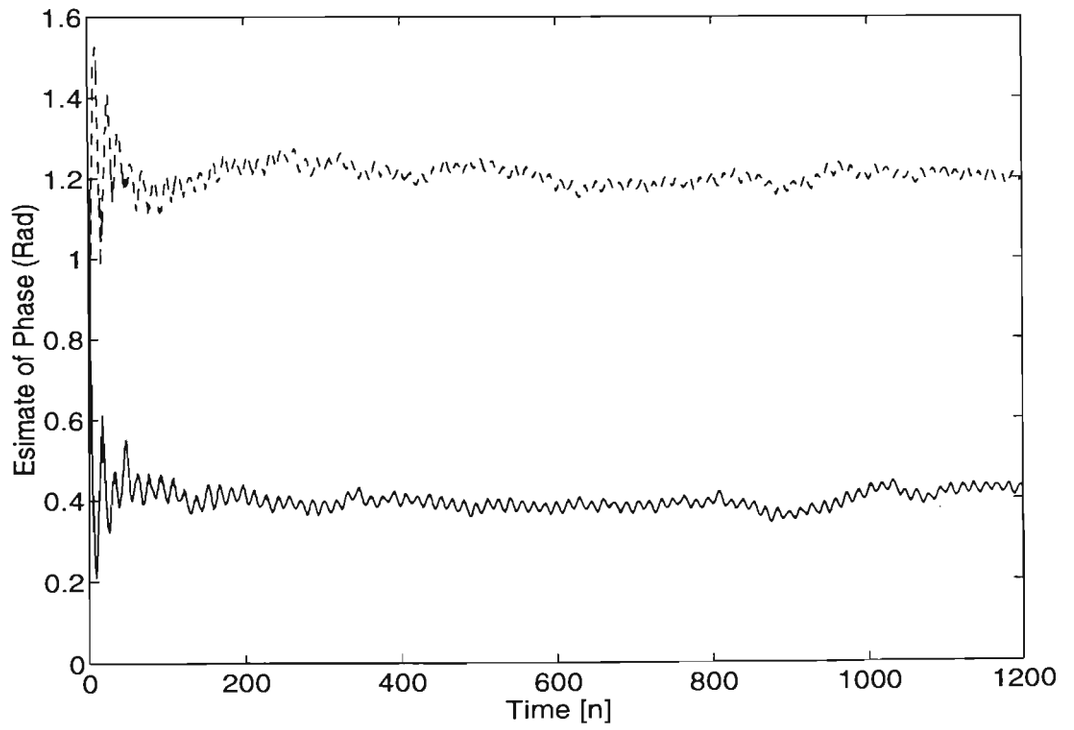

(b)

Figure 2.8: Sliding computation of the (a) amplitude and (b) phase of the nonharmonic components for the DTMF signal using a constrained second order IIR bandpass filter ($g = 0.995$), ($C_l = C_h = 3$ and $\phi_l = 0.4$ (rad), $\phi_h = 1.2$ (rad)).

From Figure 2.8, it is seen that the required number of samples for accurate amplitude estimation is approximately equal to 600 samples while for phase estimation it is only 100 samples. Even though the proposed bandpass filter parametisation needs two more multiplications per output sample than does the NFT structure, this is compensated by the fact that it requires a much smaller number of data samples to obtain the estimates. In fact, the proposed approach requires approximately one sixth of the number of samples needed by the NFT algorithm.

To compare and evaluate the accuracy of both methods, 50 independent trials were carried out and the mean and standard deviation of the amplitude and phase estimates were established for the low frequency component (f_l). In addition we also considered the scenario where two different values of g (i.e., $g = 0.99$ and $g = 0.995$) were used. The phase and amplitude estimates were taken after the 300th and 600th output samples (the appropriate output sample can be obtained using Equation (2.41)). The results are shown in Table 2.4 which also includes the required acquisition time and number of multiplications.

		2nd order BP filter		NFT
		g =0.99	g =0.995	N =4000
Amplitude $\hat{C}_l$	Ave.	2.8847	2.9371	2.9915
	Std	0.0964	0.0757	0.0202
Phase $\hat{\phi}_l$	Ave.	0.7816	0.7878	0.8026
	Std	0.0357	0.0239	0.0061
Acquisition Time		N_{acq} =300	N_{acq} =600	N_{acq} =4000
Number of Multiplications		3(N_{acq}+2) = 906	3(N_{acq}+2) = 1206	N_{acq}+2=4002

Table 2.4: The average and standard deviation of phase and amplitude estimates using NFT algorithm and the constrained second order bandpass filter.

In fact, the estimates were obtained by evaluating the algorithm (Equations (2.20), (2.36) and (2.37)) at a specific sampling time when the bandpass filters transient behaviour had settled. As stated previously, the NFT method requires a minimum of 4000 samples. Referring to the Table 2.4, it is evident that the NFT algorithm provides more accurate estimates. It is important to note that the accuracy of the proposed method can be increased by reducing the bandwidth of the bandpass filter which leads to an increase in the acquisition time. Hence, a compromise needs to be reached in practice.

2.6 Conclusion

Sliding algorithms for estimating Fourier coefficients of noise corrupted harmonic (equally spaced frequencies) and nonharmonic (arbitrary spaced frequencies) signals with known frequencies were presented.

The FIR notch filter within the NFT filter bank structure was replaced by a constrained IIR notch filter (hence, the name CNFT). This modification provides bandwidth controlled bandpass filters whose centre frequencies are equally distributed over the entire frequency band. Sliding algorithms were also developed for both NFT and CNFT methods to estimate the coefficient of enhanced sinusoid at the output of each bandpass filter. Since the resonant frequencies of the CNFT filter bank are placed at equal intervals in the frequency spectrum, it is most suitable for the enhancement and characterisation of harmonic signals. The bandwidth control parameter in the CNFT method, is used to achieve the required enhancement without increasing the order of the filter which is necessary in the NFT method. Consequently, the CNFT structure requires less memory requirements when compared with the NFT structure.

To implement individual spectral bins at arbitrary frequencies, a second order IIR bandpass filter was proposed. The centre frequency and bandwidth of the proposed bandpass filter can be easily controlled by two independent parameters. The desired spectral bin is realised by adjusting the centre frequency of the bandpass filter while the bandwidth control facility is used to obtain the required resolution and enhancement. This approach also substantially reduces the memory storage requirement when compared to the NFT method.

The issue of the required acquisition time versus frequency resolution was discussed. In the proposed technique, there is a trade off between the required acquisition time and the desired frequency resolution. This means that an increase in frequency resolution results in an increase in acquisition time. The proposed approach; however, provides faster acquisition time than the NFT method. This was particularly demonstrated for the situations where the input frequencies have the greatest common factor equal to 1Hz. This advantage is due to the fact that the centre frequency of the given bandpass filter can be arbitrarily set which is in direct contrast with the DFT and NFT filter bank structures whose resonant frequencies are equally spaced. Simulation tests for the Fourier coefficient estimation of typical harmonic and Dual-Tone Multifrequency (DTMF) signals were conducted to evaluated the relative performance of the proposed approaches with the NFT method.

CHAPTER 3:

A Generalised Frequency Sampling Filter Bank

3.1 Introduction

Spectral estimation using bandpass filtering is affected not only by the broadband noise spectrum, but also by the other sinusoidal components in the input signal. The accuracy of the estimates decreases if the unwanted spectral lines are observed at the output of the bandpass filter (spectral leakage). In the previous chapter, the effects of both the noise and leakage were reduced by using a bandwidth control parameter introduced in the bandpass filter parametisation. In this chapter another bandwidth controlled filter bank is developed which provides resonant frequencies as well as nulls at arbitrary spectral locations. As opposed to the conventional FS filter bank whose resonant frequencies and nulls are located at equally spaced points in the frequency spectrum, the proposed filter bank is referred to as Generalised Frequency Sampling (GFS) structure. The bandwidth control parameter is used to reduce the effect of noise while nulls can be placed at the frequency locations of other spectral components to effectively minimise the leakage.

A new derivation for the GFS filter bank based on the conventional LMS spectral analyser is derived. The structure of the LMS spectral analyser is shown in Figure 3.1. It is comprised of a set of sinusoids whose frequencies are equal to those of the input frequencies as reference signals. The adaptive LMS algorithm

is employed to match the weighted sum of the sinusoidal functions to the input signal. Once convergence takes place, the phases and amplitudes of input sinusoids are obtained from the adaptive weights. The relationship between LMS algorithm and the Discrete Fourier Transform (DFT) has been established by Widrow *et al.* (1987). It has been shown that the LMS algorithm can be used to determine the Fourier coefficients of the input signal in a sliding fashion. In this case, the reference signal is a set of sinusoids whose frequencies are equally distributed in frequency domain.

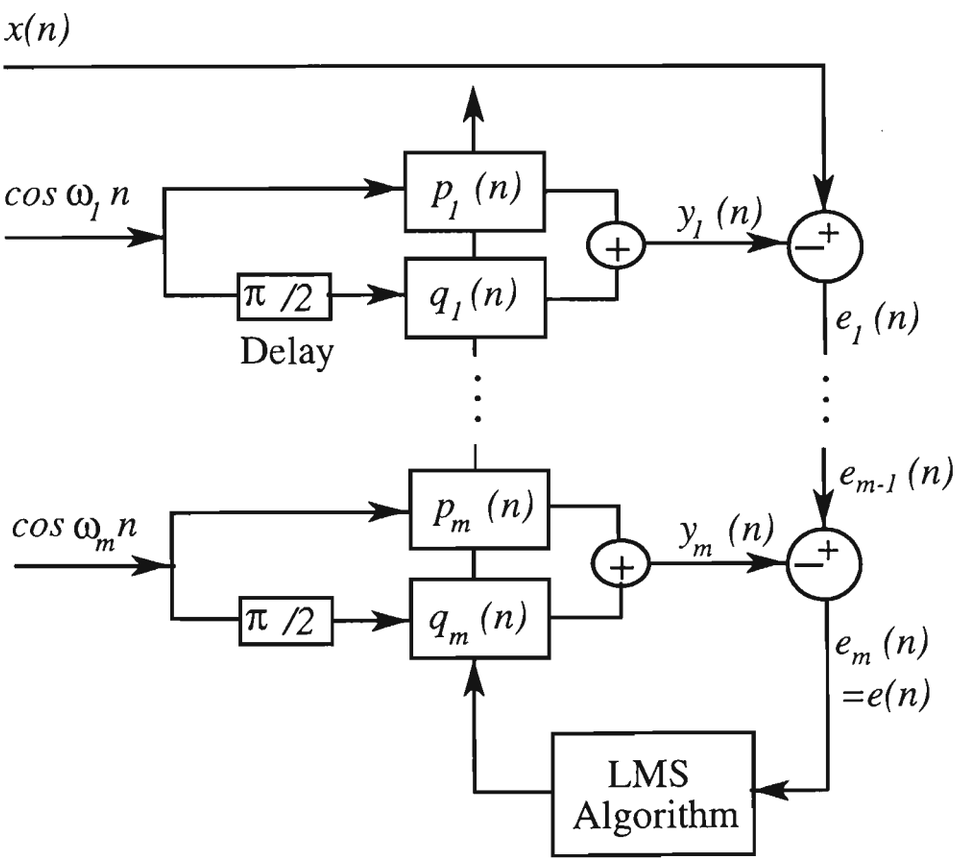

Figure 3.1: LMS spectrum analyser.

The equivalent filter transfer function from input signal, $x(n)$, to the output of each adaptive weight, $y_i(n)$, in the LMS algorithm is obtained. The resulting structure is equivalent to an IIR filter bank. The z-transform method is employed to find the parametisation of the bandpass filter at the output of each adaptive weight. Our method is similar to that used by Widrow *et al.* (1975) whereby an equivalent notch filter was obtained for adaptive noise cancellation scheme

applied to a single sinusoidal interference case. It will be shown that this method results in identical structure as suggested by Padmanabhan and Martin (1987). Different approaches but similar parametisation are also found in [McGee (1989a, 1989b), Peceli (1989)].

The important feature of the resulting filter bank is that its resonant frequencies and nulls can be arbitrarily set. In other words, using this approach, bandpass filters can be realised with the desired centre frequencies as well as arbitrary null positions. The GFS filter bank is proposed for the enhancement and characterisation of sinusoidal components buried in noise. At the resonant frequency, the phase and gain characteristics associated with each bandpass filter is equal to zero and unity, respectively. Therefore, the enhanced component is available at the output with zero phase shift and with the same amplitude as the input sinusoid. As a result, the sliding CNFT algorithm can be employed to estimate the coefficients associated with each sinusoid. It is expected that the resulting estimates will be more accurate than those obtained in Chapter 2. In Chapter 2, the leakage was reduced by decreasing the bandwidth of the bandpass filter. Unfortunately, this resulted in an undesirable increase in acquisition time. Assuming that both methods (i.e. the GFS bandpass filter and the second order IIR bandpass filter) have equal bandwidth, the effect of the leakage at the output of GFS filter bank is less than that of the second order IIR bandpass filter. This is due to the fact that the nulls of the GFS bandpass filter can be placed at those frequency locations other than the one of interest thus minimising the effect of leakage. Further, it is shown that the GFS filter bank together with the sliding CNFT algorithm is computationally more efficient when compared to the conventional LMS spectrum analyser. To evaluate the performance of both methods, simulation results are conducted to compute the phases and amplitudes of Dual Tone Multifrequency (DTMF) signals buried in noise.

This chapter is organised as follows: In Section 3.2 the GFS filter bank is derived based on the LMS spectrum analyser. The sliding CNFT algorithm is applied to the GFS filter bank and is given in Section 3.3. Simulation results are included in Sections 3.4 and finally Section 3.4 concludes the chapter.

3.2 Generalised Frequency Sampling Filter Bank

Consider Figure 3.1 and further assume that the input frequency locations are known in advance. Each of the reference sinusoidal signals are generated and passed through a two adaptive weight structure. The outputs of the adaptive weights are subtracted from the input signal to establish the error signal. This error signal is then minimised by the LMS algorithm. The transfer function from input, $x(n)$, to the error signal, $e(n)$, is equivalent to an IIR notch filter, while the transfer function from input to the output of each adaptive weight, $y_k(n)$, is equivalent to an IIR bandpass filter. To prove this, assume that the input sequence is an impulse function as follows:

$$x(n) = \delta(n) \tag{3.1}$$

The adaptive weights are updated by using the LMS algorithm and are given by [Widrow and Stearns (1985)]:

$$p_k(n+1) = p_k(n) - 2\mu e(n)\frac{\partial e(n)}{\partial p_k(n)} \tag{3.2a}$$

$$q_k(n+1) = q_k(n) - 2\mu e(n)\frac{\partial e(n)}{\partial q_k(n)} \tag{3.2b}$$

Where μ is the adaptive step size factor which controls the convergence rate of the algorithm. The error signal is written as:

$$e(n) = \delta(n) - \sum_{k=1}^{m} p_k(n)\cos\omega_k n + q_k(n)\sin\omega_k n \tag{3.3}$$

Taking the derivative of the error signal with respect to the adaptive weights, we have:

$$\frac{\partial e(n)}{\partial p_k(n)} = -\cos\omega_k n \tag{3.4a}$$

$$\frac{\partial e(n)}{\partial q_k(n)} = -\sin\omega_k n \tag{3.4b}$$

Substituting Equations (3.4) into Equations (3.2) and applying Euler's formula, we obtain:

$$p_k(n+1) = p_k(n) + \mu e(n)e^{j\omega_k n} + \mu e(n)e^{-j\omega_k n} \tag{3.5}$$

$$q_k(n+1) = q_k(n) + \frac{\mu}{j}e(n)e^{j\omega_k n} - \frac{\mu}{j}e(n)e^{-j\omega_k n} \tag{3.6}$$

Equation (3.3) can also be written as:

$$e(n) = \delta(n) - \sum_{k=1}^{m}[\frac{p_k(n)}{2}e^{j\omega_k n} + \frac{p_k(n)}{2}e^{-j\omega_k n} + \frac{q_k(n)}{2j}e^{j\omega_k n} - \frac{q_k(n)}{2j}e^{-j\omega_k n}] \tag{3.7}$$

Taking z-transform of Equations (3.5) and (3.6) and noting that:

$$e^{-j\omega n}f(n) \xleftrightarrow{z\text{-}Transform} F(e^{j\omega}z) \qquad n \geq 0 \tag{3.8}$$

we have:

$$P_k(z) = \mu\frac{E(e^{-j\omega_k}z) + E(e^{j\omega_k}z)}{z-1} \tag{3.9}$$

$$Q_k(z) = \frac{\mu}{j}\frac{E(e^{-j\omega_k}z) - E(e^{j\omega_k}z)}{z-1} \tag{3.10}$$

The z-Transform of Equation (3.7) also results in:

$$E(z) = 1 - \frac{1}{2}\sum_{k=1}^{m}\{[P_k(e^{-j\omega_k}z) + P_k(e^{j\omega_k}z)] - j[Q_k(e^{-j\omega_k}z) - Q_k(e^{j\omega_k}z)]\} \tag{3.11}$$

Substituting Equations (3.9) and (3.10) into Equation (3.11) and after some manipulations, the transfer function between the input and error signal is given by:

$$E(z) = \frac{1}{1 - 2\mu\sum_{k=1}^{m}H_r^k(z)} \tag{3.12}$$

where $H_r^k(z)$ is a second order digital resonator whose transfer function is:

$$H_r^k(z) = \frac{z^{-2} - \cos\omega_k z^{-1}}{1 - 2\cos\omega_k z^{-1} + z^{-2}} \tag{3.13}$$

Note that the transfer function as defined by Equation (3.12) yields zero transmission at the input frequency locations. In other words, the structure becomes equivalent to a $2m$ order IIR notch filter where m is equal to the number of input sinusoids. The enhanced input sinusoids are available at the outputs of the adaptive weights ($y_k(n)$). In order to obtain the transfer function between input, $x(n)$, and the output of the adaptive weights, $y_k(n)$, the error signals, $e_k(n)$ are expressed as follows (see Figure 3.1):

$$e_1(n) = \delta(n) - p_1(n)\cos\omega_1 n - q_1(n)\sin\omega_1 n \tag{3.14}$$

$$e_k(n) = e_{k-1}(n) - p_k(n)\cos\omega_k n - q_k(n)\sin\omega_k n \tag{3.15}$$

where $k = 2,\ldots,m$

Using Euler's Formula and applying Equation (3.8) to Equations (3.14) and (3.15), we obtain:

$$E_1(z) = 1 - \frac{1}{2}[P_1(e^{-j\omega_1}z) + P_1(e^{j\omega_1}z)] - \frac{1}{2j}[Q_1(e^{-j\omega_1}z) - Q_1(e^{j\omega_1}z)] \tag{3.16}$$

$$E_k(z) = E_{k-1}(z) - \frac{1}{2}[P_k(e^{-j\omega_k}z) + P_k(e^{j\omega_k}z)] - \frac{1}{2j}[Q_k(e^{-j\omega_k}z) - Q_k(e^{j\omega_k}z)] \tag{3.17}$$

Substituting Equations (3.9) and (3.10) into Equation (3.16) and (3.17) and after some straightforward manipulations it can be shown that:

$$E_1(z) = 1 + 2\mu\frac{z^{-2} - z^{-1}\cos\omega_1}{1 - 2\cos\omega_1 z^{-1} + z^{-2}}E(z) \tag{3.18}$$

and

$$E_k(z) = E_{k-1}(z) + 2\mu\frac{z^{-2} - z^{-1}\cos\omega_k}{1 - 2\cos\omega_k z + z^{-2}}E(z) \tag{3.19}$$

where $k = 2,\ldots,m$

From Figure 3.1, it is clear that:

$$Y_1(z) = 1 - E_1(z) \tag{3.20}$$

$$Y_k(z) = E_{k-1}(z) - E_k(z) \quad \text{where } k = 2,\ldots,m \tag{3.21}$$

$y_k(n)$ is the signal at the output of the kth bandpass filter. Substituting Equation (3.19) into Equation (3.21) and considering the fact that the input sequence is an impulse function, we get:

$$H_{BP}^{k}(z) = Y_k(z) = -2\mu \frac{z^{-2} - \cos\omega_k z^{-1}}{1 - 2\cos\omega_k z^{-1} + z^{-2}} E(z) \tag{3.22}$$

Based on Equations (3.12) and (3.22), the equivalent filtering structure is obtained and shown in Figure 3.2.

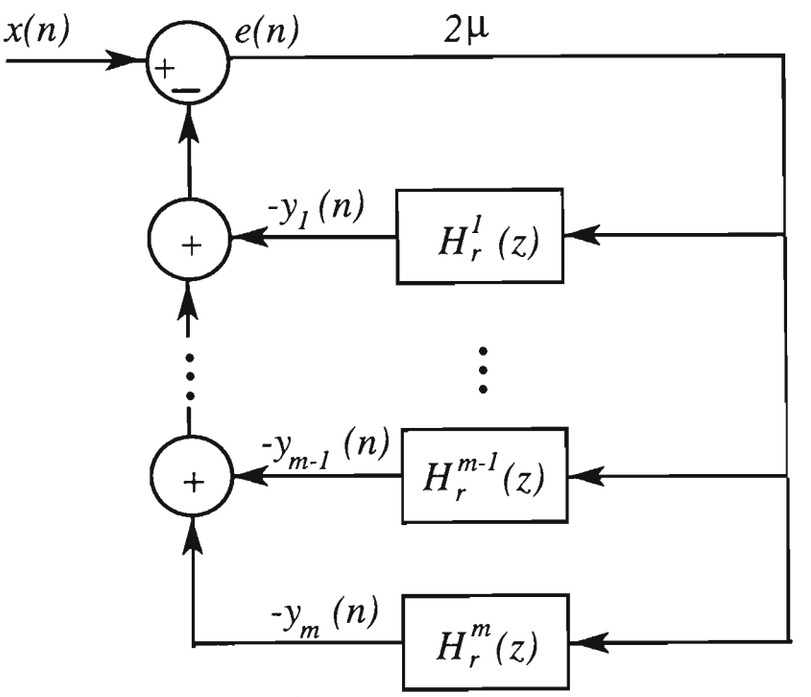

Figure 3.2: Equivalent filter bank structure for LMS spectrum analyser.

It is interesting to note that we have arrived at a similar structure to that proposed by Padmanabhan and Martin (1987) as a resonator-based filter bank. Padmanabhan and Martin (1987) derived this structure by using a singly terminated $L-C$ ladder analogue filter. Note that the phase and magnitude of each bandpass filter at resonant frequency are equal to zero and one, respectively. Each bandpass filter also has zero transmission at the other frequencies of the input signal. This is an important property which effectively eliminates the

contribution of other unwanted components at the output of the bandpass filter. A plot of magnitude response of the filter bank for $m=3$ is shown in Figure 3.3. Note that the bandwidth of each bandpass filter is controlled by parameter μ. The magnitude responses of the bandpass filters for different values of μ are also depicted in Figure 3.4. For a single sinusoid case we have:

$$E(z)=\frac{1}{1-2\mu\left(\frac{z^{-2}-\cos\omega_1 z^{-1}}{1-2\cos\omega_1 z+z^{-2}}\right)} \tag{3.23}$$

or equivalently:

$$E(z)=\frac{1-2\cos\omega_1 z^{-1}+z^{-2}}{1-2(1-\mu)\cos\omega_1 z^{-1}+(1-2\mu)z^{-2}} \tag{3.24}$$

and $H_{BP}(z)$ is given by:

$$H_{BP}(z)=1-E(z)=2\mu\frac{\cos\omega_1 z^{-1}-z^{-2}}{1-2(1-\mu)\cos\omega_1 z^{-1}+(1-2\mu)z^{-2}} \tag{3.25}$$

Equations (3.24) and (3.25) are consistent with those reported in Widrow *et al.* (1975) where the equivalent filter was derived for a single sinusoid interference cancellation scheme. The Bandwidth (BW) of the bandpass filter, Equation (3.25), is approximately given by [Widrow *et al.* (1975)]:

$$BW\approx\frac{\mu}{\pi} \tag{3.26}$$

Note that this approach includes the step size factor associated with the LMS algorithm in the IIR bandpass filter parametisation. In the LMS algorithm, as the value of μ decreases, the acquisition time increases while providing more accurate estimates. From the filter bank point of view, small values of μ result in narrow bandwidth which means that the acquisition time will be also increased. However, we expect to obtain more accurate estimates due to the fact that the amount of noise at the output of the bandpass filters is reduced.

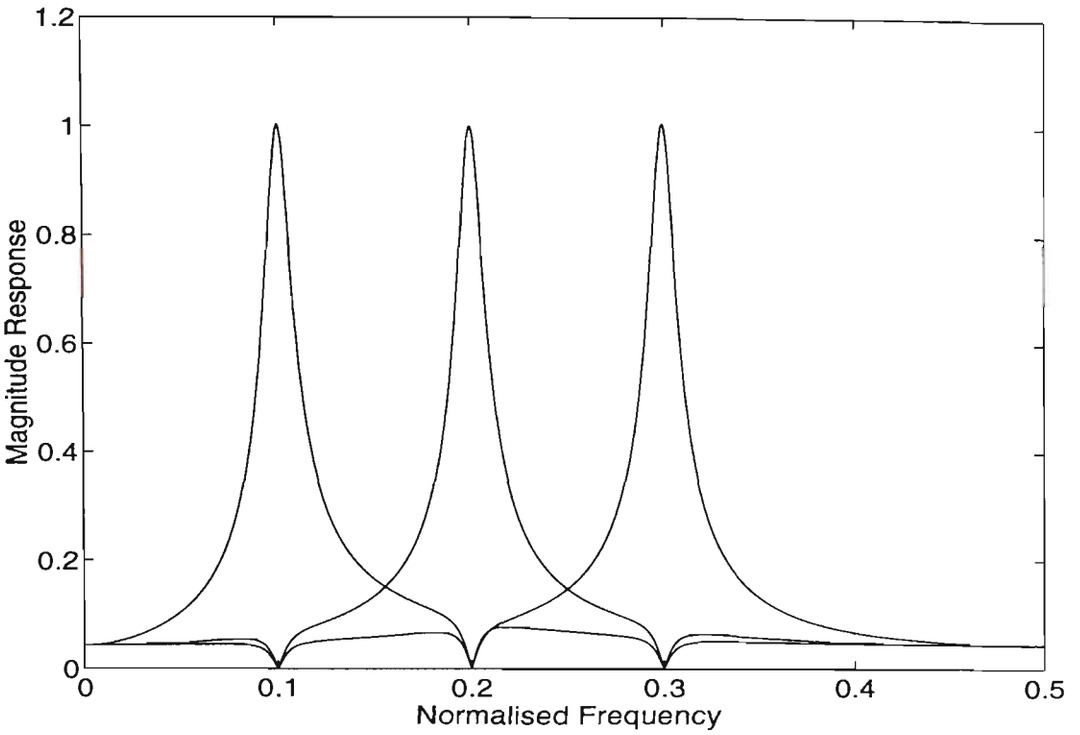

Figure 3.3: Magnitude response of filter bank for $m = 3$, $\mu = 0.05$, and $f_1 = 0.1, f_2 = 0.2, f_3 = 0.3$.

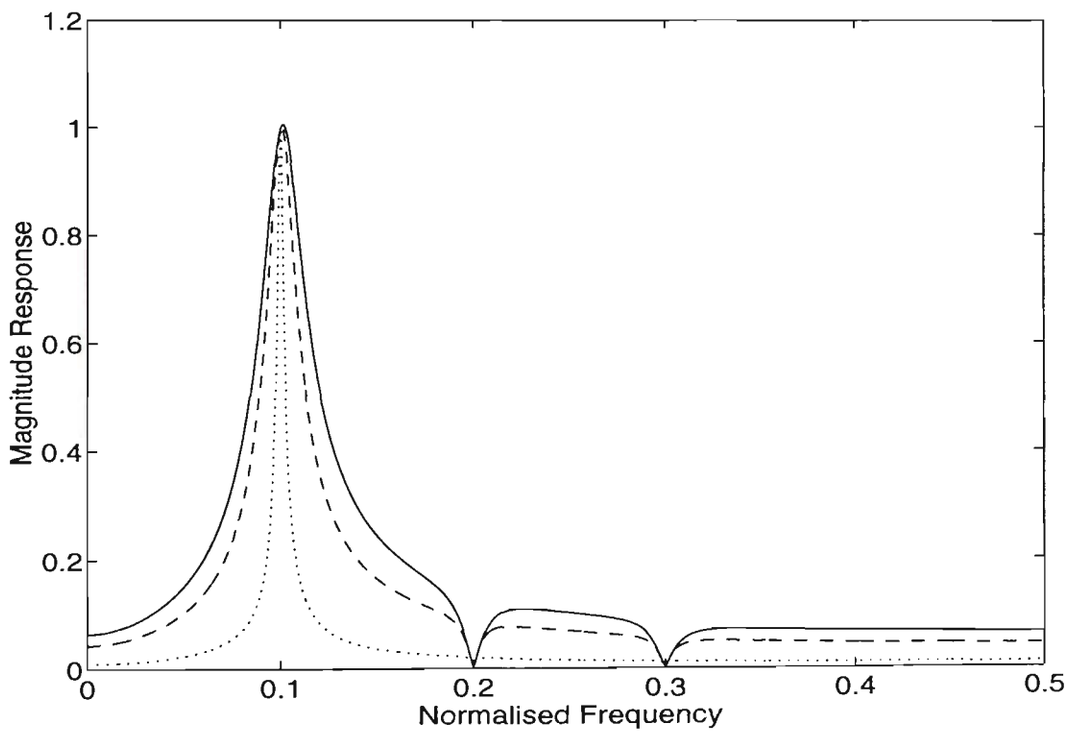

Figure 3.4: Magnitude response of bandpass filters for different values of $\mu = 0.08$ (solid line), $\mu = 0.05$ (dashed line), $\mu = 0.01$ (dotted line).

For a single sinusoid case, the LMS algorithm provides guaranteed convergence provided μ is less than unity [Widrow and Stearns (1985)]. This is particularly interesting since the IIR filter parametisation given by Equation (3.25) is also stable when $\mu < 1$. For the multisinusoid case, the necessary convergence conditions of the LMS spectrum analyser is given by [Widrow and Stearns (1985)]:

$$0 < \mu < \frac{1}{Tr(\mathbf{R})} = \frac{1}{N} \tag{3.27}$$

where $Tr(\mathbf{R})$ is the sum of the diagonal elements of the autocorrelation matrix $\mathbf{R}$ for the signal at the input of the adaptive weights. Note that $Tr(\mathbf{R})$ is the sum of the reference sinusoid's powers and therefore is equal to N. The same expression as given by Equation (3.27) was obtained for the stability of the IIR filter bank as reported by Padmanabhan and Martin (1987).

3.3 Sliding CNFT Algorithm Using GFS Filter Bank

In order to obtain a bandpass filter at any arbitrary frequency by using a conventional FS filter bank, it is necessary to increase the order of the comb filter which results in increased memory storage and acquisition time. The GFS filter bank derived in Section 3.2 can be considered as an alternative method for the case when the input sinusoids are arbitrarily distributed in the frequency spectrum. The proposed GFS filter bank can be tuned at the desired frequencies while placing zeros on the other unwanted sinusoidal frequency locations.

As mentioned earlier, the phase and gain of the GFS filter bank at the centre frequency are equal to zero and unity, respectively. Therefore, the sliding CNFT algorithm as proposed in Chapter 2 can be employed to estimate the phase and amplitude of a sinusoid at the output of each bandpass filter. Assume that the input signal is given by:

$$x(n)=\sum_{k=1}^{m} C_k \sin(\omega_k n-\phi_k)=\sum_{k=1}^{m}(a_k \cos\omega_k n+b_k \sin\omega_k n) \tag{3.28}$$

where

$$C_k=\sqrt{a_k^2+b_k^2} \quad \text{and} \quad \phi_k=-\tan^{-1}\frac{a_k}{b_k} \tag{3.29}$$

The signal at the output of the kth bandpass filter is written as:

$$y_k(n)=C_k \sin(\omega_k n-\phi_k)=a_k \cos\omega_k n+b_k \sin\omega_k n \tag{3.30}$$

Evaluating Equation (3.30) at the $(n-1)$th sampling time, we have:

$$y_k(n-1)=a_k \cos\omega_k(n-1)+b_k \sin\omega_k(n-1) \tag{3.31}$$

Solving the resulting two linear Equations (3.30) and (3.31), the following sliding algorithm is derived:

$$A_k(n)=y_k(n)=a_k \cos\omega_k n+b_k \sin\omega_k n \tag{3.32}$$

$$B_k(n)=\frac{-1}{\sin\omega_k}\{y_k(n-1)-\cos\omega_k y_k(n)\}=b_k \cos\omega_k n-a_k \sin\omega_k n \tag{3.33}$$

The two coefficients, a_k and b_k are updated at every sampling time as follows:

$$\begin{bmatrix} a_k(n) \\ b_k(n) \end{bmatrix}=\begin{bmatrix} \cos\omega_k n & -\sin\omega_k n \\ \sin\omega_k n & \cos\omega_k n \end{bmatrix}\begin{bmatrix} A_k(n) \\ B_k(n) \end{bmatrix} \tag{3.34}$$

Note that the GFS filter bank is equivalent to the LMS algorithm. Therefore, the same performance is expected for the acquisition time and accuracy. However, the number of multiplications based on using the sliding CNFT algorithm is less than that in the LMS algorithm (see Figure 3.1). For m sinusoids, the LMS algorithm requires $6m$ multiplications at every sample update. By contrast, the realisation of the GFS filter bank as shown in Figure 3.2, requires $2m+1$ multiplications to compute each sample at the outputs of all bandpass filters. Note that, in the CNFT method, Equations (3.32), (3.33) and (3.34) do not need to be performed at every sample time but rather after the transient time of the filter has elapsed. The performance of both methods are assessed by using simulation tests in the next section.

3.4 Simulation Results

Simulations have been carried out to evaluate the relative performance of both the direct LMS and the CNFT algorithms. The algorithms have been applied for the task of phase and amplitude estimation of Dual-Tone Multifrequency (DTMF) Signal. In this case, f_l and f_h were chosen to be equal to $852Hz$ and $1336Hz$, respectively and the sampling frequency was selected as $4000Hz$. The input signal was corrupted by noise and is expressed as follows:

$$x(n) = \sum_{k=1}^{2} a_k \cos \omega_k n + b_k \sin \omega_k + \nu(n) \qquad (3.34)$$

where $\nu(n)$ is a unit variance, zero mean white noise sequence. The coefficients a_1 and b_1 are both chosen to be equal to 4, while a_2 and b_2 are both set equal to 5. Note that the frequencies are mutually prime factors which means that $1Hz$ resolution is required if conventional DFT or NFT algorithms are used. In other words, to estimate the Fourier coefficients accurately, at least 4000 samples are needed as was the case in simulation studies in Chapter 2.

The GFS bandpass filter together with the sliding CNFT algorithm is used for estimating the sinusoidal coefficients and the results are depicted in Figure 3.5. For comparison purposes, the results of the LMS algorithm are also included. It is seen that both methods have similar acquisition times for the same value for μ as expected. Note that in the CNFT algorithm the initial state of the filters must be set equal to zero. In the LMS algorithm, however, initial values for adaptive weights can be selected arbitrarily. The initial values for the adaptive parameters in the LMS algorithm were chosen to be half of the actual values of the coefficients.

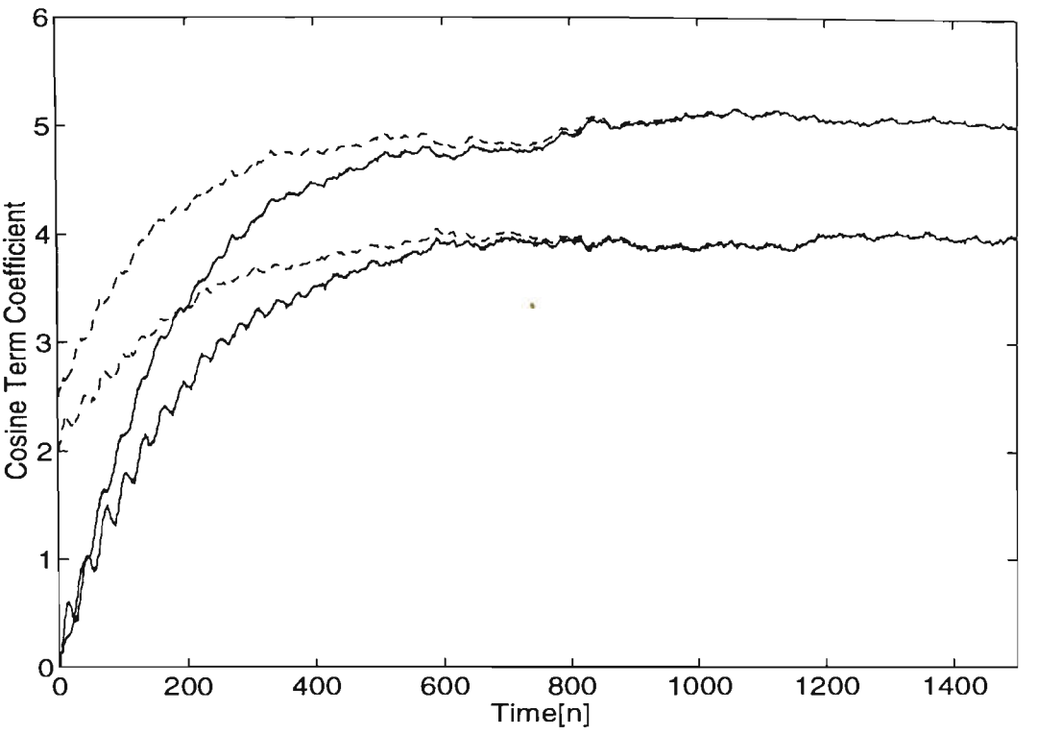

(a)

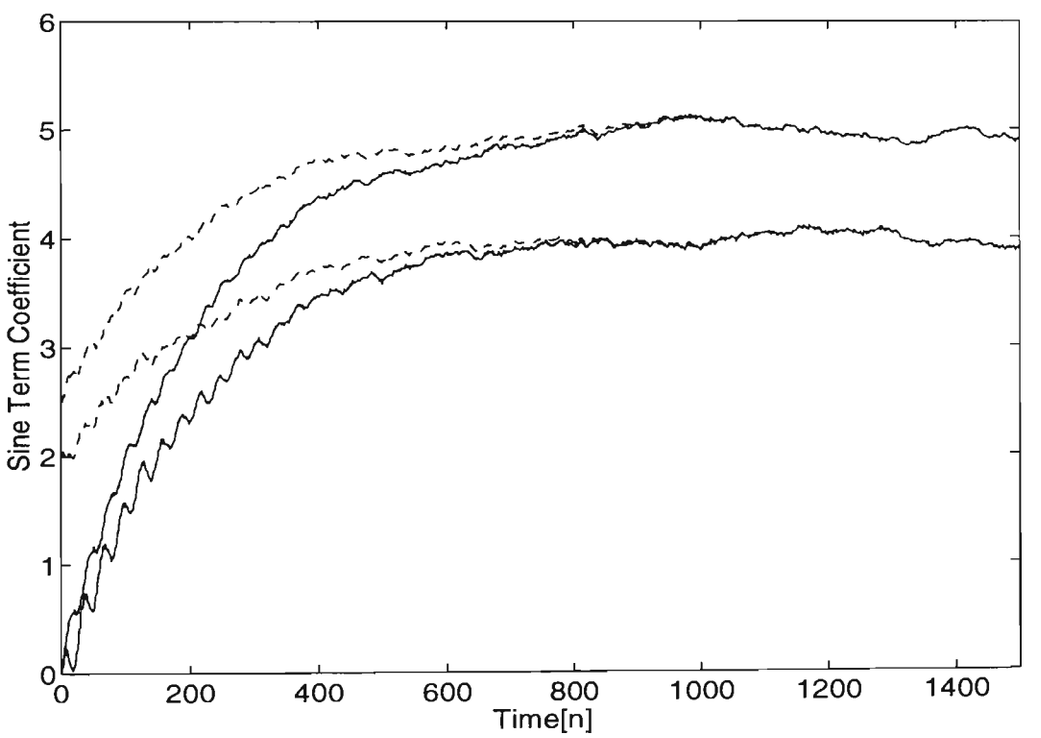

(b)

Figure 3.5: The sliding estimates of (a) cosine and (b) sine terms coefficients using CNFT (solid line) and LMS (dashed line) algorithms, $\mu = 0.01$, $f_1 = 852/4000$, $f_2 = 1336/4000$, $a_1 = 4$, $a_2 = 5$, $b_1 = 4$, $b_2 = 5$.

To compare the accuracy of both methods, the mean and standard deviation of the estimates for both components have been determined based on 100 independent trials. The results are shown in Table 3.1 and 3.2. From the Tables, it is evident that both methods have also similar accuracy characteristics as expected.

		LMS Algorithm	CNFT Algorithm
Average	$\hat{a}_1$	4.0058	3.9844
	$\hat{a}_2$	4.9984	4.9920
STD	$\hat{a}_1$	0.0737	0.0766
	$\hat{a}_2$	0.0685	0.0623

Table 3.1: The average and standard deviation of the cosine term coefficient.

		LMS Algorithm	CNFT Algoritm
Average	$\hat{b}_1$	4.0026	3.9965
	$\hat{b}_2$	5.0013	4.9940
STD	$\hat{b}_1$	0.0680	0.0666
	$\hat{b}_2$	0.0723	0.0775

Table 3.2: The average and standard deviation of the sine term coefficient.

3.5 Conclusion

A new derivation for the equivalent filter bank for the LMS spectrum analyser was presented. The main advantage of the filter is that it provides a bandwidth controlled bandpass filter whose resonant frequencies can be set arbitrarily. Further, the filter bank possesses a very desirable feature in that we can place nulls at any frequency location. Hence, the filter bank is referred to as the Generalised Frequency Sampling (GFS) structure. The bandwidth control parameter is used to reduce the effect of noise while the nulls are placed at those unwanted spectral lines to minimise the leakage.

This filter bank can be used to enhance and characterise sinusoidal signals corrupted by noise. The phase and gain characteristics of the bandpass filter are equal to zero and one, respectively. As a result, if the bandpass filters are tuned at the input frequencies, the enhanced components will be available at the outputs of bandpass filters with zero phase shift and with same amplitude as the input components. The sliding CNFT algorithm as proposed in Chapter 2 was employed to estimate the phase and amplitude of each enhanced sinusoid. It was shown that the GFS filter together with the sliding CNFT algorithm is computationally efficient when compared with the LMS algorithm.

CHAPTER 4:

Resonator-Based Sliding Goertzel Algorithm

4.1 Introduction

In low Signal to Noise Ratio (SNR) conditions, the IIR bandpass filters proposed in Chapters 2 and 3 require a narrow bandwidth thus resulting in increased acquisition time. This chapter presents a sliding Goertzel (SG) algorithm based on a second order digital resonator whose resonant frequency is tuned at the input frequency location. The proposed technique accurately estimates the coefficients of the sinusoidal signal in less than one period of the signal and provides good performance in low SNR conditions.

The leakage problem associated with the DFT can be avoided provided that at least a block length equal to the ratio of sampling frequency to the greatest common factor of the input frequencies is used. Clearly, in situations where the greatest common factor of the input frequencies is small, a large number of samples is required. Note that the same situation exists for the Frequency Sampling (FS) and NFT filter banks as discussed in the previous chapters. For the DFT method, windowing techniques are employed to reduce the detrimental effects of the noise and spectral leakage [Harris (1973), Rife and Vincent (1969)]. These techniques apply a weighting function to the input data before performing the DFT. In fact, the leakage is caused by the discontinuity at the boundaries of the input block. The objective of the windowing function is to

bring data smoothly to zero at the boundaries thus minimising the effect of discontinuity. The windows are designed such that their spectra exhibit a narrow main lobe and low amplitude side lobes. As a result, the effect of noise also reduces. A concise review of data windows and their effect on the estimation of the sinusoidal signals in the presence of noise are found in [Harris (1973), Rife and Vincent (1970)]. Windowing techniques; however, increase the computational burden particularly when the input sinusoidal coefficients need to be updated at every sample time (in the case of sliding measurements).

It is known that the conventional Goertzel algorithm is an efficient implementation of the DFT when the number of coefficients required is small [Oppenheim and Schafer (1989)]. The transfer function of the equivalent Goertzel algorithm filter is defined as follows [Oppenheim and Schafer (1989)]:

$$H_k(z^{-1}) = \frac{1 - e^{j\omega_k} z^{-1}}{1 - 2\cos\omega_k z^{-1} + z^{-2}} \qquad (4.1)$$

where $\omega_k = 2\pi k / N$. The DFT coefficients are obtained as the output of the system after N iterations. The signal flow graph of the transfer function given by Equation (4.1) is shown in Figure 4.1. Note that the Goertzel filter is composed of a recursive part (left hand side of delay elements) and a nonrecursive part (right hand side of the delay elements). The recursive part is a second order digital resonator. The resonant frequency of the resonator is set at equally spaced frequency points; that is, $\omega_k = 2\pi k / N$. In practice, we only compute the recursive part of the filter at every sample update and the nonrecursive part is computed only after the Nth time instant when the Fourier coefficients are to be determined.

Since the Goertzel algorithm is only an efficient realisation of the DFT, it requires the same acquisition time as the DFT. Often a large number of samples

are required which reduces the tracking capability of the Goertzel technique when the parameters of an input sinusoid are time-varying. Further, it increases the possibility of overflow at the output of the Goertzel filter for fixed-point arithmetic implementation [Beraldin and Steenaart (1989)].

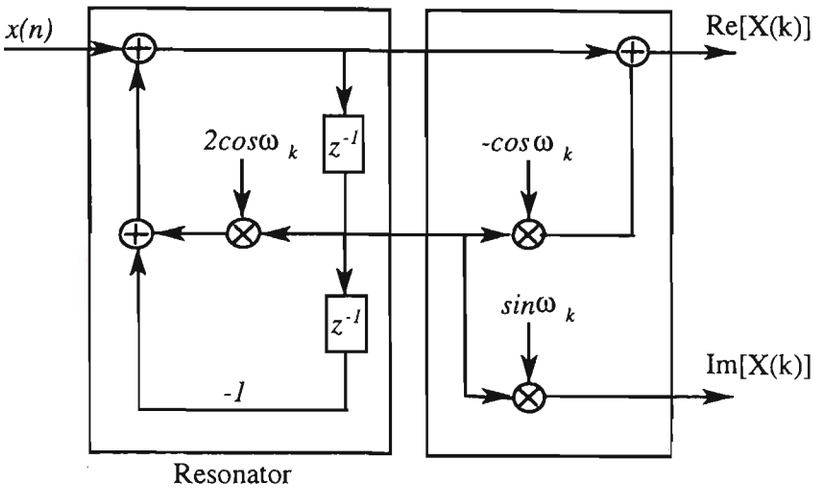

Figure 4.1: Filter realisation of the Goertzel algorithm.

The resolution can be improved by using the modified Goertzel algorithm proposed by Gay *et al.* (1989). In the modified Goertzel algorithm, Equation (4.1) is evaluated at the exact frequency of interest which means that the resonator is set arbitrarily at the angular frequency (ω_k) of the kth component. This modification results in faster acquisition time for estimating the amplitude of the input sinusoid. The modified Goertzel algorithm; however, requires the same acquisition time as the conventional Goertzel algorithm for estimating both the phase and amplitude. In fact, the conventional Goertzel algorithm yields accurate estimates of the sinusoidal parameters provided that the input frequency falls exactly at the resonant frequency of the resonator. Under these circumstances both the conventional and modified Goertzel algorithms become equivalent.

This chapter considers the required acquisition time associated with the DFT technique for estimating coefficients of sinusoidal signals. In order to obtain a

faster acquisition time as well as good performance in low SNR, a new technique is presented. The proposed technique applies an input sinusoid to a second order digital resonator whose resonance frequency is tuned to the exact input frequency. The signal characteristics at the output of the resonator is derived in the time domain by means of the z-Transform. An algorithm similar to the real valued Goertzel algorithm is then established which estimates the phase and amplitude of the input sinusoid for successive values of n. This new approach provides the following features when compared with the conventional and modified Goertzel algorithms. Firstly, it computes accurate sinusoidal coefficients before a complete signal period has elapsed. As a result, faster acquisition time is achieved. Secondly, since the required number of samples is significantly reduced, the possibility of numerical overflows reduces when implemented in hardware with only fixed-point arithmetic [Beraldin and Steenaart (1989)]. Experimental tests are performed to assess the performance of the proposed method and the results are compared with those obtained by the conventional and modified Goertzel algorithms.

This chapter is organised as follows: In Section 4.2, the problem associated with the Goertzel algorithm is discussed and the sliding Goertzel algorithm based on a second order resonator as a solution is proposed in Section 4.3. Simulation tests are included in Section 4.4. Finally, Section 4.5 concludes the chapter.

4.2 Problem Statement

One problem associated with the DFT and Goertzel techniques is that they can not accurately compute the Fourier coefficients until the end of a complete signal period. This means that in order to accurately estimate the phase and amplitude of sinusoidal components of a Multifrequency (MF) signal, the required number of samples should be taken over the whole period of the input sequence. Clearly,

the period of an MF signal depends on the constituent input frequencies. In situations where the input frequencies are prime factor or very closely spaced, a large number of samples will be required which results in an undesirable increase in acquisition time. In the case where the greatest common measure frequency of the input frequencies is equal to Δf Hz, the minimum number of samples ($N_{\min}$) which is required to accurately compute sinusoidal coefficients is given by:

$$N_{\min} = \frac{f_s}{\Delta f} \tag{4.2}$$

where f_s is the sampling frequency (f_s is assumed to be an integer factor of Δf). It is seen that the $N_{\min}$ is inversely proportional to Δf, that is, for small value of Δf a large number of samples are required. To prove Equation (4.2), consider the following composite signal:

$$x(n) = \sum_{i=1}^{m} C_i e^{j\frac{2\pi f_i}{f_s}n} \tag{4.3}$$

where C_i and f_i are amplitude and frequency of the i th complex sinusoidal input component, respectively. The DFT of a sequence $x(n)$ of length N is then given by:

$$X(k) = \sum_{n=0}^{N-1} x(n) e^{-j\frac{2\pi}{N}nk} \qquad 0 \le k \le N-1 \tag{4.4}$$

Substituting Equation (4.3) into Equation (4.4) results in:

$$X(k) = \sum_{i=1}^{m}\sum_{n=0}^{N-1} C_i e^{-j\frac{2\pi}{N}n(k-\frac{Nf_i}{f_s})} \tag{4.5}$$

Rearranging Equation (4.5), we obtain:

$$X(k) = C_l \sum_{n=0}^{N-1} e^{-j\frac{2\pi}{N}n(k-\frac{Nf_l}{f_s})} + \sum_{\substack{i=1,\\ i\neq l}}^{m}\sum_{n=0}^{N-1} C_i e^{-j\frac{2\pi}{N}n(k-\frac{Nf_i}{f_s})} \tag{4.6}$$

To compute the l th component (C_l), the appropriate index k_l is required so that:

$$X(k_l) = NC_l \tag{4.7}$$

This implies that the first summation and the second term in Equation (4.6) must be equal to N and zero respectively. To meet these two requirements we use the fact that [Oppenheim and Schafer (1989)]:

$$\sum_{n=0}^{N-1} e^{-j\frac{2\pi}{N}(k-l)n} = \begin{cases} N & \text{for } k-l = LN \text{ and } L \text{ is an integer} \\ 0 & \text{for other integer values of } l \end{cases} \tag{4.8}$$

In order to satisfy the first requirement we obtain:

$$k_i - \frac{Nf_i}{f_s} = L_i N \quad \text{for } i = 1,\ldots,m \tag{4.9}$$

Since k_i are integer values which lie in the range of $0 \le k_i \le N-1$ and $f_i < f_s$, it is clear that $L_i = 0$. Assuming there exists at least two frequencies (say f_p and f_q) that have no greater common factor than Δf, we have:

$$f_p = M_p \Delta f \;;\; f_q = M_q \Delta f \tag{4.10}$$

where M_p and M_q are integers with the greatest common measure equal to one. From Equations (4.9) and (4.10), we obtain:

$$k_p = \frac{NM_p}{f_s / \Delta f} \;;\; k_q = \frac{NM_q}{f_s / \Delta f} \tag{4.11}$$

and, therefore:

$$\frac{M_p}{M_q} = \frac{k_p}{k_q} \tag{4.12}$$

Since M_p and M_q are integer numbers with prime factor, the indexes k_p and k_q should be equal to the values of M_p and M_q, respectively. Applying this fact to Equation (4.11), the required block length is given as follows:

$$N = \frac{f_s M_p}{f_p} = \frac{f_s}{\Delta f} \tag{4.13}$$

Now we show that the second requirement is satisfied when the block length given by Equation (4.13) is used. From Equation (4.13), we get:

$$\frac{Nf_i}{f_s} = \frac{f_i}{\Delta f} \quad \text{for } i = 1,\ldots,m \tag{4.14}$$

and

$$k_j - \frac{Nf_i}{f_s} = \frac{f_j - f_i}{\Delta f} = r \quad \text{for } i \neq j \tag{4.15}$$

Since the values of frequencies are integer factors of Δf, r is an integer number (less than N) as well. Hence, the second term in Equation (4.6) becomes equal to zero. By evaluating Equation (4.15) for the case of $j = p$ and $i = q$, it can be shown that the block length given by Equation (4.13) is a minimum, that is:

$$k_p - \frac{Nf_q}{f_s} = M_p - \frac{N}{f_s / \Delta f} M_q = r \tag{4.16}$$

Since M_p and M_q are integer numbers with common measure equal to one, the value of r becomes noninteger for $N < (f_s / \Delta f)$. Therefore the second term in Equation (4.6) will not be identical to zero and this ends the proof.

It is assumed when using DFT and Goertzel algorithms that the phase and amplitude must be fixed during each block of data. If the input signal parameters vary within each frame of data, the estimates will be degraded. This means that the required large number of samples given by Equation (4.2) also reduces the tracking capability of the Goertzel technique when the sinusoidal parameters (phase and amplitude) are time varying.

4.3 Resonator-Based Sliding Goertzel Algorithm

This section presents the sliding Goertzel algorithm based on a second order digital resonator. Consider a real valued signal composed of arbitrary frequencies expressed as follows:

$$x(n) = \sum_{k=1}^{m} a_k \cos \omega_k n + b_k \sin \omega_k n + \nu(n) \tag{4.17}$$

where m is the number of components and $\nu(n)$ is the noise component. The task is to compute the coefficients (a_k and b_k) of the sinusoidal components of

$x(n)$. Let us begin by examining the case where the input signal consists of a single component as follows:

$$x_k(n) = a_k \cos\omega_k n + b_k \sin\omega_k n \tag{4.18}$$

Applying $x_k(n)$ to the resonator, in terms of z-Transform, the output, $Y_k(z^{-1})$, is given by:

$$Y_k(z^{-1}) = X_k(z^{-1}) H_r(z^{-1}) \tag{4.19}$$

where $X_k(z^{-1})$ is:

$$X_k(z^{-1}) = \frac{a_k(1-\cos\omega_k z^{-1}) + b_k \sin\omega_k z^{-1}}{1-2\cos\omega_k z^{-1} + z^{-2}} \tag{4.20}$$

$H_r(z^{-1})$ is the transfer function of a second order resonator. Taking the inverse z-Transform of Equation (4.19), it is shown that the output, $y_k(n)$, is given by [see Appendix (C)]:

$$\begin{aligned} y_k(n) = {} & \frac{b_k}{2\sin^2\omega_k}\{(n+2)\cos\omega_k \sin[\omega_k(n+1)] - (n+1)\sin[\omega_k(n+2)]\} \\ & + \frac{a_k}{2\sin^2\omega_k}\{(n+2)\sin\omega_k \sin[\omega_k(n+1)]\} \end{aligned} \tag{4.21}$$

Evaluating Equation (4.21) at nth and $(n-1)$th sampling time and after some manipulations we obtain:

$$\begin{aligned} y_k(n) = {} & \frac{n}{2\sin\omega_k}\{a_k \sin[\omega_k(n+1)] - b_k \cos[\omega_k(n+1)]\} \\ & + \frac{1}{2\sin^2\omega_k}\{2a_k \sin\omega_k \sin[\omega_k(n+1)] + b_k \sin\omega_k n\} \end{aligned} \tag{4.22}$$

and

$$\begin{aligned} y_k(n-1) = {} & \frac{n}{2\sin\omega_k}(a_k \sin\omega_k n - b_k \cos\omega_k n) \\ & + \frac{1}{2\sin^2\omega_k}[(b_k \cos\omega_k + a_k \sin\omega_k)\sin\omega_k n] \end{aligned} \tag{4.23}$$

It is evident that as the number of samples increases, the output values will also increase in magnitude. This is expected since the input frequency is equal to the

resonance frequency of the resonator. For large values of n, the second terms in Equations (4.22) and (4.23) can be ignored and, with some straightforward manipulations, the following equations are obtained:

$$\begin{aligned}\hat{A}_k(n) &= \frac{2(y(n)-y(n-1)\cos\omega_k)}{n} \approx a_k\cos\omega_k n + b_k\sin\omega_k n \\ \hat{B}_k(n) &= -\frac{2\sin\omega_k y(n-1)}{n} \approx -a_k\sin\omega_k n + b_k\cos\omega_k n\end{aligned} \tag{4.24}$$

This algorithm has similar parametisation to the real valued conventional Goertzel algorithm which is now presented in sliding form. In the conventional Goertzel algorithm the left hand side of Equation (4.24) is only evaluated at the Nth sample time and the resonator is tuned at equally spaced frequency points, that is; $\omega_k = 2\pi k / N$. The proposed and modified Goertzel techniques are similar in the sense that both employ a resonator tuned exactly at the input frequency location. The modified Goertzel algorithm takes $\hat{A}_k$ and $\hat{B}_k$ as the estimates of a_k and b_k, respectively. In the proposed algorithm; however, the equality in the right hand side of Equation (4.24) provides a suitable means for updating both the phase and amplitude at every sample time. In other words, by solving the resulting linear Equations (Equations (4.24)), the sliding algorithm for Fourier coefficients are obtained as follows:

$$\begin{bmatrix} a_k(n) \\ b_k(n) \end{bmatrix} \approx \begin{bmatrix} \cos\omega_k n & -\sin\omega_k n \\ \sin\omega_k n & \cos\omega_k n \end{bmatrix} \begin{bmatrix} \hat{A}_k(n) \\ \hat{B}_k(n) \end{bmatrix} \tag{4.25}$$

From Equations (4.24) it can be shown:

$$\hat{A}_k^2(n) + \hat{B}_k^2(n) \approx a_k^2 + b_k^2 \tag{4.26}$$

which means that the amplitude of the sinusoidal component can be updated at every sample time without performing Equation (4.25). The phase associated with each sinusoid is obtained as follows:

$$\phi_k(n) = -\tan^{-1}\left(\frac{a_k(n)}{b_k(n)}\right) \tag{4.27}$$

In the case where the input signal is composed of m sinusoids buried in noise, m resonators are required where each resonator is tuned at a particular input sinusoidal frequency.

At this point it is important to consider the issue of the acquisition time (t_{acq}). Note that although the algorithm provides the sinusoidal coefficients at every sample update, one does not need to evaluate Equations (4.24) and (4.25) at every sample time but only after the transient time has elapsed and the output of the resonator has settled. In other words, accurate estimates of the Fourier coefficients are available after a specific sampling number (say N_{acq}) when the contribution of noise and other components can be ignored at the output of the resonator. Clearly we can write:

$$t_{acq} = N_{acq} / f_s \tag{4.28}$$

In the proposed technique, the acquisition time depends on the power of the noise and the required resolution. In other words, when the input spectral lines are closely spaced or the input signal is heavily corrupted by noise, a greater value for N_{acq} will be required. For situations where the frequency of the input sinusoid is different from the resonance frequency of the resonator the output is given by [see Appendix C]:

$$y(n) = \frac{1}{-2(\cos\omega_r - \cos\omega_k)}\{\frac{-b_k \sin\omega_k}{\sin\omega_r}\sin[\omega_r(n+1)] + b_k \sin[\omega_k(n+1)]\} \tag{4.29}$$

where ω_r is the resonance frequency of the resonator. ω_k and b_k are the frequency and amplitude of the input sinusoid, respectively. From Equation (4.29), it is seen that the output magnitude is inversely proportional to the factor $(\cos(\omega_r) - \cos(\omega_k))$ which means that the contribution of the unwanted component will be greatest when it is close to the desired component. Note that the magnitude of the output component associated with the desired sinusoid linearly increases in time (see Equation (4.22)) while the output component due

to the unwanted frequency is constant. Therefore, the individual sinusoids are quickly separated and enhanced through the resonator. The algorithm also provides a good performance in low SNR. This is due to the fact that the resonator can be considered as an ideal matched filter for sinusoids buried in noise. Since an estimate for phase and amplitude of each sinusoid is available at every sample time, the value of N_{acq} can be selected arbitrarily large to get more accurate results. This is not the case for the conventional Goertzel algorithm. The appropriate selection of N_{acq} and performance of the proposed method will be discussed in more detail by means of simulation tests in the next section. The complete algorithm is summarised in Table 4.1 and the signal flow graph of the resonator and algorithm is shown in Figure 4.2. Note that the sampler in Figure 4.1 has a frequency given by:

$$f_{sampler} = \frac{1}{t_{acq}} = \frac{f_s}{N_{acq}} \tag{4.30}$$

for $k = 1, \ldots, m$:

$$\hat{A}_k(n) = \frac{2(y_k(n) - y_k(n-1)\cos\omega_k)}{n}$$

$$\hat{B}_k(n) = -\frac{2\sin\omega_k y_k(n-1)}{n}$$

$$\begin{bmatrix} a_k(n) \\ b_k(n) \end{bmatrix} \approx \begin{bmatrix} \cos\omega_k n & -\sin\omega_k n \\ \sin\omega_k n & \cos\omega_k n \end{bmatrix} \begin{bmatrix} \hat{A}_k(n) \\ \hat{B}_k(n) \end{bmatrix}$$

$$\hat{A}_k^2(n) + \hat{B}_k^2(n) \approx a_k^2(n) + b_k^2(n)$$

$$\phi_k(n) \approx -\tan^{-1}\left(\frac{a_k(n)}{b_k(n)}\right)$$

Table 4.1: Sliding Goertzel algorithm.

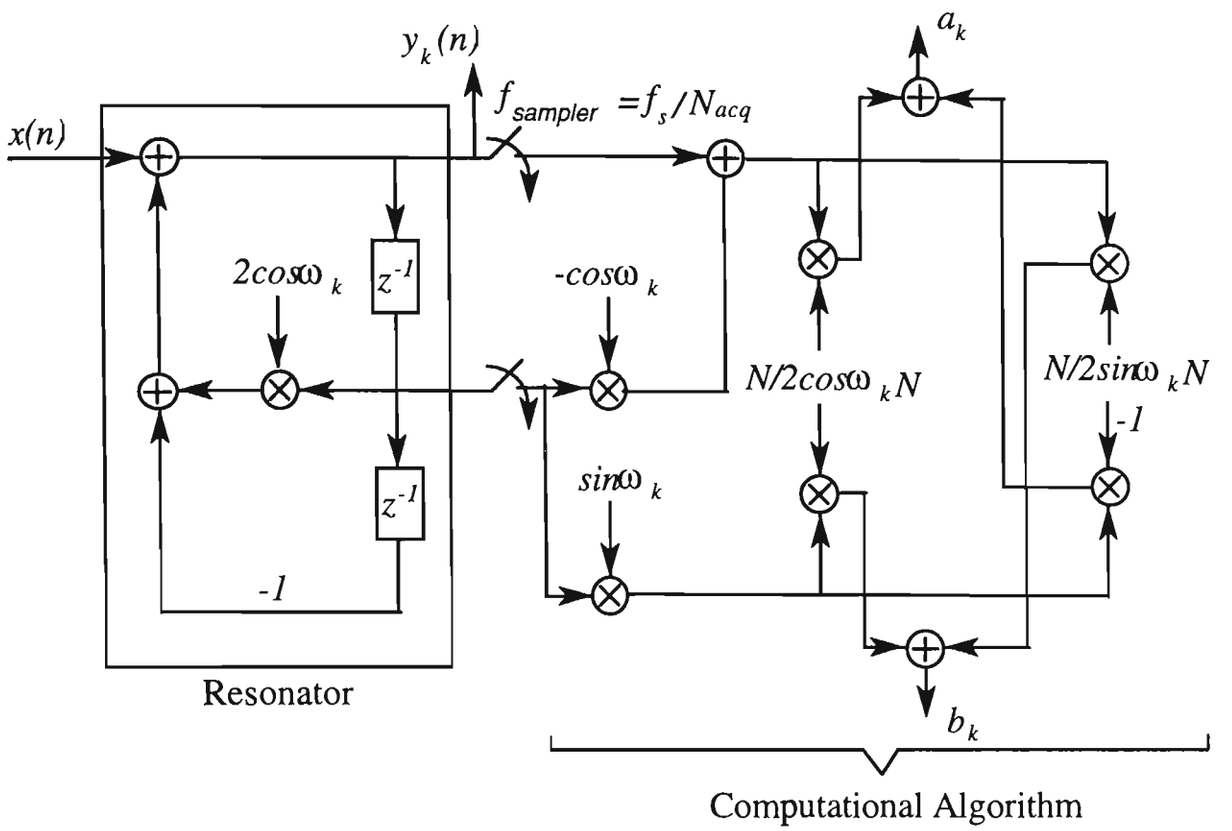

Figure 4.2: Digital resonator and sliding Goertzel algorithm realisation.

4.4 Simulation Results

Simulation tests have been carried out to evaluate the performance of the proposed algorithm. Two cases are considered. First, the algorithm is used for the detection of a DTMF signal. Secondly, the algorithm will estimate the phase and amplitude of a single sinusoid whose parameters are time varying within the successive sequences.

Example 1. The proposed sliding Goertzel algorithm is used for the task of Fourier coefficient estimation of a DTMF signal. Consider the following DTMF signal:

$$x(n) = \sum_{i=l,h} C_i \cos(\frac{2\pi f_i}{f_s} - \phi_i) + \nu(n) \qquad (4.31)$$

where $\upsilon(n)$ is zero mean white noise. The parameters of the signal are given in Table 4.2.

	Low Freq. component	High Freq. component
Freq.	941Hz	1209Hz
Amplitude	2	2
Phase	1(rad)	1(rad)
Sampling Freq.	4000Hz	
SNR	3dB	

Table 4.2: Parameters of DTMF signal.

Figures 4.3 and 4.4 show the resulting trajectories for amplitude and phase estimates of the input signal components, respectively. The amplitude estimates when the frequencies have not been transmitted is also depicted in Figure 4.5. From Figure 4.5 it is clear that the contribution of noise is insignificant after 100 samples when compared with the magnitude of the sinusoidal component.

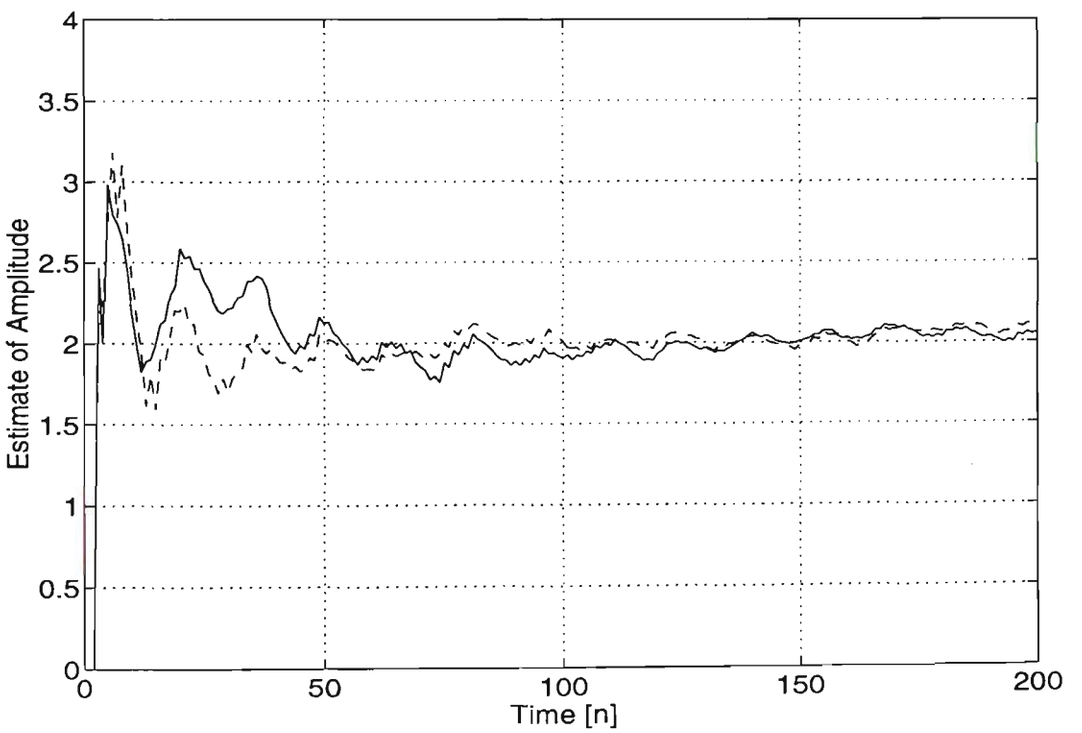

Figure 4.3: Sliding computation of amplitude (C_l, C_h) of the DTMF (low frequency component (Dashed line), high frequency component (Solid Line)).

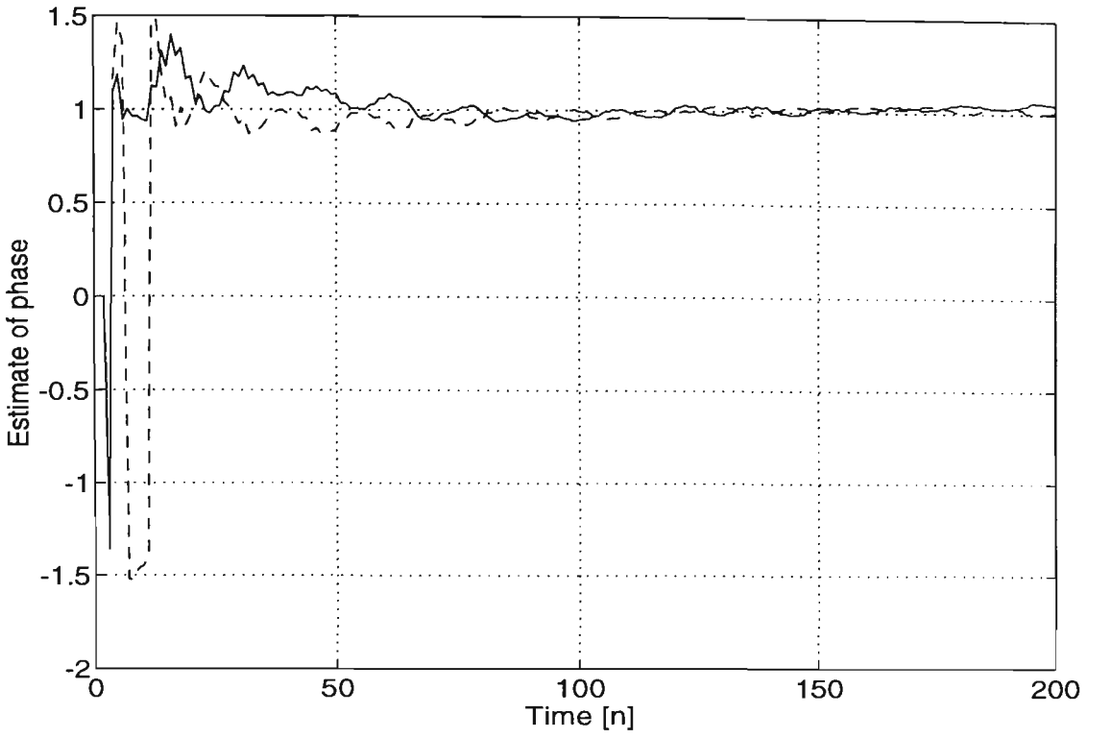

Figure 4.4: Sliding computation of phase (ϕ_l, ϕ_h) of the DTMF (low frequency component (Dashed line), high frequency component (Solid Line)).

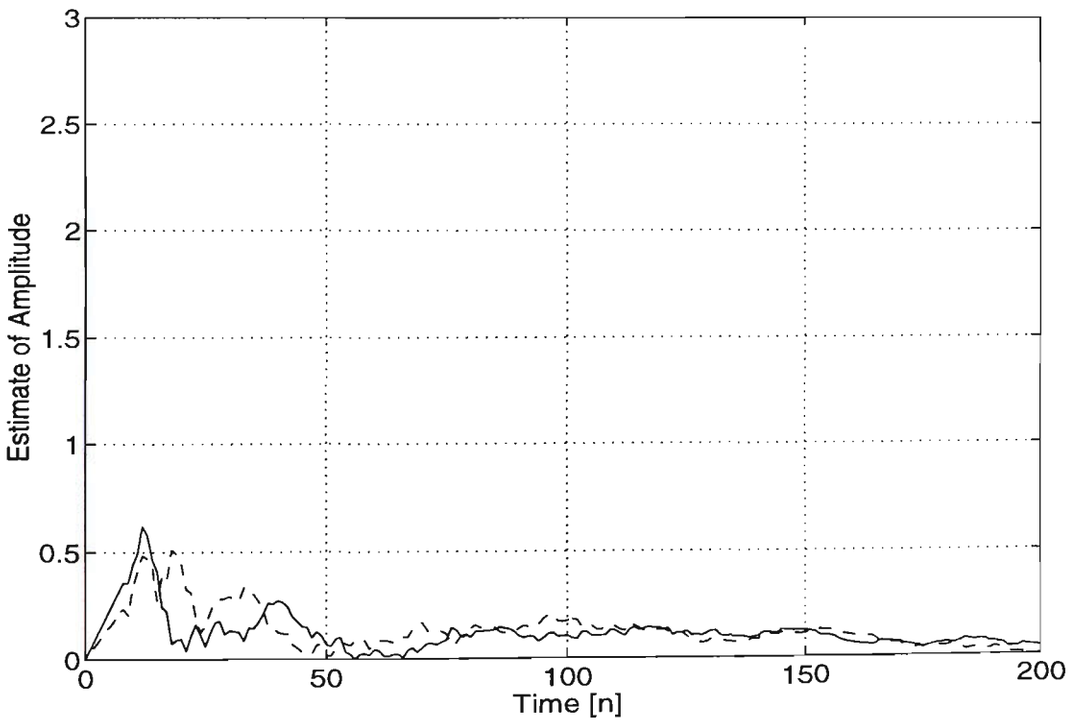

Figure 4.5: Sliding amplitude computation (C_l, C_h) using sliding Goertzel algorithm in the presence of unit variance, zero mean white noise only (low frequency component (Dashed line), high frequency component (Solid Line)).

Figure 4.6 corresponds to the case when the two closest frequencies, in the DTMF signal ($f_l = 852$Hz and $f_h = 1336$Hz), are transmitted while the resonators are tuned at 941Hz and 1209Hz. It is evident that when the two most adjacent frequencies are transmitted, after 100 samples the receiver does not falsely detect another DTMF signal. Once the transient behaviour of the filter has elapsed, detection can be accomplished by using an appropriate threshold. The threshold value is application dependent. The signal is detected as a valid transmitted frequency when the magnitude is larger than the threshold. These results clearly show that the coefficients are computed very fast. Note that if the conventional or modified Goertzel algorithms are used at least 4000 samples are needed to accurately estimate the phase and amplitude of the components. Based on 100 independent experiments, the average and standard deviation of amplitude estimates of low frequency component (f_l) using the proposed, conventional and modified Goertzel algorithms were computed at the 256th time instant and the results are given in Table 4.3. For the conventional Goertzel algorithm, the index k is found to be equal to 30.

		Sliding Goertzel algorithm	Modified Goertzel algorithm	conventional Goertzel algorithm
		$N_{acq} = 256$		SNR=3dB
Amplitude (f_l)	Ave.	2.0158	1.9874	1.9610
	STD	0.0910	0.1115	0.1312
Phase (f_l)	Ave.	0.9900	–	–
	STD	0.0441	–	–

Table. 4.3: The average and standard deviation of phase and amplitude estimates of low frequency component (f_l) of DTMF signal (Example 1) using sliding, conventional and modified Goertzel algorithms.

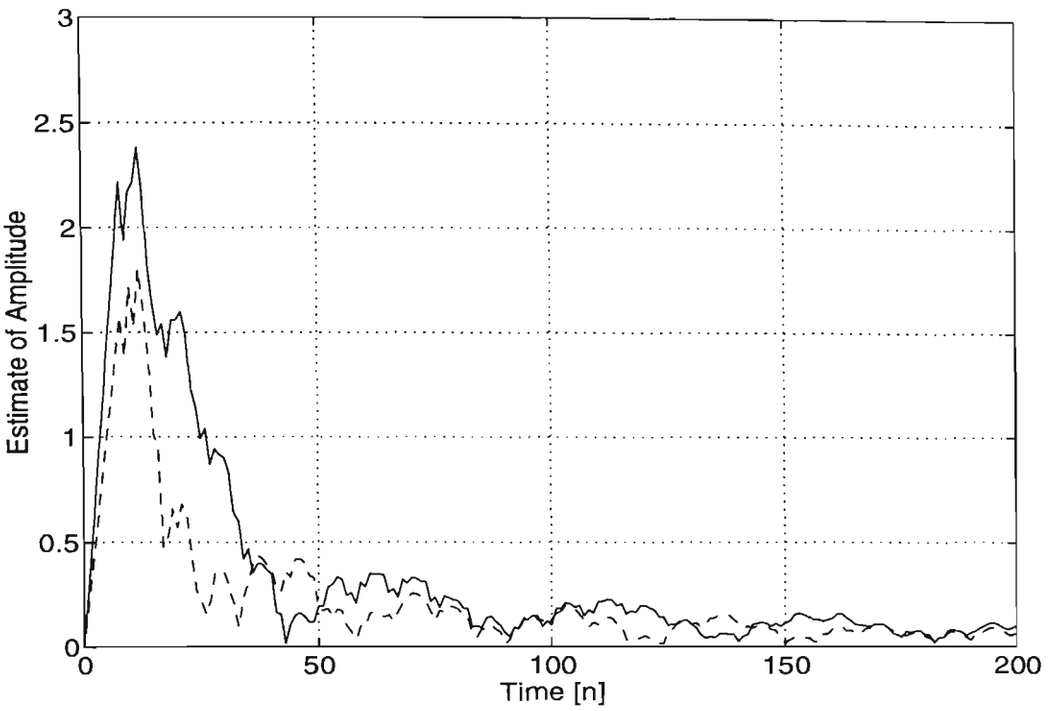

Figure 4.6: Sliding amplitude computation using sliding Goertzel algorithm when the two most adjacent frequencies ($f_l = 852Hz$, $f_h = 1336Hz$) are transmitted (C_l (Dashed line), C_h (Solid Line)).

Note that, since the conventional and modified Goertzel algorithms can not estimate phase of the component by using 256 samples, these are not included in Table 4.3. It is seen that the sliding Goertzel algorithm provides similar accuracy for amplitude computation as does the modified Goertzel algorithm. Both the sliding and modified Goertzel algorithms perform better than the conventional Goertzel algorithm. The performance of the sliding Goertzel algorithm under various SNR conditions has also been examined. For each SNR condition, the estimates are computed based on 100 independent experiments. The standard deviation and average error of the estimates for the amplitude and phase are shown in Figures 4.7 and 4.8, respectively. In these figures, the parameter N indicates the sample number at which the algorithm was performed. It is seen that the algorithm exhibits good performance at low SNR.

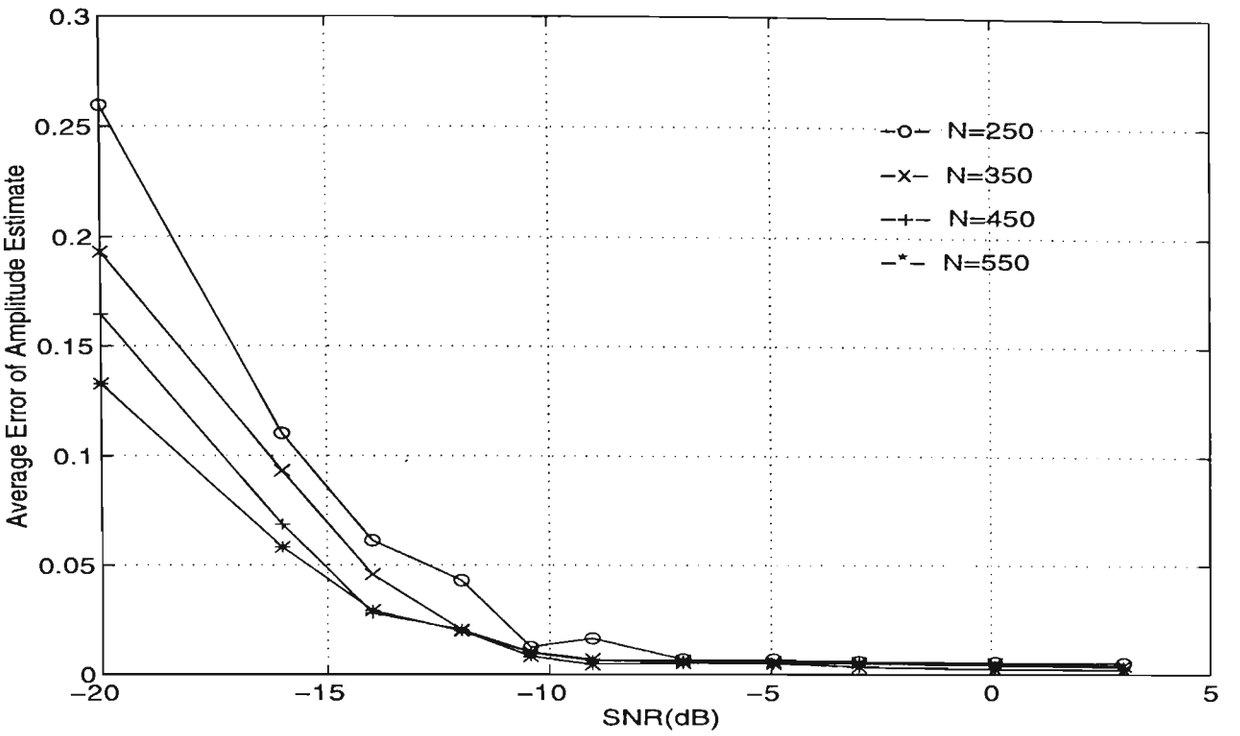

(a)

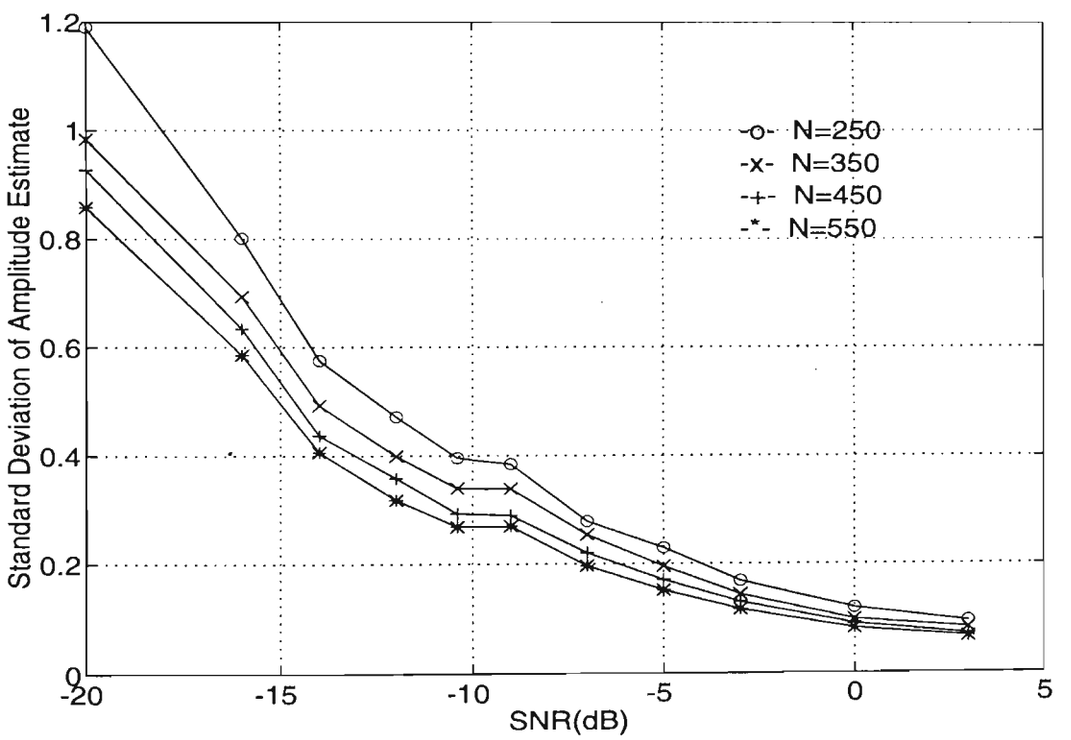

(b)

Figure 4.7: (a) error ($\left|(\bar{\hat{C}} - C_{actual}) / C_{actual}\right|$) and (b) standard deviation of amplitude estimate versus SNR.

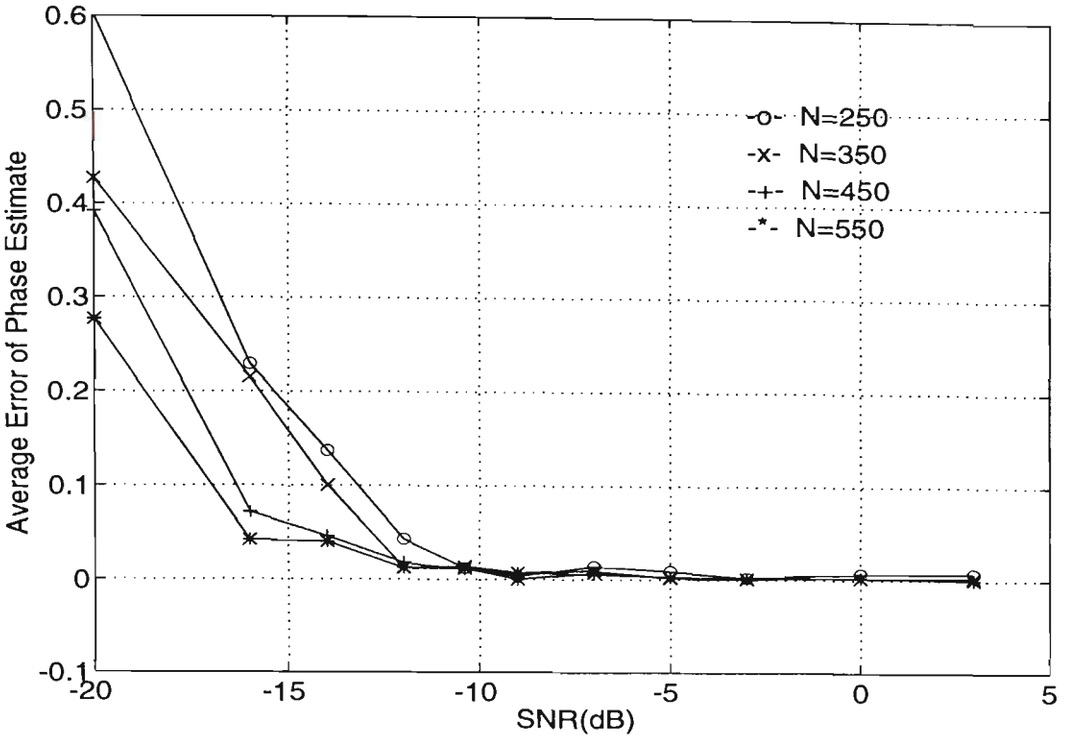

(a)

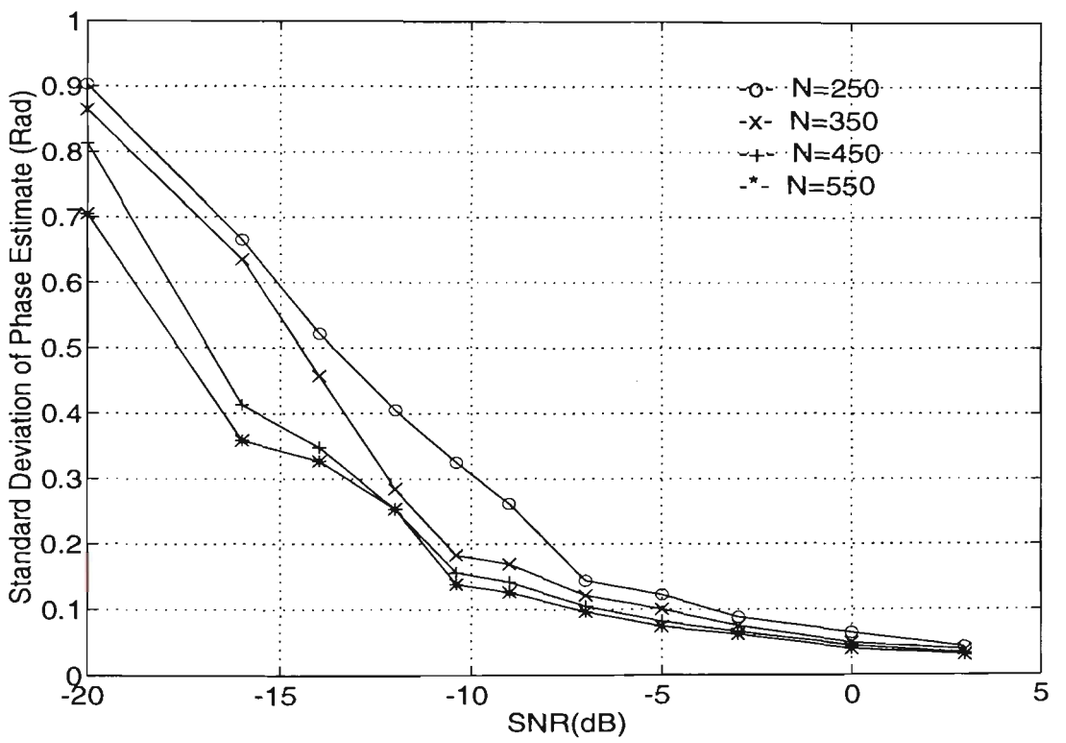

(b)

Figure 4.8: (a) error ($\left|(\bar{\hat{\phi}} - \phi_{actual})/\phi_{actual}\right|$) and (b) standard deviation of phase estimate versus SNR.

Note that N can be selected large to increase the accuracy of the estimates. This, however; leads to an increase in acquisition time which means that one needs to trade acquisition time for accuracy, or *vice versa.*

Now we consider the condition when a mismatch exists between the resonance frequency of the resonator and the actual input sinusoidal frequencies. In other words, in practice, there may exist some deviation in input frequencies. For the given example, assume ±1.0% frequency deviation in the low frequency component of the input signal. Using 100 different trials, the standard deviation and the average of Fourier coefficients have been carried out and the results are depicted in Table 4.4. The input frequency was randomly selected from the range of $f_l - 0.01f_l < f < f_l + 0.01f_l$. As can be observed the accuracy of the proposed and modified Goertzel algorithms are similar and both provide more accurate estimates when compared with the conventional Goertzel algorithm. Obviously, the accuracy depends on the degree of uncertainty in the input frequency, that is, a more accurate estimate can be obtained as the amount of mismatch reduces.

		Sliding Goertzel algorithm	conventional Goertzel algorithm	Modified Goertzel algorithm
		N_{acq}=256 SNR=3dB Freq. Deviation=1%		
Amplitude (f_l)	Ave.	2.0434	2.0454	1.8806
	STD	0.1305	0.1285	0.2253
Phase (f_l)	Ave.	1.0120	–	–
	STD	0.1036	–	–

Table 4.4: The average and standard deviation of phase and amplitude estimates of low frequency component (Example 1) using sliding, modified and conventional Goertzel algorithms for 1% deviations in frequency.

Example 2. This example considers the situation where the signals are time-varying. Even though the proposed technique provides an estimate update at every sample time, one needs to wait for a minimum of N_{acq} samples before the estimate can be considered reliable. Note, however, that N_{acq} is less than one period of the signal. Figures 4.9 and 4.10 show amplitude and phase computation at every 30 samples of a single sinusoid, respectively. The phase and amplitude of the sinusoid change within successive sequences simultaneously. The input and sampling frequencies were chosen to be equal to 1209Hz and 4000Hz, respectively, while the SNR was set at 20dB. Step changes in amplitude (from 1 to 2) and phase (from 0 to 1 radian) were applied to the input sinusoid. From Figures 4.9 and 4.10, it is evident that the given algorithm is capable of tracking the rapid changes in the parameters of the input sinusoid.

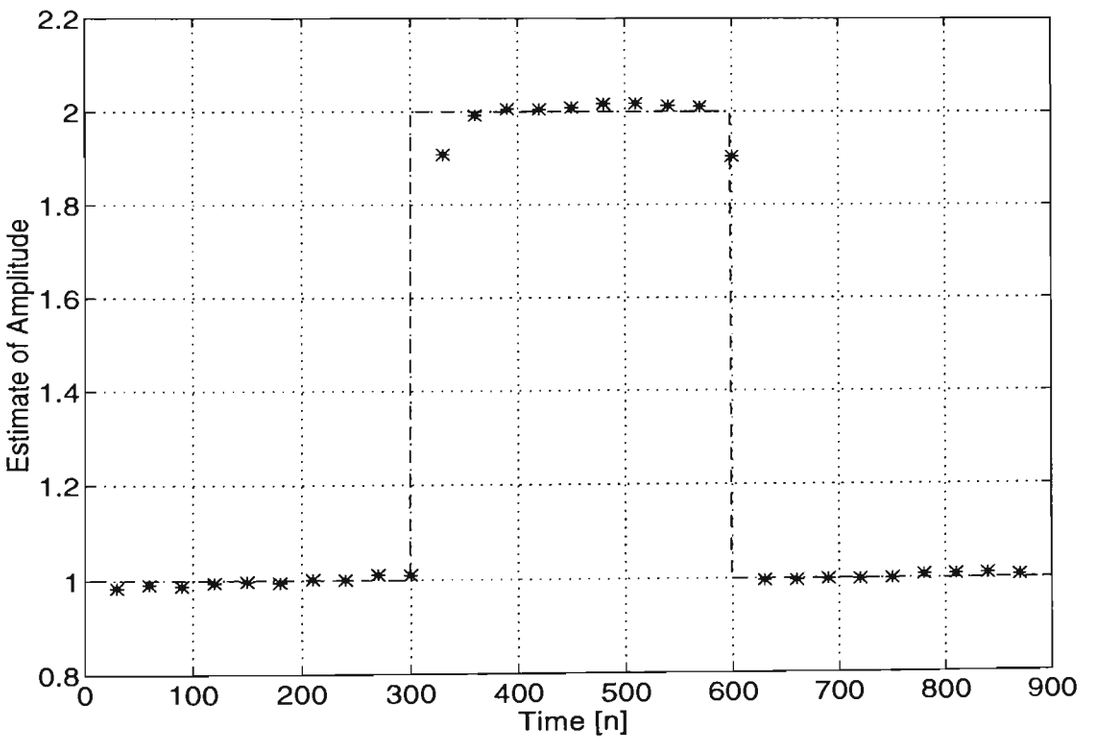

Figure 4.9: Amplitude computation of single sinusoid at every 30 samples with step changes in the input sinusoid's parameter.

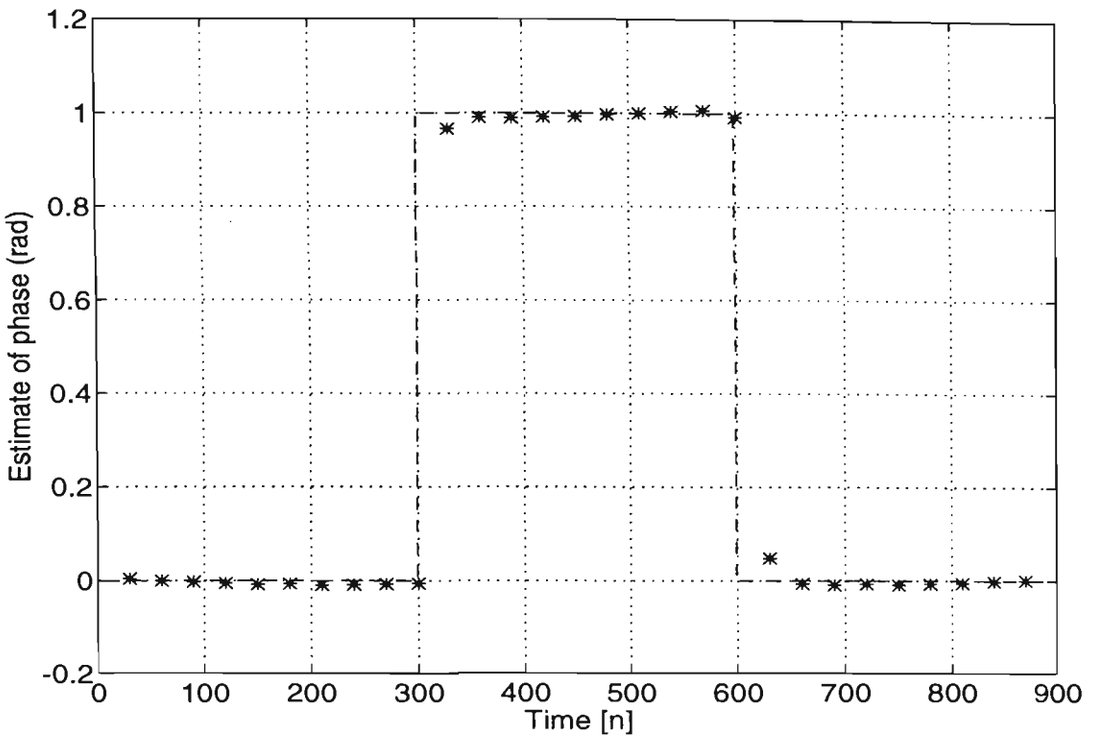

Figure 4.10: Phase computation of single sinusoid at every 30 samples with step changes in the input sinusoid's parameter.

4.5 Conclusion

The required acquisition time associated with the Goertzel algorithm for estimating the coefficients of sinusoidal signals was discussed. It was shown that the Goertzel algorithm requires a large number of samples when the common factor of input frequencies are small. This increases the required acquisition time of the algorithm and therefore reduces its tracking capability when the sinusoids parameters are time-varying.

A Sliding Goertzel (SG) algorithm was developed based on using second order digital resonators which are tuned to the input spectral frequencies. The proposed method provides good performance in low SNR situations and estimates accurate Fourier coefficients in less than one period of the signal. As a result, a significant reduction in acquisition time is achieved when compared to the conventional Goertzel algorithm. The accuracy versus the acquisition time of

the SG algorithm was also discussed. Further, the proposed approach is better suited to the estimation of Fourier coefficients when the parameters are time-varying within successive sequences. Simulation tests for the Fourier coefficient estimation of a typical DTMF signal were conducted to evaluate the relative performance of the sliding, modified and conventional Goertzel algorithms.

CHAPTER 5:

An Adaptive IIR Frequency Sampling Filter Bank

5.1 Introduction

So far the enhancement and characterisation of noise-corrupted sinusoidal signals have been performed based on the assumption that the frequencies of the input components are known *a priori*. We now consider the case when the input frequencies are unknown. In this chapter, the enhancement and frequency estimation of the input frequencies are performed by using an adaptive Frequency Sampling (FS) filter bank. The problem of large spectral overlap amongst the bandpass filters of the FS structure which decreases the convergence speed is discussed. A new adaptive IIR FS filter bank is proposed in an attempt to overcome the problem.

Traditionally, enhancement of unknown sinusoids buried in broadband noise is performed by using Tapped Delay Line (TDL) Adaptive Line Enhancers (ALE) [Widrow *et al.* (1975)]. A block diagram of the traditional ALE is shown in Figure 5.1. It is comprised of an N-weight TDL filter which is adapted by using the Least Mean Square (LMS) algorithm. Once convergence takes place, the enhanced sinusoidal signal is available at the output, $y(n)$, of the FIR filter. The location of the input frequencies are determined by taking the DFT of the FIR filter weights. The frequencies are validated if there is any spectral peak above the background noise [Widrow *et al.* (1975)]. Clearly, the desired enhancement

as well as the required resolution of the conventional ALE can be improved by increasing the length of the FIR filter.

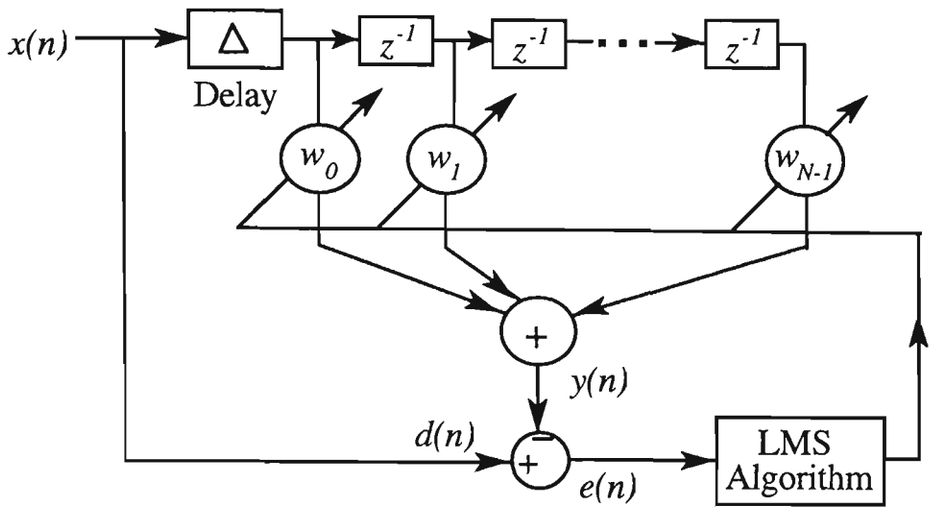

Figure 5.1: Traditional ALE structure.

It is well known that the convergence speed of the conventional ALE depends on the eigenvalue disparity of the input autocorrelation function [Widrow *et al.* (1976)]. In situations where the powers of the input sinusoids are widely spread, the input correlation matrix will have a bigger eigenvalue disparity thus resulting in slow convergence speed. Transform domain LMS adaptive algorithms have been proposed partly with the aim of improving the convergence speed [Narayan and Peterson (1981), Narayan *et al.* (1983), Bitmead and Anderson (1981)]. This approach also provides more uniform convergence rate for all the adaptive weights. The method is similar to the TDL LMS adaptive filter, except that a transformation such as the DFT or the Discrete Cosine Transform (DCT) is first performed on the input sequence in a sliding fashion. Each transform can be considered as a bank of narrow-band bandpass filters. An equivalent filter bank structure is more efficient in terms of computational burden. The FS structures are generally regarded as having a reduced computational complexity of the sliding spectral measurements. These structures are composed of an FIR comb

filter followed by parallel resonators. Alternative realisations for the real valued FS filter bank have been described in [Bitmead and Anderson (1981)].

The purpose of using a filter bank is to separate the energy of the input signal into N approximately nonoverlapping frequency bins as shown in Figure 5.2. At first, the filter bank splits the input signal $x(n)$ into N approximately orthogonal signals $y_k(n)$. These signals, $[y_k(n)]$, are filtered by a bank of adaptive subfilters $F_k(n,z)$. The outputs of the subfilters are added to obtain the overall filter output $z(n)$. The output, $z(n)$, is compared with the desired signal $d(n)$ to produce a common error signal $e(n)$. A self-orthogonalising LMS adaptive algorithm is then employed to adjust the coefficients of the adaptive subfilters so that the MSE is minimised [Narayan *et al.* (1983), Lee and Un (1986)].

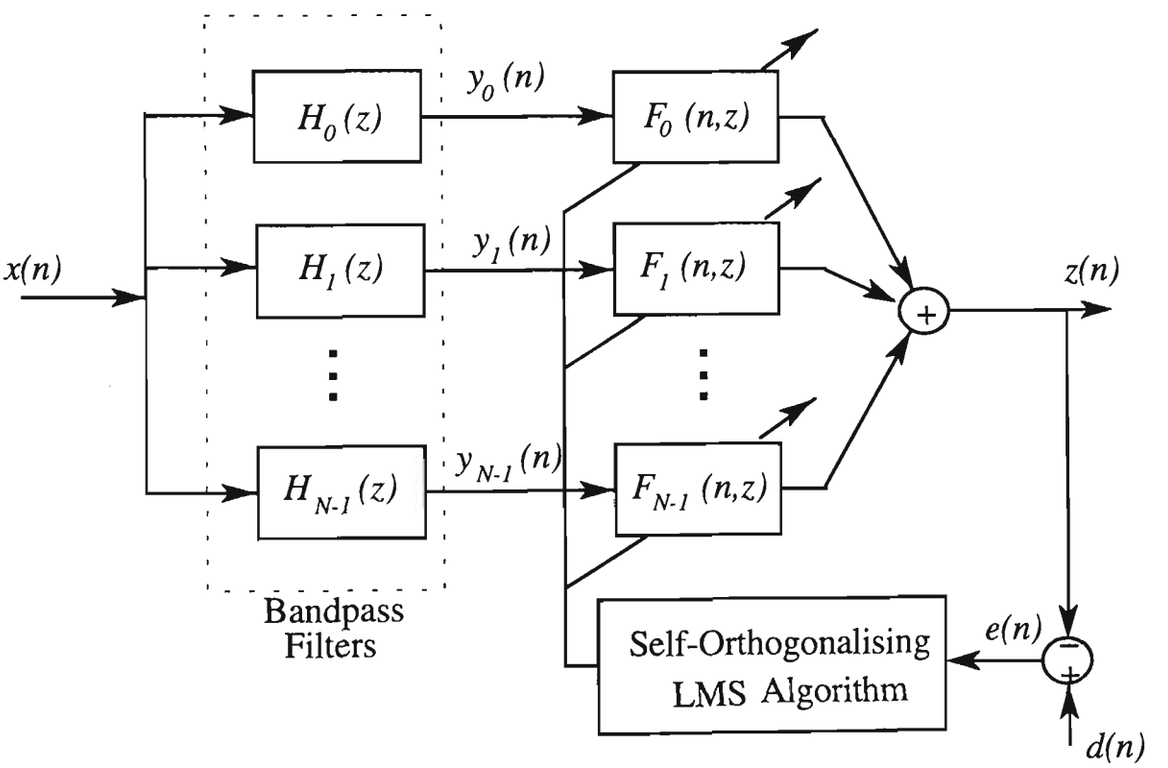

Figure 5.2: Filter bank based adaptive filtering.

The self-orthogonalising algorithm is similar to the conventional LMS algorithm except that it uses a time-varying step size factor for each adaptive weight which is inversely proportional to the power of the signal at the output of each bin. This

algorithm, in fact, normalises the power of the signal in each bin to unity thus resulting in reduced eigenvalue disparity. Therefore faster convergence speed is expected when compared with TDL LMS algorithm. The algorithm is sometimes called transform domain normalised LMS algorithm [Farhang-Boroujeny and Gazor (1992)].

When adaptive filters are realised using a filter bank, two important issues must be considered. The first is the amount of overlap and the second is the spectral holes which occur between two adjacent bins. The steady state performance of the adaptive algorithm is adversely affected by the spectral hole. In other words, the adaptive process may not give adequate enhancement to the unknown sinusoids lying in these spectral gaps [Shynk (1992)]. On the other hand, the existence of a large degree of spectral overlap results in reduced convergence rate [Shynk (1992), Petraglia and Mitra (1988)]. Although FS filter banks are computationally efficient, they suffer from a large degree of spectral overlap.

In this chapter we present a new IIR FS filter bank. The proposed structure is composed of a constrained IIR comb filter followed by parallel digital resonators. The IIR comb filter comprises N zeros equally spaced on the unit circle along with N uniformly distributed zeros and poles inside the unit circle. Two adjacent zeros of the comb filter on the unit circle are eliminated by using two successive digital resonators and the resulting structure is an IIR bandpass filter. The spectral overlap as well as the spectral hole between adjacent channels of the proposed method are significantly reduced when compared to the conventional FS structures. Further, by using the self-orthogonalising LMS algorithm, the proposed filter bank approach provides faster convergence speed when compared with both the TDL (normalised LMS) and conventional FS methods under the

same steady-state Mean-Squared-Error (MSE). The convergence conditions, the minimum and excess MSE of the adaptive FS filter bank are also studied.

Since the poles of the proposed IIR parametisation are constrained to be within the unit circle, it has guaranteed stability. Further, it provides approximately linear phase characteristics in the passband. The proposed structure is modular in design which means that it lends itself to easy implementation. The proposed filter bank is used for the task of ALE and simulation tests are carried out to establish the performance. The results are compared with those obtained by the TDL and the conventional FS methods.

This chapter is organised as follows: Section 5.2 presents the formulation for the proposed filter bank. Performance analysis of the self-orthogonalising LMS algorithm using filter bank is described in Section 5.3. Simulation tests are included in Section 5.4 and finally Section 5.5 concludes the chapter.

5.2 The Proposed Filter Bank

Conventional FS filter banks are commonly used when implementing sliding spectral measurements. The DFT can be implemented in sliding form using an FIR comb filter followed by parallel digital resonators. For example, the transfer function of DFT filter bank becomes [Rabiner and Gold (1975)]:

$$H_k(z^{-1}) = H_c(z^{-1})H_r(z^{-1}) = \frac{1-z^{-N}}{1-e^{-j\frac{2\pi k}{N}}z^{-1}} \qquad k = 0,\ldots,N-1 \qquad (5.1)$$

where $H_c(z^{-1})$ and $H_r(z^{-1})$ are the transfer functions of the comb filter and resonator, respectively. The pole of each resonator (denominator) eliminates the corresponding zero of the comb filter (numerator) and the result is an FIR complex bandpass filter. An equivalent approach of implementing the DCT is via a digital filter bank defined as follows, [Narayan *et al.* (1983)]:

$$H_k(z^{-1}) = H_c(z^{-1})H_r(z^{-1}) = \frac{(1-z^{-1})(1-(-1)^k z^{-N})}{1-2\cos\frac{\pi k}{N}z^{-1}+z^{-2}} \qquad (5.2)$$

for $k = 0,\ldots,N$. It is evident that the poles of each resonator cancels the corresponding zeros of the comb filter (numerator). Each branch in this structure results in a real FIR bandpass filter. For the DCT case, the bandpass filters are spaced at equal intervals of π/N rather than $2\pi/N$ radians as seen in the DFT filter bank implementation. Unlike the DFT case, the bandpass filter outputs of the DCT filter bank are real and therefore no complex arithmetic is involved. These structures have become attractive because of their modularity and lower computational burden. The frequency response of two adjacent bins for the DFT and the DCT filter banks are shown in Figures 5.3 and 5.4, respectively. It is evident that in the case of DCT the size of the spectral hole between two adjacent bins has decreased. However, the amount of spectral overlap in the main lobe has increased. Further, it can be seen that the side lobes contain less overlap when compared to the DFT filter bank implementation. Note that in both methods (i.e., DFT and DCT), the first side lobe is about 13dB below the main lobe.

Our objective is to obtain bandpass filters with less spectral overlap and reduced spectral hole between adjacent bins, while preserving the modularity of the FS structures. To achieve these requirements, we propose an IIR comb filter rather than FIR comb filter as follows:

$$H_c(z^{-1}) = (1-z^{-N})\frac{1-\alpha z^{-N}}{1-\beta z^{-N}} \qquad (5.3)$$

where N is an even number and $0 < \alpha < \beta < 1$.

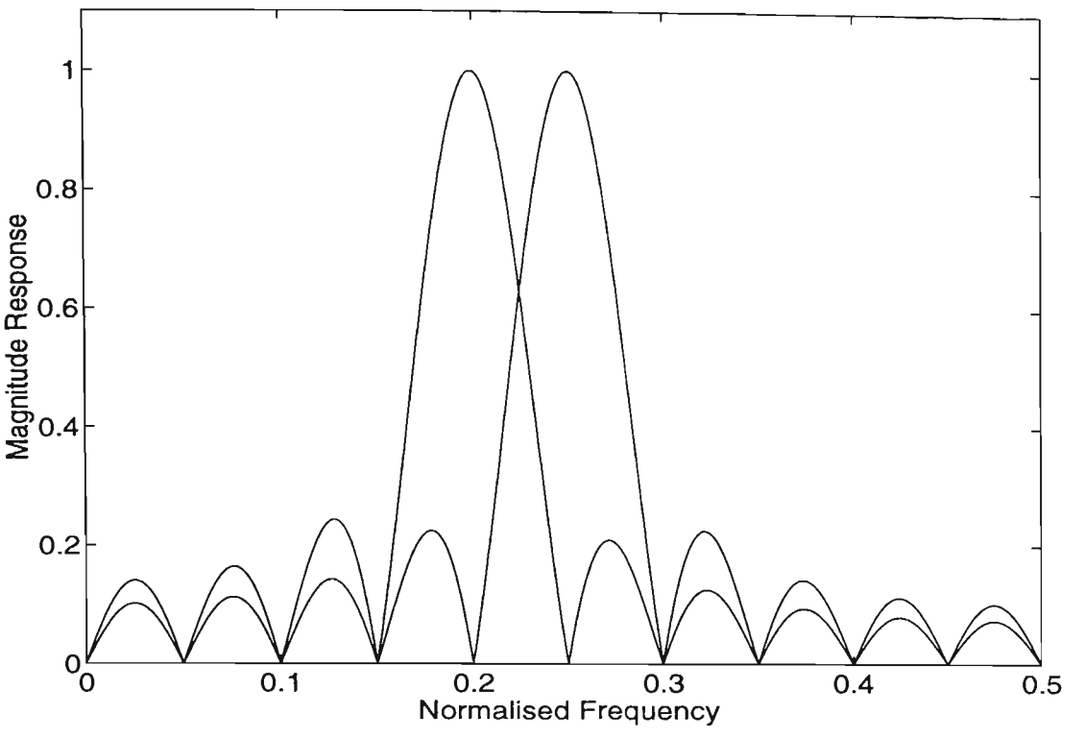

Figure 5.3: Magnitude response of two adjacent bins for the DFT filter bank.

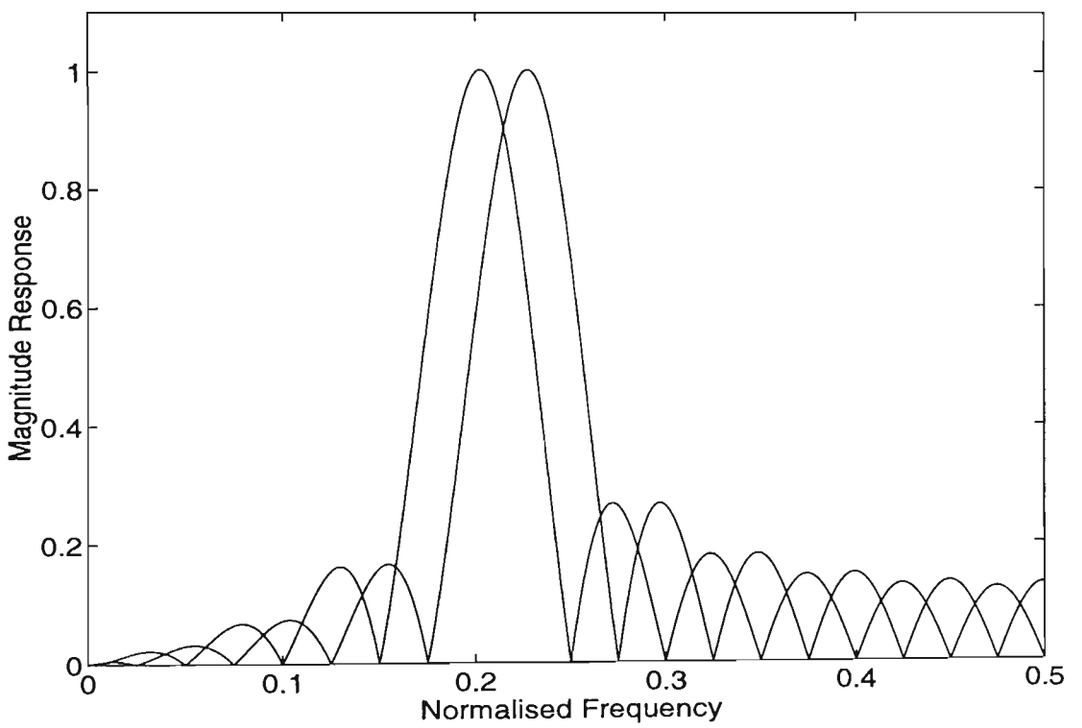

Figure 5.4: Magnitude response of two adjacent bins for the DCT filter bank.

The comb filter, as described by Equation (5.3), has N equally spaced zeros on the unit circle as well as N equally distributed zeros and poles within the unit circle. The two parameters α and β can be used to control the position of zeros and poles, respectively. In addition, two resonators will be used in each branch to eliminate the two corresponding adjacent zeros of the comb filter on the unit circle as follows:

$$H_r(z^{-1}) = [\frac{1}{1-e^{-j\frac{2\pi k}{N}}z^{-1}}][\frac{1}{1-e^{-j\frac{2\pi(k+1)}{N}}z^{-1}}] \qquad k = 0,....N-1 \qquad (5.4)$$

The normalised magnitude response of two adjacent bins are depicted in Figure 5.5. From Figure 5.5, it is evident that the transition band of each bandpass filter has decreased, which leads to a reduction in the spectral hole between adjacent channels.

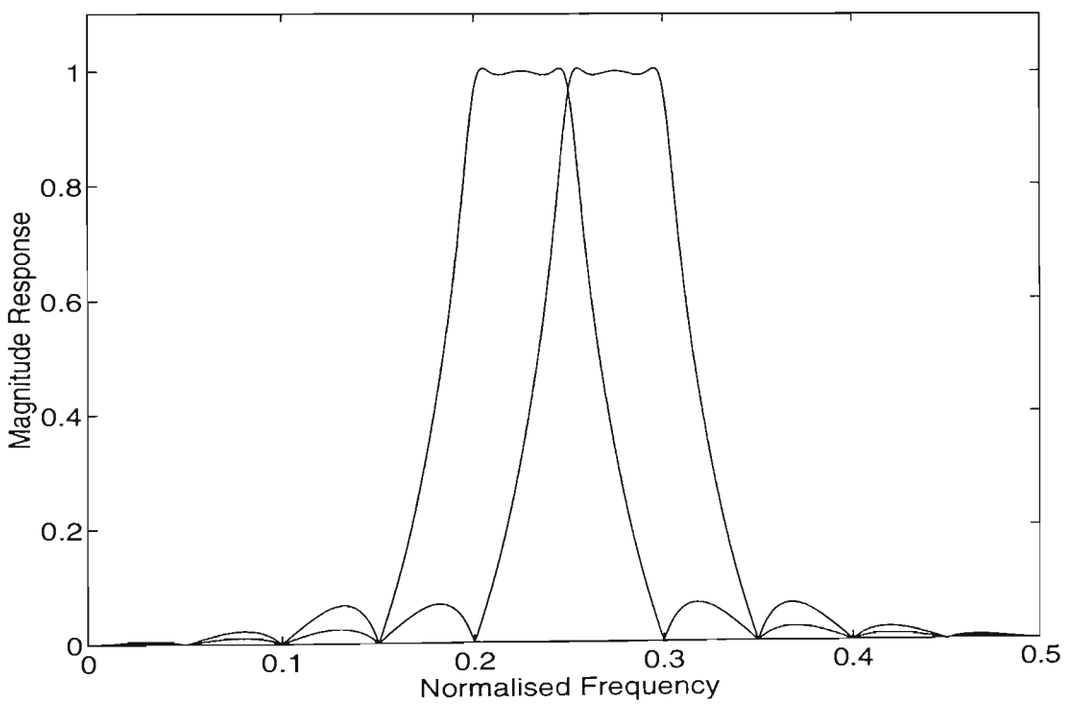

Figure 5.5: Magnitude response of two adjacent bins for the proposed structure ($N = 20$, $\alpha = 0.2$, $\beta = 0.3$).

Further, the amount of overlap particularly through the side lobes is reduced. The first side lobe is now about 24dB below the main lobe which is significantly

reduced when compared with that of the FS structure (-13dB side lobe). In order to obtain an appropriate selection of the parameters (α and β), β is defined as follows:

$$\beta = \alpha + \eta \tag{5.5}$$

The transition band (bin) and the passband ripple (dB) versus α for different values of η are plotted in Figures 5.6 and 5.7, respectively. The bandwidth of the transition band in which the magnitude response drops from the passband to the stopband is given in terms of frequency bin. Each frequency bin is equal to the distance between the centre frequencies of two adjacent bandpass filters. In this case, the stopband cutoff frequency corresponds to the frequency where the magnitude of the response is equal to -20dB. Figures 5.6 and 5.7 can be used for design purposes. Note that when α and β are close to the origin, the spectral hole as well as the transition band will be increased. However, when α and β are close to unity, the filter characteristics become sharper. Unfortunately in this case, the ripple in the passband will also increase.

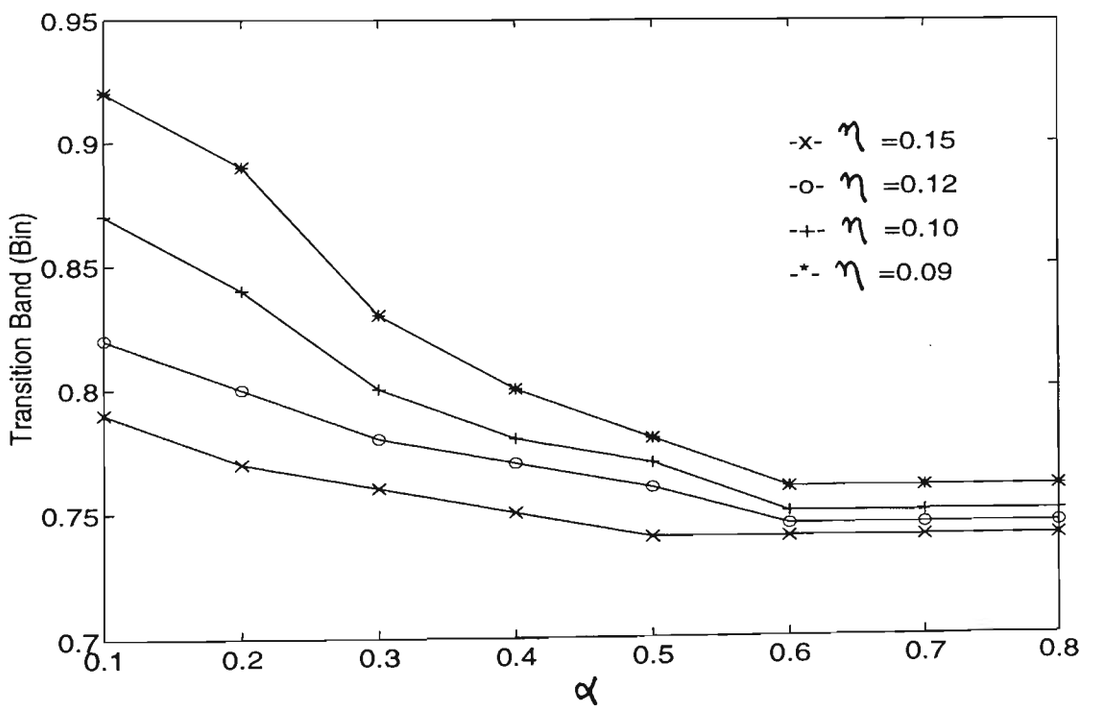

Figure 5.6: Transition band versus α for individual channel while η is the parameter.

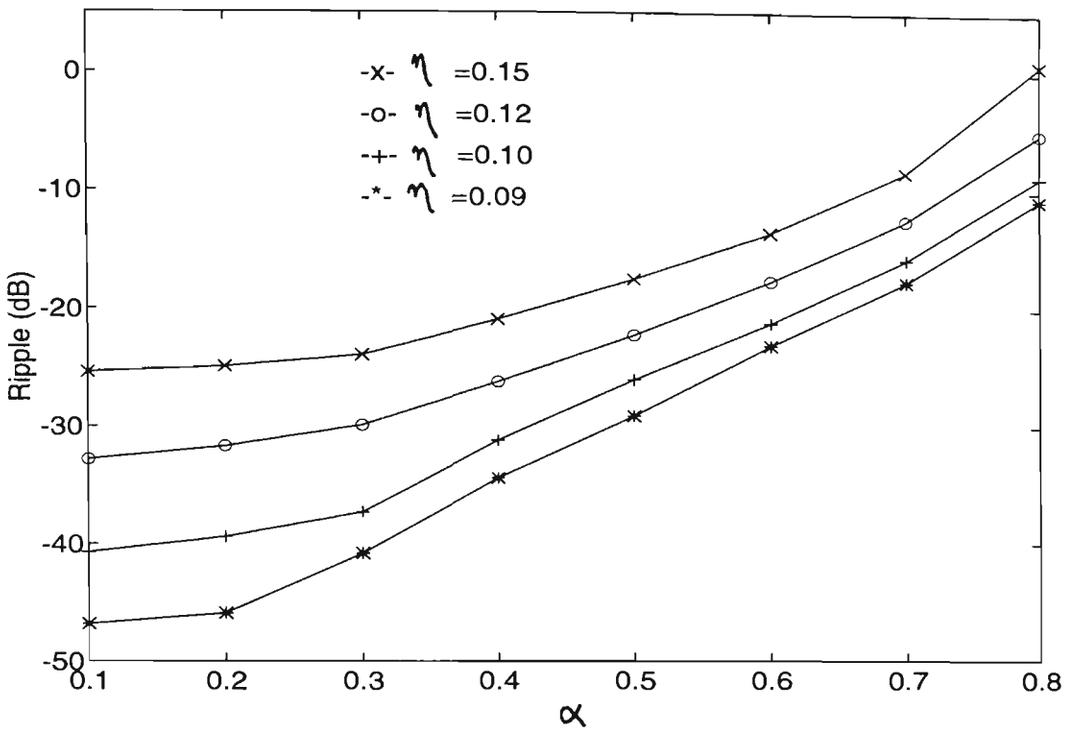

Figure 5.7: Ripple versus α for individual channel while η is the parameter.

A plot of the phase characteristics versus normalised frequency for a specific bin when α is equal to 0.2 and for different values of η is depicted in Figure 5.8. It is seen that the phase response of the proposed structure is approximately linear in the passband of each bandpass filter.

Since the proposed filter bank provides reduced overlap as well as minimal spectral hole characteristics between adjacent channels, it is an attractive solution for adaptive filtering. In other words, due to improved orthogonalisation properties of the proposed filter bank (reduced overlap), it is expected this will lead to faster convergence when compared to the conventional adaptive FS structures. Referring to Figure 5.2, each subfilter is generally comprised of a single complex coefficient while the complex LMS algorithm [Widrow *et al.* (1975)] is employed to recursively update the weight vector. Other types of subfilters such as pole-zero filters can also be used [Shynk (1989a)]. Assuming that one is dealing with real signals, it is desirable to use real operations. In such

cases, the kth and the $(N-k)$th bandpass filters can be combined together. The resulting bandpass filter is realised by using the IIR comb filter together with two second order digital resonators in series as follows:

$$H_r(z^{-1}) = \frac{1}{1-2\cos\frac{\pi k}{N}z^{-1}+z^{-2}} \frac{1}{1-2\cos\frac{\pi(k+1)}{N}z^{-1}+z^{-2}} \qquad (5.6)$$

$$K = 1,\ldots,(N/2)-2$$

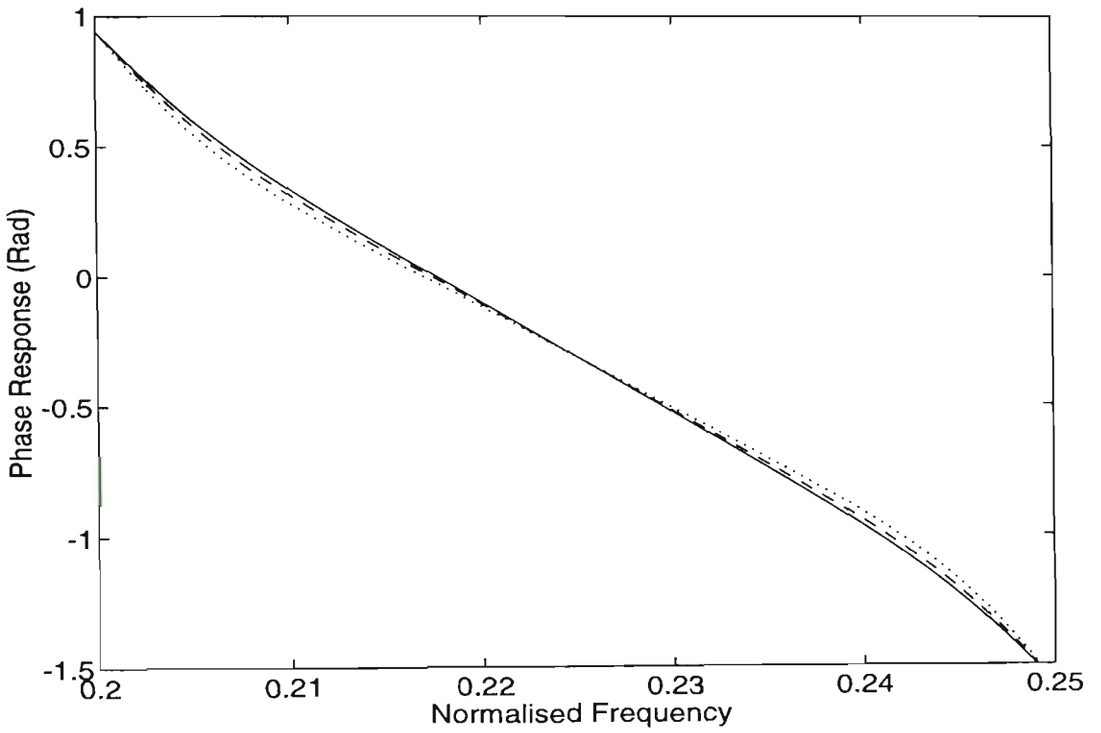

Figure 5.8: Phase response of the proposed bandpass filter ($N=20$, $\alpha=0.2$, $f_c=0.225$, $\eta=0.1$ (solid line), $\eta=0.12$ (dashed line), $\eta=0.15$ (dotted line)).

In order to provide symmetric conditions, two additional zeros are added to the comb filter using $1-z^{-2}$. Hence, the transfer function given by Equation (5.6) can also be used for $k=0$ and $k=(N/2)-1$. The proposed real valued implementation requires a subfilter which consists of a two tap delay line with real weights as follows:

$$F_k(n,z) = w_{1k}(n) + w_{2k}(n)z^{-1} \qquad (5.7)$$

The centre frequency of k th bandpass filter occurs at:

$$\omega_c = \frac{2\pi k}{N} + \frac{\pi}{N} \tag{5.8}$$

To ensure that the bandpass filter gain is unity, the transfer function can be normalised as follows:

$$|G| = [\frac{1+\alpha}{1+\beta}] \frac{\sin(\frac{2\pi k}{N} + \frac{\pi}{N})}{4\sin^2(\frac{\pi}{2N})\sin(\frac{2\pi k}{N} + \frac{3\pi}{N})\sin(\frac{2\pi k}{N} + \frac{\pi}{2N})} \tag{5.9}$$

where G is the gain of the bandpass filter at the centre frequency. For adaptive filtering applications, the constant gain criteria can be dropped, as it is absorbed by the corresponding adaptive subfilters. Note that there are 6 multiplications per channel per output sample for the proposed approach which is three times the number required by the conventional FS structure. Clearly, in situations where computational burden is not a main concern then the proposed approach will provide superior performance in terms of improved convergence rate.

In practice for finite word length arithmetic implementation of the proposed approach one needs to consider two important issues. First, because the poles of each resonator lie exactly on the unit circle, it is clear that any round-off errors could result in filter instability. In this case, it is suggested that z^{-1} be replaced by ξz^{-1}, where $0 << \xi < 1$ [Shynk (1989a), (1992)]. Secondly, even if poles and zeros are moved inside the unit circle, the zeros may not be exactly cancelled by the poles of the resonator due to the coefficient quantisation noise. That is, the poles may be placed either before or after the zeros of the comb filter. Depending on the extent to which this mismatch occurs it may cause notches or peaks in the bandpass region of the proposed filters. It is important to note that typical Digital Signal Processing (DSP) chips are characterised by 32-bit fixed-point arithmetic (multiplication and accumulation) and 16-bit memory allocation.

In this case the degradation in filter characteristics and its performance is negligible as verified by our simulations and confirmed by the independent work of Kuo and Rodrigues [Kuo and Rodrigues (1986)] where an implementation of a conventional FS structure (based on pole-zero cancellation) was done using the TMS32010 chip.

5.3 Performance Analysis

The properties of the conventional and normalised TDL LMS algorithms are reviewed in this section. These properties are used for comparison purposes. The performance of the adaptive self-orthogonalising LMS algorithm using a filter bank in terms of the convergence condition, minimum of MSE and the excess MSE is then presented.

5.3.1 Conventional and Normalised TDL LMS Algorithm

The adaptive weights ($\mathbf{W}$) in the TDL adaptive digital filter as shown in Figure 5.1 are adjusted by the conventional LMS algorithm as follows [Widrow and Stearns (1985)]:

$$\mathbf{W}(n+1) = \mathbf{W}(n) + 2\mu_t \overline{\mathbf{X}}(\mathbf{n})e(n) \qquad (5.10)$$

$\mathbf{W}(n)=[w_1(n)\ w_2(n)\ \ldots\ w_n(n)]^T$ where T denotes transpose of a matrix and μ_t is a convergence factor which controls stability and the performance of the algorithm. $\mathbf{X}(n)=[x(n)\ x(n-1)\ \ldots\ x(n-(N-1))]^T$ and N is equal to the number of adaptive weights. This algorithm minimises the MSE that is defined as:

$$MSE = E[e(n)\bar{e}(n)] \qquad (5.11)$$

where the $\bar{\cdot}$ indicates the complex conjugate and $E[.]$ denotes the statistical expectation. After convergence, the optimum weight vector ($\mathbf{W}_{opt}$) and minimum of MSE ($\varepsilon_{\min}$) are given respectively, by:

$$\mathbf{W}_{opt} = \mathbf{R}_x^{-1}\mathbf{P}_x \quad \text{and} \quad \varepsilon_{\min} = E[d(n)\bar{d}(n)] - \mathbf{P}_x^{*}\mathbf{R}_x^{-1}\mathbf{P}_x \qquad (5.12)$$

where the asterisk denotes complex conjugate transpose of a matrix. $\mathbf{R}_x$ and $\mathbf{P}_x$ are the input autocorrelation matrix and cross-correlation vector, respectively. These are defined as follows:

$$\mathbf{R}_x = E[\overline{\mathbf{X}}(n)\mathbf{X}^T(n)] \quad \text{and} \quad \mathbf{P}_x = E[d(n)\overline{\mathbf{X}}(n)] \tag{5.13}$$

The excess MSE (ε_Δ) and the time constants (τ_i) relating to relaxation of the learning curve are given respectively by [Widrow and Stearns (1985)]:

$$\varepsilon_\Delta = \mu_t Tr(\mathbf{R}_x)\varepsilon_{\min} = \mu_t N\sigma_x^2\varepsilon_{\min} \quad \text{and} \quad \tau_i = \frac{1}{4\mu_t\lambda_i} \tag{5.14}$$

where $1 \le i < N$, λ_i's are the eigenvalues of the input autocorrelation matrix. $Tr(\mathbf{R}_x)$ denotes the sum of the principal diagonal elements of the matrix $\mathbf{R}_x$ and is equal to $N\sigma_x^2$. The time domain normalised LMS algorithm uses a time varying convergence factor as follows [Lee and Un (1986)]:

$$\mu_t(n) = \frac{\mu_{t0}}{\hat{\sigma}_x^2(n)} \tag{5.15}$$

where $\sigma_x^2(n)$ is the power of the input signal and is estimated as follows:

$$\hat{\sigma}_x^2(n) = \gamma\hat{\sigma}_x^2(n-1) + (1-\gamma)x(n)\bar{x}(n), \qquad 0 < \gamma < 1 \tag{5.16}$$

where γ is the so-called smoothing constant which controls estimation accuracy and tracking capability of time variations. Consequently, the excess MSE for this algorithm is written as [Lee and Un (1986)]:

$$\varepsilon_\Delta = \mu_{t0} N\varepsilon_{\min} \tag{5.17}$$

It is seen from Equation (5.17) that the steady-state performance of the normalised LMS is independent of the input signal power. Equations (5.14) and (5.17) will be used later for comparing the TDL LMS with the FS filter bank approach.

From Equation (5.14), it is clear that the convergence speed is most affected by the largest time constant (τ_m) corresponding to the minimum eigenvalue. Therefore, in order to speed up the convergence rate, the value of $\lambda_{\min}$ must be

increased. Note that the convergence speed of different methods must be compared under the same steady-state MSE. This means that $Tr(\mathbf{R}_x)$ which is equal to the sum of eigenvalues must be fixed (see Equation (5.14)). As a result, the value of λ_{min} becomes maximum, when all the eigenvalues are identical [Lee and Un (1986)].

5.3.2 Adaptive Self-Orthogonalising LMS Algorithm

Using a two tap delay line filter as given by Equation (5.7) at the output of each bandpass filter, the self-orthogonalising LMS algorithm updates the weights as follows [Narayan et al. (1983), Lee and Un (1986)]:

$$w_{1k}(n+1) = w_{1k}(n) + 2\mu_{fk}(n) y_k(n) e(n) \tag{5.18}$$

$$w_{2k}(n+1) = w_{2k}(n) + 2\mu_{fk}(n) y_k(n-1) e(n) \tag{5.19}$$

where $y_k(n)$ is the signal at the output of kth bandpass filter and

$$\mu_{fk}(n) = \frac{\mu_f}{\hat{\sigma}^2_{y_k}(n)} \tag{5.20}$$

is the time-varying adaptive step size for the kth bandpass filter and μ_f is a positive constant. The signal power can be estimated using a single-pole lowpass filter [Lee and Un (1986)] as follows:

$$\hat{\sigma}^2_{y_k}(n) = \gamma \hat{\sigma}^2_{y_k}(n-1) + (1-\gamma) y_k^2(n) \qquad 0 < \gamma < 1 \tag{5.21}$$

It is well known that the eigenvalue disparity of the input correlation matrix is related to the power variation in the input signal spectrum [Makhoul (1975)]. Passing the input signal through a filter bank provides an effective means for compensating the power variation. This can be done by properly normalising the signal power at the output of each bin. Under these circumstances, the elements of the main diagonal of the autocorrelation matrix will be equal to unity (assuming perfect orthogonalisation) which means that fast convergence is obtained. This implies that if the filter bank provides less correlated output the

speed of the convergence will be increased. The output of the filter bank is expressed as:

$$\mathbf{y}(n) = \mathbf{R}\mathbf{x}(n) \tag{5.22}$$

where

$$\mathbf{y}(n) = [y_0(n), y_1(n), \ldots, y_{N-1}(n)]^T \tag{5.23}$$

and

$$[\mathbf{R}]_{km} = r_k(m) \quad \text{for } k = 0,1,\ldots,N\text{-}1 \text{ and } m = 0,1,\ldots,N\text{-}1 \tag{5.24}$$

where in this case N is equal to the number of bins and $r_k(m)$ is the impulse response of the kth bandpass filter and it is assumed that its value for m greater than N, is approximately equal to zero. This approximation is justified by examining the impulse responses of the bandpass filters which are very close to zero for $m \geq N$. The autocorrelation matrix of the new input to the adaptive weights (the output of the bandpass filters) is:

$$\begin{aligned} \mathbf{R}_y &= E[\bar{\mathbf{y}}(n)\mathbf{y}^T(n)] = \bar{\mathbf{R}}E[\bar{\mathbf{x}}(n)\mathbf{x}^T(n)]\mathbf{R}^T \\ &= \bar{\mathbf{R}}\mathbf{R}_x\mathbf{R}^T \end{aligned} \tag{5.25}$$

The Wiener optimal solution is obtained as follows:

$$\mathbf{W}_{opt}^f = \mathbf{R}_y^{-1}\mathbf{P}_y \tag{5.26}$$

using

$$\mathbf{P}_y = E[d(n)\bar{\mathbf{y}}(n)] = E[d(n)\bar{\mathbf{R}}\bar{\mathbf{x}}(n)] = \bar{\mathbf{R}}\mathbf{P}_x \tag{5.27}$$

and substituting Equations (5.27) and (5.12) into Equation (5.26), we have:

$$\begin{aligned} \mathbf{W}_{opt}^f &= \mathbf{R}_y^{-1}\bar{\mathbf{R}}\mathbf{P}_x = \mathbf{R}_y^{-1}\bar{\mathbf{R}}\mathbf{R}_x\mathbf{R}_x^{-1}\mathbf{P}_x \\ &= \mathbf{R}_y^{-1}\bar{\mathbf{R}}\mathbf{R}_x\mathbf{W}_{opt} \end{aligned} \tag{5.28}$$

The minimum MSE for the adaptive bandpass filtering ($\varepsilon_{\min}^f$) becomes:

$$\begin{aligned} \varepsilon_{\min}^f &= E[d(n)\bar{d}(n)] - \mathbf{P}_y^*\mathbf{R}_y^{-1}\mathbf{P}_y \\ &= E[d(n)\bar{d}(n)] - \mathbf{P}_x^*\mathbf{R}^T\mathbf{R}_y^{-1}\bar{\mathbf{R}}\mathbf{P}_x \end{aligned} \tag{5.29}$$

Assuming that $\mathbf{R}$ is not singular, substituting Equation (5.25) into Equation (5.29) leads to:

$$\varepsilon_{\min}^f = E[d(n)\bar{d}(n)] - \mathbf{P}_x^*\mathbf{R}_x^{-1}\mathbf{P}_x = \varepsilon_{\min} \tag{5.30}$$

Note that for the case of any transform ($\mathbf{R}$) (such as DCT or DFT) applied to the input vector, the minimum MSE is also obtained to be equal to ε_{min} [Lee and Un (1986)]. The excess MSE of the LMS for the filter bank is given by:

$$\varepsilon_{\Delta}^{f} \approx \mu_f Tr[\mathbf{R}_y]\varepsilon_{min}^{f} = \mu_f Tr[\mathbf{R}_y]\varepsilon_{min} \qquad (5.31)$$

First we consider the case when a fixed step size factor is used. Also, assume that the filter bank perfectly orthogonalises the input signal. In this case, the matrix $\mathbf{R}_y$, only has non zero elements on principal diagonal $r_y(k,k)$ and their values correspond to the power of the signal at the kth bin which are approximately equivalent to the eigenvalues of the input autocorrelation matrix. The eigenvalue disparity can be considered as the signal power variation among the filter bank bins. Note that the filter bank only diagonalises the autocorrelation matrix and does not affect the eigenvalue disparity of the autocorrelation matrix. It is also clear that the sum of the signal power of the filter bank output is equal to the input signal power. So, we can write:

$$Tr(\mathbf{R}_y) \approx \frac{1}{N} Tr(\mathbf{R}_x) \qquad (5.32)$$

From Equations (5.14), (5.31) and (5.32), it can be concluded that the TDL and filter bank methods both have the same steady-state MSE and the same time constant provided that $\mu_f = N\mu_t$.

Now if the signals at the output of the individual bins are normalised, the equivalent autocorrelation matrix becomes equal to an identity matrix (assuming perfect orthogonalisation conditions). This means that all the eigenvalues become equal to unity thus resulting in fast convergence speed ($\lambda_{max}/\lambda_{min} \rightarrow 1$). This normalisation is, in fact, performed by using a time varying convergence factor which is inversely proportional to the signal power at the output of each bin (see Equations (5.20) and (5.21)). In this case, we obtain:

$$Tr(\mathbf{R}_y) \approx N \qquad (5.33)$$

Note that the steady-state performance (that is, the excess MSE) becomes independent of the input signal power and is equivalent to the normalised TDL LMS algorithm provided $\mu_{f0} = \mu_{t0}$ (see Equation (5.17)). Considering Equation (5.33), the self-orthogonalising LMS algorithm converges provided that:

$$0 < \mu_f < \frac{1}{Tr[\mathbf{R}_y]} \approx \frac{1}{N} \tag{5.34}$$

In summary, orthogonalising the input sequence through the use of the proposed filter bank increases the convergence speed; however, it does not improve the steady state error performance. These results are consistent with those reported in [Lee and Un (1986), Marshal *et al.* (1989)] where orthogonalisation is carried out by multiplying the input sequence by a unitary transformation matrix.

5.4 Simulation Results

The proposed filter bank was used for the implementation of the ALE. For the comparison purposes, the adaptive line enhancer was also implemented using TDL and conventional FS filter bank. For the TDL method the structure shown in Figure 5.1 is employed while for the FS method the equivalent FS filter bank of the DFT transform is used (see Equation 5.2). It has been shown that for the ALE application, both the DCT and the DFT FS filter banks have similar performance [Narayan *et al.* (1983)].

In each method, the reference signal (input of the adaptive filter) is formed by delaying the input signal by Δ to provide uncorrelated noise components. For situations where the broadband noise component of the input signal is white, Δ is usually selected equal to one sample delay. This is justified by the fact that the correlation between two adjacent samples of a white noise sequence is equal to zero. It has been shown that there exists an optimum choice for Δ that slightly improves the performance of the TDL method in terms of bias and noise variance

of the input frequency estimates [Reddy *et al.* (1981), Gupta (1985), Yoganandam *et al.* (1988)]. However, this optimum value which has only been given for the case of one and two sinusoids buried in white noise is a function of the input frequencies. Since the input frequencies are not known *a priori*, an estimation technique is required to obtain a near-optimum value for Δ which results in increased computational complexity. In our simulation for simplification purposes, the value of Δ is set equal to one step delay. The filter input consists of two sinusoidal components plus white noise as follows:

$$x(n) = C_1 \cos(0.275\pi n) + C_2 \cos(0.475\pi n) + \nu(n) \qquad (5.35)$$

where $\nu(n)$ is a zero mean white noise sequence. Note that the frequencies were chosen such that they do not fall exactly on the null of the bandpass filters. Otherwise, the effect of the leakage could not be observed. The eigenvalues of the input signal correlation matrix are widely spread by setting the power of the two components at different values.

In the FS method, the frequency resolution is determined by the number of the bins in the filter bank. The input frequency is detected by examining the sum of the squares of the adaptive weight (i.e., $w_{1k}^2 + w_{2k}^2$) at the output of each bin. Detection is said to be accomplished if this value is above a specific threshold. Clearly, the threshold value is application dependent. If the two input spectral lines fall in the passband of a particular bandpass filter, the algorithm will not be able to distinguish them. On the other hand, the frequency resolution of the TDL method is determined by the number of TDL filter weights. In order to estimate the input frequency, one needs to take an FFT from the adaptive weights after the adaptation process is completed. The input frequency is detected if there is any peak above the background noise. Clearly, both the TDL and FS methods yield the same frequency resolution provided the number of adaptive weights in the TDL filter is equal to the number of frequency bins in the FS filter bank. In these

simulations, the number of TDL adaptive weights and the number of bandpass filters (N) of the FS structures (i.e., the proposed IIR and DFT FS filter banks) are chosen to be equal to 40. The values of α and β are set equal to 0.2 and 0.3, respectively. Referring to Figures 5.6 and 5.7, the amount of the ripple in the passband and the transition bandwidth become approximately equal to –38dB and 0.84bin (bin$=1/N$), respectively.

Using a self-orthogonalising LMS algorithm for the filter banks (i.e., the proposed IIR and DFT FS filter bank) and normalised LMS algorithm for the conventional TDL method ($\mu_{f0}=\mu_{t0}=0.01,\ \gamma=0.9$), the learning curves are obtained. Note that the values of the step size factors (μ_{t0} and μ_{f0}) should be equal so that the same steady state performance (i.e., $\varepsilon_{min}^{f}=\varepsilon_{min}$ and $\varepsilon_{\Delta}^{f}=\varepsilon_{\Delta}$), is achieved. Figure 5.9 shows the learning curves for the case when ($C_1=1,\ C_2=0.1$).

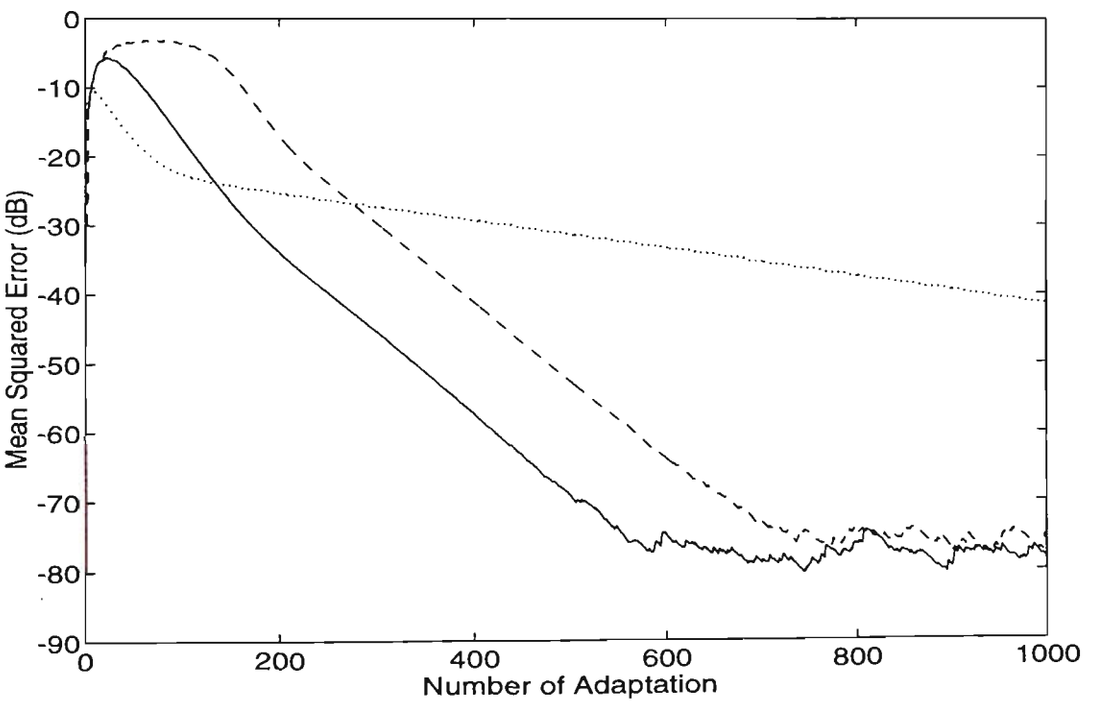

Figure 5.9: Learning curves using self-orthogonalising LMS algorithm for proposed filter bank (solid line) and DCT (dashed line) and normalised LMS algorithm for TDL method (dotted line) ($\mu_{f0}=\mu_{t0}=0.01,\ \gamma=0.95,\ SNR=80dB,\ C_1=1,\ C_2=0.1$).

Figure 5.10 corresponds to the case when the eigenvalues of the input signal correlation matrix are widely spread ($C_1 = 1$, $C_2 = 0.05$). From the given results, it is clear that the proposed method provides faster convergence rate when compared to the TDL and conventional FS method.

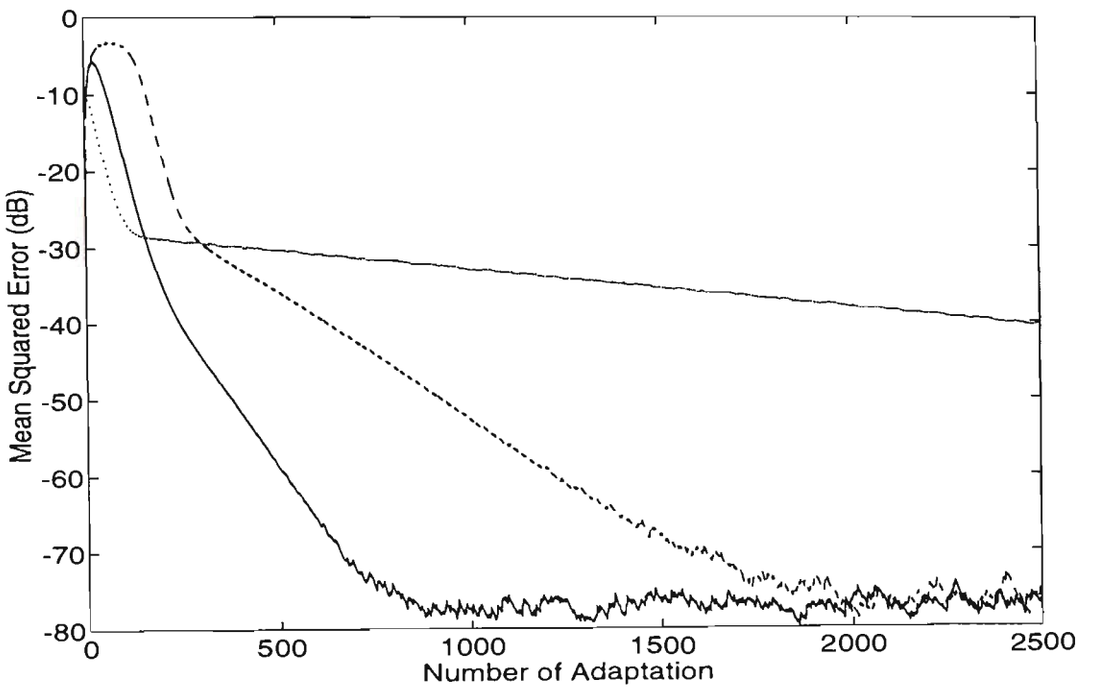

Figure 5.10: Learning curves using self-orthogonalising LMS algorithm for proposed filter bank (solid line) and DCT (dashed line), normalised LMS algorithm for TDL method (dotted line) ($\mu_{f0} = \mu_{t0} = 0.01$, $\gamma = 0.95$, $SNR = 80dB$, $C_1 = 1$, $C_2 = 0.05$.

Figure 5.11 shows the learning curves of the TDL and DFT domain and the proposed structure for the case of the $SNR = 40dB$. In this case, since the correlation amongst the input samples is reduced, the TDL method also results in fast convergence rate. The learning curves for the proposed filter bank and TDL method for fixed step size factor is shown in Figure 5.12 ($SNR = 40dB$). It is evident from Figure 5.12 that both methods have similar convergence speed under the same MSE condition (that is, $\mu_f / (Number\ of\ bins) = \mu_t = 0.03$).

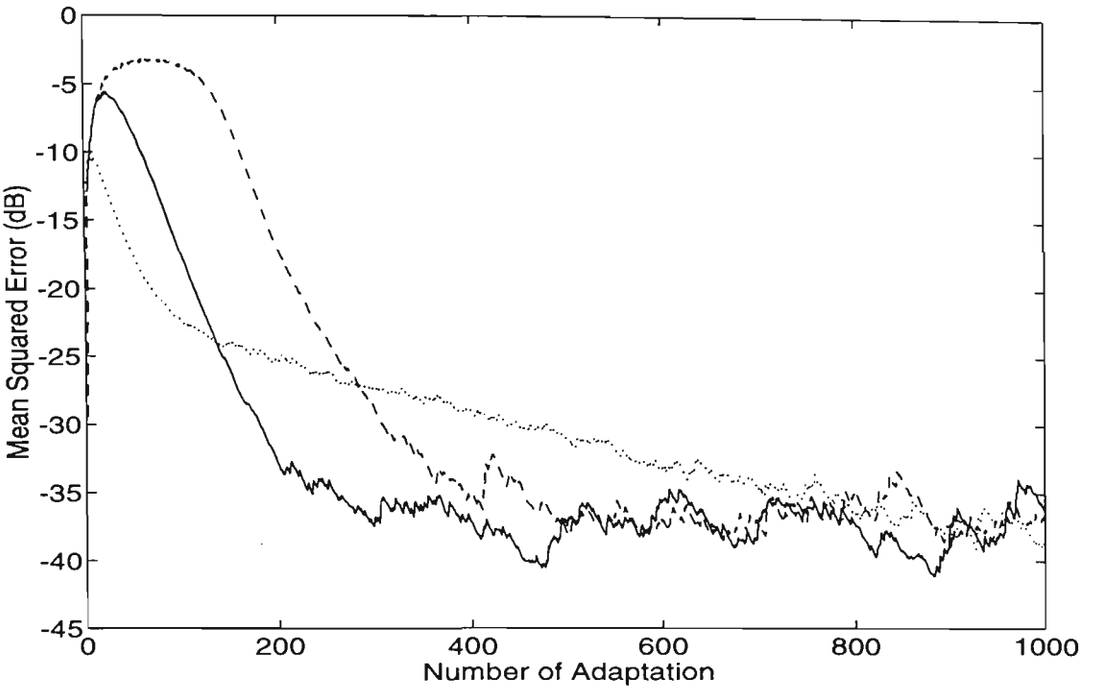

Figure 5.11: MSE learning curves using self-orthogonalising LMS algorithm for proposed filter bank (solid line) and DCT (dashed line) and using normalised LMS algorithm for TDL method (dotted line) ($\mu_{f0} = \mu_{t0} = 0.01$, $\gamma = 0.95$, $SNR = 40dB$, $C_1 = 1$, $C_2 = 0.1$).

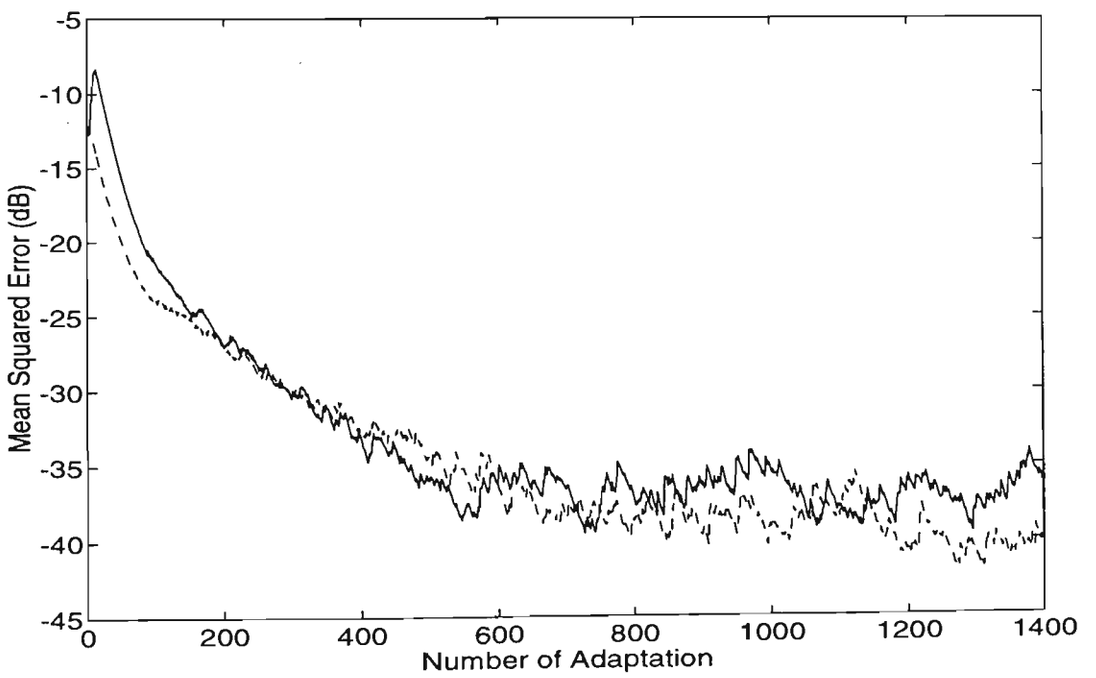

Figure 5.12: MSE Learning curves using fixed step size factor for proposed IIR filter bank (solid line) and TDL (dashed line), $SNR = 40dB$, $C_1 = 1$, $C_2 = 0.1$, $\mu_f / (Number\ of\ bins) = \mu_t = 0.03$.

5.5 Conclusion

A novel modular Infinite-Impulse-Response (IIR) filter bank primarily aimed at adaptive line enhancement applications was introduced. The proposed IIR FS filter is composed of a constrained IIR comb filter followed by parallel digital resonators. The comb filter consists of N equally spaced zeros on the unit circle as well as zeros and poles whose positions are controlled by two parameters within the unit circle. The appropriate selection of these parameters using graphical characteristics is given so that the desired transition band and the ripple in the passband are obtained.

The proposed filter bank is characterised by reduced spectral overlap as well as reduced spectral hole between adjacent channels when compared to the conventional Frequency Sampling (FS) structures. As a result, the signals at the outputs of the proposed bandpass filters are less correlated. This property is expected to lead to improved convergence rate characteristics. The proposed filter bank also possesses the desirable features in that it is modular and has approximately linear phase characteristics in the passband.

The analysis of minimum of Mean-Squared-Error (MSE), excess MSE and convergence condition was also given and compared with Tapped-Delay-Line (TDL) method. Computer simulations for Adaptive Line Enhancer (ALE) application were included to demonstrate the performance of the proposed structure. Under the same steady-state MSE conditions, the performance of the proposed approach was compared with those obtained by the TDL and FS methods. It is clear from the results that the proposed approach provides superior performance in terms of improved convergence rate as expected.

CHAPTER 6:

Parallel IIR Adaptive Line Enhancer

6.1 Introduction

This chapter considers the use of an IIR Parallel Adaptive Line Enhancer (PALE) for enhancement and frequency estimation of sinusoids buried in noise. The problems resulting from local minima and saddle points associated with the error surface of the conventional PALE are addressed and a new structure is proposed as a solution.

ALE's based on the TDL filter and FS structures require a large number of adaptive weights to provide adequate enhancement of sinusoidal signals. In an effort to reduce the number of weights, adaptive IIR filtering has been proposed for ALE application. Different forms of implementation including direct [Friedlander (1982, 1984), Rao and Kung (1984), Nehorai (1985), Ng (1987)], cascaded and parallel [Chicharo and Ng (1990a) David (1984), Hush and Ahmed. (1984), Hush *et al.* (1986), Ahmed *et al.* (1984), Kwan and Martin (1989)] structures for the IIR ALE have been suggested. In order to estimate and to enhance a number (N) of sinusoids buried in noise, the order of numerator and denominator polynomials in direct form are equal to $2N$. In modular structures, however, each module is usually composed of a second order IIR bandpass filter which is itself used to estimate one input frequency. Modular structures have some advantages when compared to the direct form implementation. Firstly,

since the order of the denominator of each module is a polynomial of order two, they offer simple stability monitoring. Secondly, estimation of frequencies which are equivalent to the resonant frequencies of the bandpass filter can be easily computed. Finally, individual components are available at the output of bandpass filters in the time domain for further processing.

Various adaptive algorithms have been proposed for the IIR ALE [Friedlander and Smith (1984), Rao and Kung (1984), Nehorai (1985), Chicharo and Ng (1990)]. Chicharo and Ng (1992) in a comparative study of various algorithms conclude that the selection of an appropriate algorithm depends on the application. They suggest, however; that for applications where the signal to noise ratio is moderate, the gradient based algorithms are suitable, particularly where minimal computational burden is desired.

This chapter presents a novel IIR PALE model structure which can be viewed as a modification of the conventional IIR PALE scheme introduced by David (1984) and Hush and Ahmed (1984). The conventional PALE is shown in Figure 6.1 which is composed of parallel IIR bandpass filters whose peaks are allowed to vary adaptively. One problem associated with the conventional recursive PALE is that its error surface is not quadratic. Therefore, if gradient-based algorithms are used the adaptive parameters may converge to local minima or saddle points. For the situations where the input frequencies are completely unknown *a priori,* it has been recommended to initialise the adaptive parameters at equally spaced intervals in the range from dc to $f_s / 2$ [Hush and Ahmed (1984)]. However, even if the initial values are chosen as suggested, it is possible for some of the parameters to get trapped in the saddle points or local minima.

For the proposed structure, the error signal is established separately for each module as depicted in Figure 6.2. It will be shown that this modification provides an effective means of retrieving all the input sinusoidal components for situations where there is no *a priori* information regarding the location of the input frequencies.

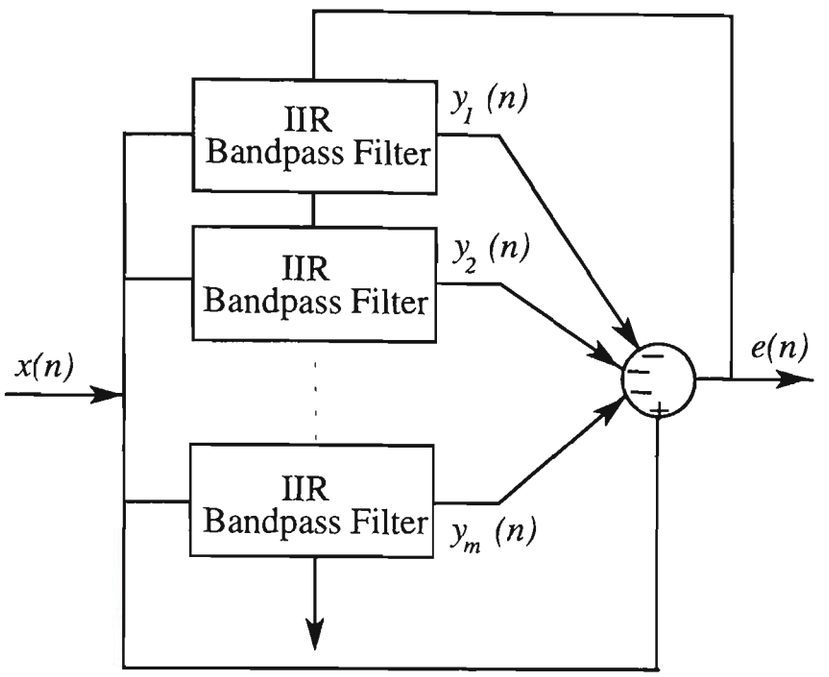

Figure 6.1: Conventional parallel recursive ALE.

Gradient-based algorithms such as Recursive Prediction Error (RPE) and Pseudolinear Regression (PLR) algorithms for the proposed structure are derived. These algorithms have been found to converge under a wide variety of conditions and are very straightforward to implement in real time [Bitmead *et al.* (1986), Widrow and Stearns (1986)]. Error surface analysis is used to provide some insight into the convergence behaviour of the given structure. It is shown that the error surface of successive modules in the proposed structure are improved by the module which has just converged to a particular frequency. In this aspect, the proposed PALE model structure can be regarded as a hybrid combination of conventional parallel and cascaded configuration.

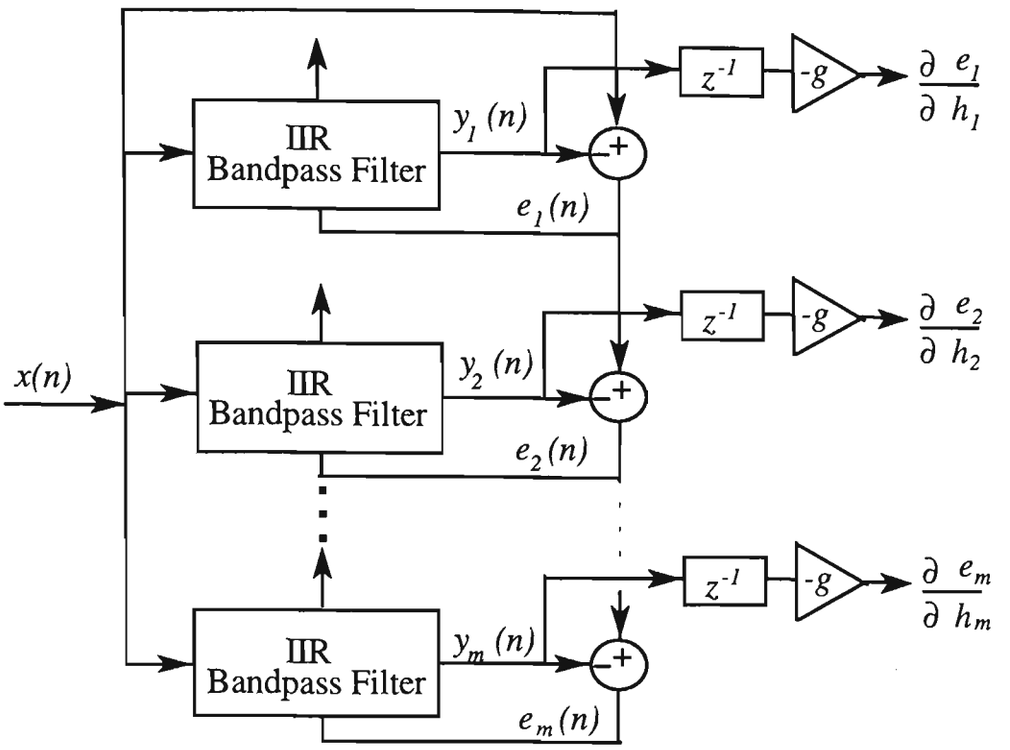

Figure 6.2: The proposed IIR parallel ALE.

Extensive experiments were performed and the results show that the proposed method has similar convergence rates as the cascaded configuration. However, it is superior to the serial structure in terms of phase and amplitude distortion associated with individual sinusoids. In other words, each sinusoid only passes through one module rather than successive modules as in the case of cascaded structures. It is worth noting that parallel structures have the lower degradation in performance due to quantisation noise for a fixed number of bits and round off accumulation error when compared with direct or cascaded configurations [Rabiner and Gold (1975), Liu and Kaneko (1969)].

The proposed structure is very suitable for the detection of a set or comb of frequencies which are used in Frequency Comb Multiple Access (FCMA) scheme [Stevenson and Yates (1989)]. The FCMA scheme is efficient in the sense that the information is carried within the phase and frequency of each sinusoid. The receiver requires the detection of many frequencies across the transmission bandwidth. The detection is commonly performed using the FFT

technique. For situations where the signal frequencies are prime factor, the DFT (or equivalently FFT) requires a large number of samples to accurately estimate the parameters of the sinusoids thus resulting in an increased acquisition time as stated earlier. In such cases, the proposed technique can be considered as an alternative method. Once the bandpass filters in the PALE structure converges to the input sinusoidal locations, the input frequencies become equivalent to the resonant frequencies of the bandpass filters. Since the individual sinusoids are available at the outputs, the CNFT algorithm developed in Chapter 2 can be employed to obtain the phase and amplitude associated with each sinusoid.

This chapter is organised as follows: In Section 6.2, the IIR bandpass filter parametisation is presented. The adaptive algorithm is derived in Section 6.3 while the error surface analysis is given in Section 6.4. Simulation results are included in Section 6.5 and finally, Section 6.6 concludes the paper.

6.2 The IIR Bandpass Filter Parametisation

A number of filter parametisations have been suggested for a second order module of IIR bandpass filter. One such parametisation is the bilinear bandpass filter which is computationally more efficient [Kwan and Martin (1989)] when compared to the filter structure proposed by Chicharo and Ng (1990), David (1984) and Hush and Ahmed (1984). Further, it provides unbiased frequency estimates when the input signal is composed of single sinusoid buried in white noise [Kwan and Martin (1990)]. This filter is designed based on a bilinear transformation of a second order analogue bandpass filter and its transfer function is given by:

$$H_{BP}(h,z) = (1-g)\frac{1-z^{-2}}{1+hgz^{-1}+(2g-1)z^{-2}} \qquad (6.1)$$

where $-2 \le h \le 2$ and g is the parameter which controls the bandwidth. In order to obtain guaranteed stability it is necessary to satisfy the inequality; $0.5 \le g < 1$. The parameter g determines the bandwidth of the filter and the centre frequency can be set independently from the bandwidth of the filter and is given by [see Appendix (A)]:

$$f_p = \frac{1}{2\pi}\cos^{-1}\left(\frac{-h}{2}\right) \tag{6.2}$$

Using the above bandpass filter for the ALE, the parameter h is adapted such that the centre frequency is located at the input spectral lines. The parameter g is either fixed or time varying during the adaptation process. In order to speed up the convergence, a wider bandwidth can be used at the beginning of the process [David (1986), Nehorai (1985)]. For such cases the value of g changes according to some heuristic rule as the adaptive algorithm proceeds. After the adaptation process, the input frequency is obtained from Equation (6.2).

The above bandpass filter has exactly unity gain and zero phase characteristics at the resonant frequency. Therefore, individual enhanced sinusoids are available at the output of the bandpass filter with undistorted amplitude and phase characteristics. These signals can be used for further processing such as estimating phase and amplitude parameters. Note that the bandpass filter given by Equation (6.1) was used in Chapter 2 to enhance the known sinusoids buried in noise.

6.3 Gradient-Based Adaptive Algorithms

Gradient-based adaptive algorithms are used to adjust the h coefficients in the bandpass filter transfer functions. From Figure 6.2, the error signals are described as follows:

$$e_i^2(n) = x(n) - \sum_{j=1}^{i} y_j(n) \tag{6.3}$$

where $y_i(n)$ is the output of i th bandpass filter. The recursive gradient-based formula for updating the coefficients is given by [Widrow and Stearns (1986)]:

$$h_i(n+1) = h_i(n) - \mu_i \nabla_{h_i} \tag{6.4}$$

where μ_i is a positive scalar step size which controls the algorithm convergence rate and ∇_{h_i} is the partial derivative of the mean squared error with respect to h_i. The goal of this algorithm is to search for the values of h_i which minimises the mean squared error $\zeta_i = E[e_i^2(n)]$. For on-line processing the error signal is examined at each instant of time and an instantaneous estimate of ζ_i is used and given by $\zeta_i = e_i^2(n)$. Although this approximation leads to noisy estimates of the filter coefficients, it provides a simple and computationally efficient approach. A normalised factor based on the instantaneous estimate of power of the gradient signal can be used which makes the algorithm faster as well as providing good performance in low SNR situations [Chicharo and Ng (1990a), Hush and Ahmed (1984)]. The normalisation factor is incorporated in Equation (6.4) as follows:

$$h_i(n+1) = h_i(n) - \mu_i \frac{\nabla_{h_i}}{\varepsilon + \Gamma_i} \tag{6.5}$$

ε is a small real number to ensure that division by zero does not occur. Γ_i is a smoothed estimate of the power of the ∇_{h_i} and is given by:

$$\Gamma_i(n+1) = \gamma \Gamma_i(n) + (1-\gamma) \nabla_{h_i}^2 \tag{6.6}$$

γ is a forgetting factor in the range of $0 < \gamma < 1$ and provides an averaging effect. The derivative of the squared error (Equation (6.3)) with respect to h_i results in:

$$\nabla_{h_i} = -2e_i(n)\frac{\partial y_i}{\partial h_i} = -2e_i(n)y_i^f(n) \tag{6.7}$$

where $y_i^f(n)$ is the filtered version of $y_i(n)$ and is an estimate for $\frac{\partial y_i(n)}{\partial h_i}$. Taking the derivative of the output of the i th bandpass filter with respect to h_i, we have:

$$\frac{\partial y_i(n)}{\partial h_i} = -g y_i(n-1) - h_i g \frac{\partial y_i(n-1)}{\partial h_i} - (2g-1)\frac{\partial y_i(n-2)}{\partial h_i} \tag{6.8}$$

Assuming that the adaptation step size μ_i is chosen sufficiently small, the coefficients adapt slowly and the following approximation is valid:

$$\frac{\partial y_i(n-1)}{\partial h_i(n)} \approx \frac{\partial y_i(n-1)}{\partial h_i(n-1)} \quad ; \quad \frac{\partial y_i(n-2)}{\partial h_i(n)} \approx \frac{\partial y_i(n-2)}{\partial h_i(n-2)} \tag{6.9}$$

Therefore, Equation (6.7) leads to the following recursive form:

$$y_i^f(n) = -gy_i(n-1) - gh_i y_i^f(n-1) - (2g-1)y_i^f(n-2)\} \tag{6.10}$$

Using Equation (6.10) together with Equations (6.5), (6.6) and (6.7), provides the means for updating the coefficients. This algorithm is referred to as a Recursive Prediction Error (RPE) method and can be further simplified by ignoring the recursive part of Equation (6.10), that is [Shynk (1989b)]:

$$y_i^f(k) = -g\{y_i(k-1)\} \tag{6.11}$$

The resulting algorithm is often referred to as an approximate gradient or Pseudolinear Regression (PLR) algorithm [Shynk (1989b)]. It is interesting to note that the gradient signal is easily implemented by multiplying the one step delay of the output of the bandpass filter by the value of g (see Figure 6.2).

6.4 Error Surface Analysis

In this section, error surface analysis is employed to provide some insight into the convergence behaviour of the proposed structure. It is well known that IIR filters can produce nonquadratic error surfaces with local minima and saddle points. Hence special care must be taken when gradient search techniques are used [Widrow and Stearns (1986)]. First, the error surface associated with each module of the proposed structure is derived. It is shown that these error surfaces have minima occurring at the input frequency locations as well as local minima and saddle points. Based on the characteristics of these error surfaces, then a novel scheme is presented so that convergence to the saddle points and local minima is avoided. The error signal associated with the first module is given by [Stearns (1981), Chicharo and Ng (1990a), Chicharo (1992)]:

$$E(e_1^2) = \frac{1}{2\pi j}\oint \Phi_{xx}(z)\left|1 - H_{BP}^1(h_1, z)\right|^2 \frac{dz}{z} \tag{6.12}$$

where $H_{BP}^1(h_1, z)$ is given by Equation (6.1) and $\Phi_{xx}(z)$ is the power spectrum of the input signal and the path of integration is along the unit circle on the z-plane. It is assumed that the input signal is composed of multiple sinusoidal components buried in white noise of power σ_n^2. Hence, the power spectrum will be equal to:

$$\Phi_{xx}(z) = \frac{1}{2}\sum_{k=1}^{m} C_k^2 + \sigma_n^2 \tag{6.13}$$

where C_i is the amplitude of the i th input frequency. Substituting Equation (6.13) into Equation (6.12) we obtain:

$$\begin{aligned} E(e_1^2) = {} & \frac{C_1^2}{2}\left|1 - H_{BP}^1(h_1, \omega_1)\right|^2 + \cdots + \frac{C_m^2}{2}\left|1 - H_{BP}^1(h_1, \omega_m)\right|^2 \\ & + \frac{\sigma_n^2}{2\pi}\int_0^{2\pi}\left|1 - H_{BP}^1(h_1, \omega)\right|^2 d\omega \end{aligned} \tag{6.14}$$

Using the analytical solution given in Appendix D, the integral on the right hand side of Equation (6.14) is:

$$\frac{1}{2\pi}\int_0^{2\pi}\left|1 - H_{BP}^1(h_1, \omega)\right|^2 d\omega = g \tag{6.15}$$

Note that the output noise power does not depend on the updated filter coefficient. The output noise power only depends on the bandwidth control parameter. This property leads to asymptotically unbiased frequency estimates for the case where the input signal is composed of a single sinusoid buried in white noise. A straightforward proof is given in Appendix E. Figure 6.3(a) shows the error surface associated with $E(e_1^2)$. In this case we have three ($m = 3$) sinusoids buried in white noise. The sinusoidal components have an amplitude equal to 5, while the white noise is zero mean with unit variance. It is evident that the error surface has three unique minima, one corresponding to each of the input frequencies. If the first module is initialised at -2, it converges to the

closest minimum to the dc frequency ($h_1 \rightarrow h_1^*$) provided the step size factor is sufficiently small. Therefore the error surface associated with the second module ($E(e_2^2)$) is given by:

$$E(e_2^2) = \frac{1}{2\pi}\int_0^{2\pi} \Phi_{xx}(\omega)\left|1 - H_{BP}^1(h_1^*, \omega) - H_{BP}^2(h_2, \omega)\right|^2 d\omega \qquad (6.16)$$

Equation (6.16) is computed by using a numerical algorithm developed by Astrom *et al.* (1970) for evaluating complex integrals of this form. The error surface given by Equation (6.16) is depicted in Figure 6.3(b). It has a saddle point at dc frequency, one maximum corresponding to the frequency which has been detected by the first module and two minima related to the two left frequencies in the input signal. When module one has converged, the value of the next parameter (h_2) must lie on the right hand side of the maximum of the error surface. This can be achieved simply by checking the second adaptive parameter at each time step to ensure that it is greater than h_1. Otherwise, it may converge to the saddle point which occurs at dc. Once the second parameter has converged to the next minimum ($h_2 \rightarrow h_2^*$), the error surface for the third module ($E(e_3^2)$) is expressed as:

$$E(e_3^2) = \frac{1}{2\pi}\int_0^{2\pi} \Phi_{xx}(\omega)\left|1 - H_{BP}^1(h_1^*, \omega) - H_{BP}^2(h_2^*, \omega) - H_{BP}^3(h_3, \omega)\right|^2 d\omega \qquad (6.17)$$

Equation (6.17) was computed and the result is shown in Figure 6.3(c). In this case, there exits two maxima, two saddle points and one minimum. The maxima occurs at the frequencies which have already been identified by the previous modules. The minimum corresponds to the third component in the input signal. The third module converges to this minimum provided the parameter h_3 is located on the right hand side of the second maximum.

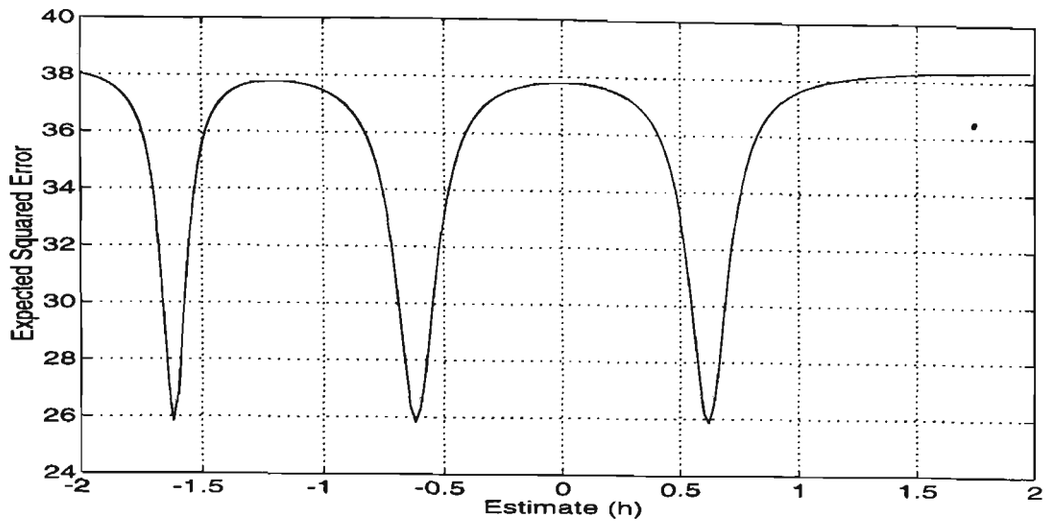

(a)

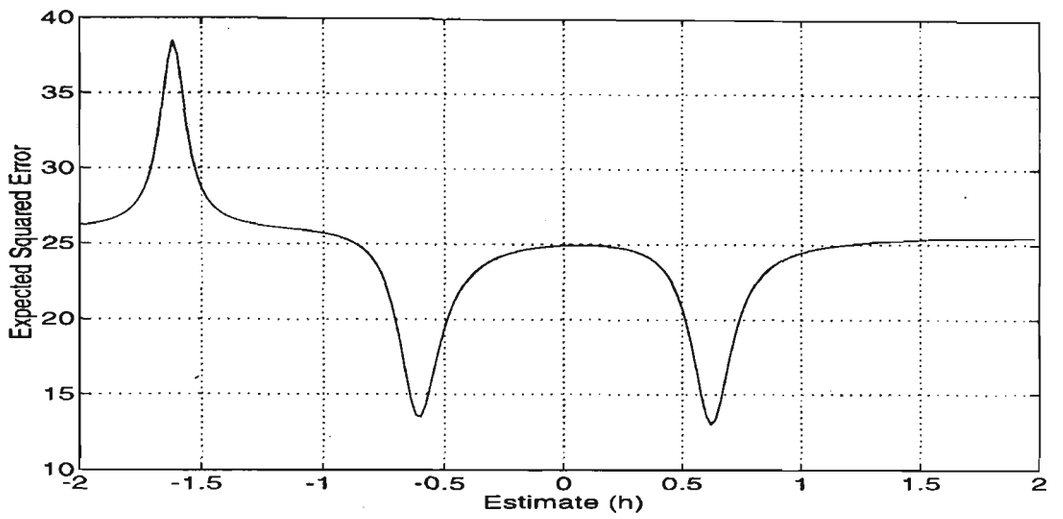

(b)

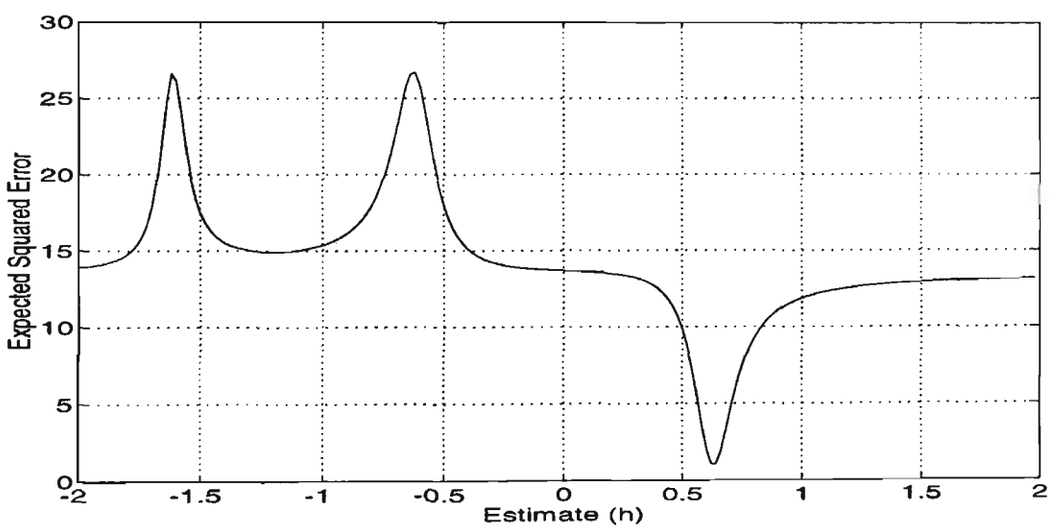

(c)

Figure 6.3: The error surfaces associated with a) $E(e_1^2)$, b) $E(e_2^2)$, c) $E(e_3^2)$,

$C_1 = C_2 = C_3 = 5$, $\sigma_n = 1$, $h_1^* = -1.618$, $h_2^* = -0.618$, $h_3^* = 0.618$.

From the error surfaces shown in Figure 6.3, it is evident that each module converges to optimum weights provided $h_{i+1} > h_i$ during the adaptation process. This can be easily accomplished by checking the adaptive parameters at each time instant to see if h_{i+1} is greater than h_i, and if not, to replace h_{i+1} by a value slightly bigger than h_i. If all the adaptive parameters are identically initialised close to -2, the whole frequency range is swept by the adaptive algorithm. Once the i th module has converged, the next adaptive parameter is placed at an appropriate location which ensures the convergence to the next optimum weight. In this way, the first module converges to the minimum closest the dc frequency and the next modules converge to the next minimum and so on.

Now consider the situation where the number of modules are greater than the number of input frequencies. In this case the error surfaces of the last modules have saddle points at half the sampling frequency. As a result, the last adaptive parameters will converge to the value of 2. This fact may be used for determining the number of input components without any further processing.

6.5 Simulation Results

Computer simulations were used to establish the performance of the proposed structure and adaptive processes described in the previous sections. The objective is to show that although the performance surface is not uni-modal, the proposed scheme is able to identify all input frequencies. First consider the case where the input sequence is composed of 3 sinusoids buried in zero mean, unit variance white noise and three modules are used. The input data is expressed as follows:

$$x(n) = \sum_{i=1}^{3} C_i \sin(2\pi f_i n) + \upsilon(n) \qquad (6.18)$$

The amplitude of each component is set to the value of 5 and the input normalised frequencies are equal to 0.1, 0.2 and 0.3. The actual values of adaptive parameters, h_1, h_2 and h_3 are -1.618, -0.618 and 0.618, respectively. Using the RPE algorithm, the parameter estimate trajectories for the conventional parallel structure is depicted in Figure 6.4. For this case we have assumed that the frequencies are completely unknown, so the initial values for adaptive parameter are set in a comb pattern in the possible range of h which is between -2 and 2. It is seen that only two frequencies have been identified and one parameter has been trapped in a local minima. The results of the trajectories of the estimates using the suggested scheme and RPE algorithm are plotted in Figure 6.5 which clearly shows that all frequencies have been successfully identified.

Under the same signal conditions and filter bandwidth (g), simulation tests were also conducted for the cascaded configuration using the RPE algorithm. It was observed that the proposed structure provides the same convergence speed as the cascaded implementation under the same steady state Mean-Squared-Error (MSE) conditions. The same steady state error conditions can be achieved by using the same bandwidth and step size factor for both methods. The trajectories of the estimates for the serial configuration are given in Figure 6.6(a). A typical learning curve for the third module of the serial configuration is also shown in Figure 6.6(b). For comparison purposes, the learning curve of the proposed method is also included. Note that in the serial structure, individual sinusoids are distorted in phase and amplitude by successive filter characteristics. For example, the third sinusoid must pass through those filters which have already been converged to the other input frequencies. While in the proposed structure, the input sinusoid only passes through one filter which also possesses approximately linear phase characteristics.

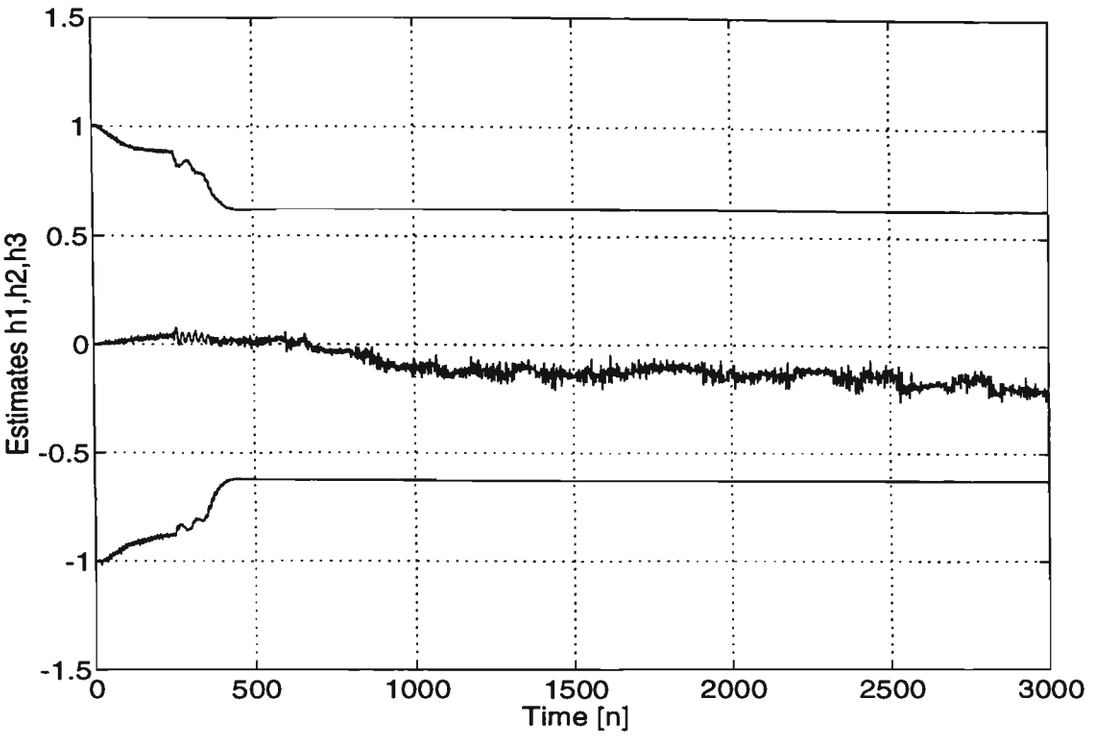

Figure 6.4: Parameter estimate trajectories for conventional PALE using RPE algorithm, $C_1 = C_2 = C_3 = 5$, $\sigma_n = 1$, $g = 0.95$, $\gamma = 0.95$, $\mu_1 = \mu_2 = \mu_3 = 0.008$, $h_1^* = -1.618$, $h_2^* = -0.618$, $h_3^* = 0.618$.

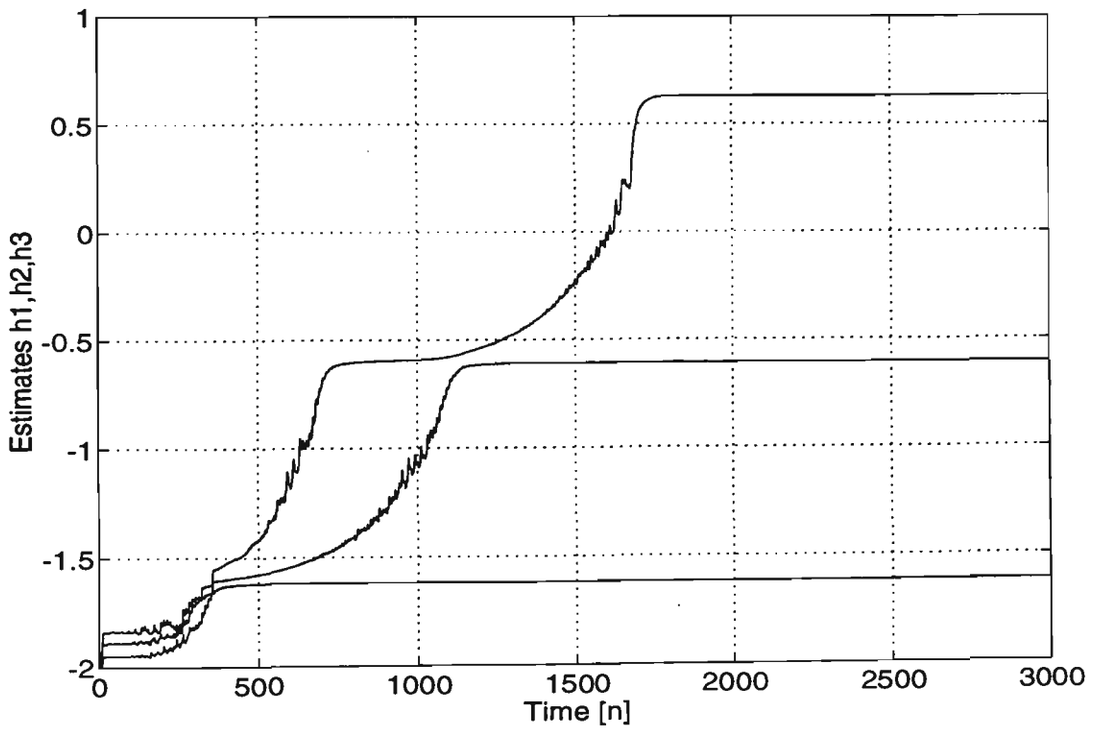

Figure 6.5: Parameter estimate trajectories for the proposed PALE using RPE method, $C_1 = C_2 = C_3 = 5$, $\sigma_n = 1$, $\mu_1 = \mu_2 = \mu_3 = 0.008$, $g = 0.95$, $\xi = 0.95$, $h_1^* = -1.618$, $h_2^* = -0.618$, $h_3^* = 0.618$.

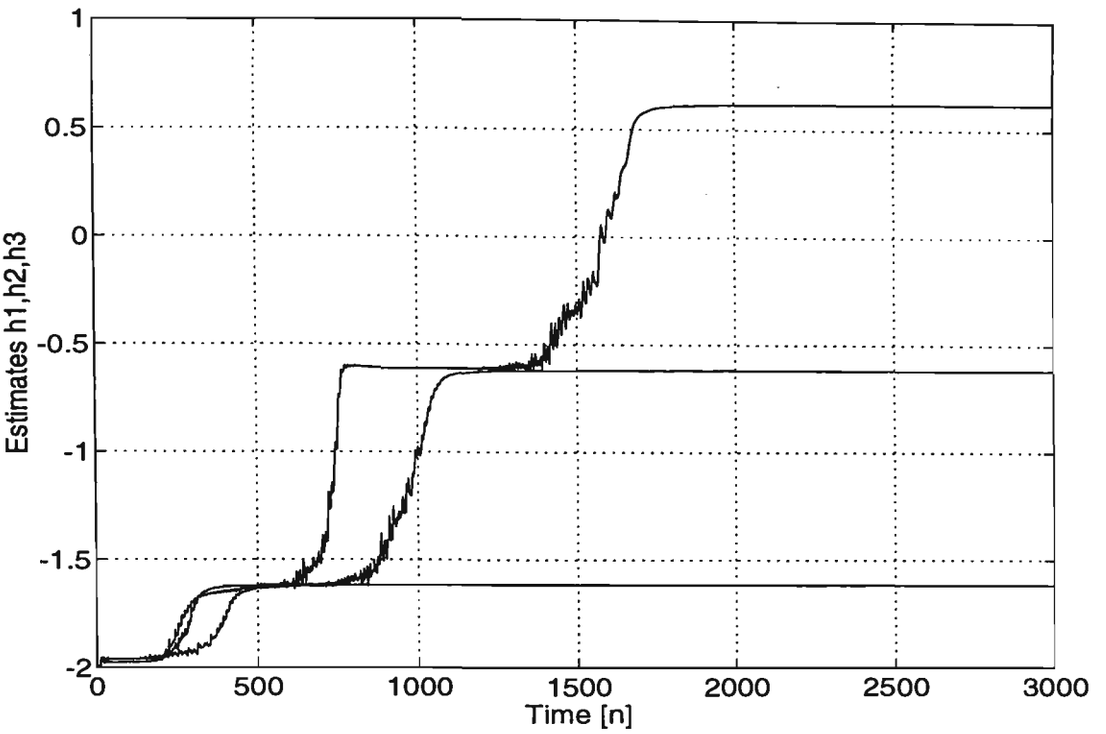

(a)

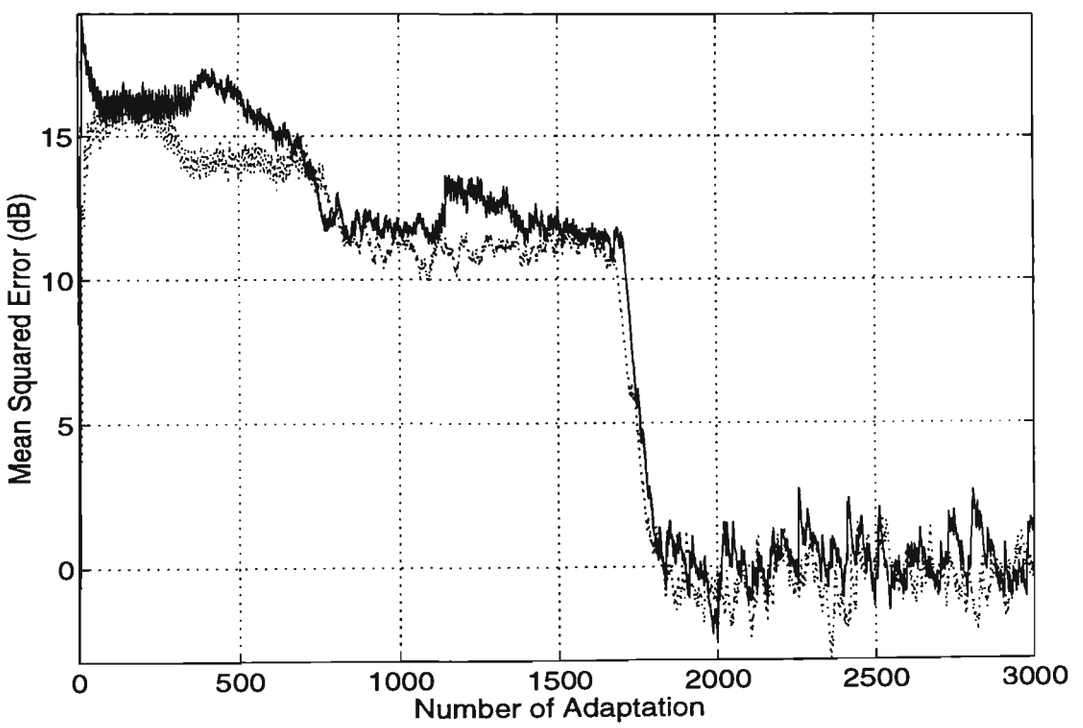

(b)

Figure 6.6: (a) Parameter estimate trajectories for serial configuration using RPE method, $C_1 = C_2 = C_3 = 5$, $\sigma_n = 1$, $g = 0.95$, $\gamma = 0.95$, $\mu_1 = \mu_2 = \mu_3 = 0.008$, $h_1^* = -1.618$, $h_2^* = -0.618$, $h_3^* = 0.618$, (b) Learning curves of the third module in the proposed (solid line) and serial (dotted line) structures.

Extensive simulation tests were also performed and it was observed that by using the PLR algorithm, the parameters converge to the minima corresponding to the input frequencies without the need for a checking procedure as suggested in the previous section. A typical result is depicted in Figure 6.7. From Figure 6.7, it is evident that when the first module has converged, the second and the third adaptive parameters are located in the vicinity of a local minimum (see Figure 6.3). However, they successfully converged to the optimum weights (h_2^* and h_3^*). This result is consistent with those reported in [Ng (1987)] where an Adaptive Notch Filtering (ANF) was implemented using a direct form structure. Ng (1987) showed by simulation results that the PLR algorithm for ANF may work when RPE method does not. Figure 6.8 plots the parameter estimate trajectories for the case when the number of input components were equal to 2 while four modules were used. It is seen that the parameters of the last two modules have converged to the saddle points which occurs at the value of 2. One can possibly use this fact to determine the number of sinusoids present in the input signal.

6.6 Conclusion

The existence of local minima and saddle points in the error surface associated with the conventional parallel IIR adaptive line enhancer was discussed. It was stated that because of these characteristics the adaptive weights may converge to local minima and saddle points if gradient search algorithms are used.

The conventional parallel structure was modified such that the convergence to local minima is avoided. The proposed structure employs a bilinear transformed second order IIR bandpass filter as a building block. The normalised Recursive Prediction Error (RPE) and Pseudolinear Regression (PLR) algorithms were derived for the proposed filter parametisation.

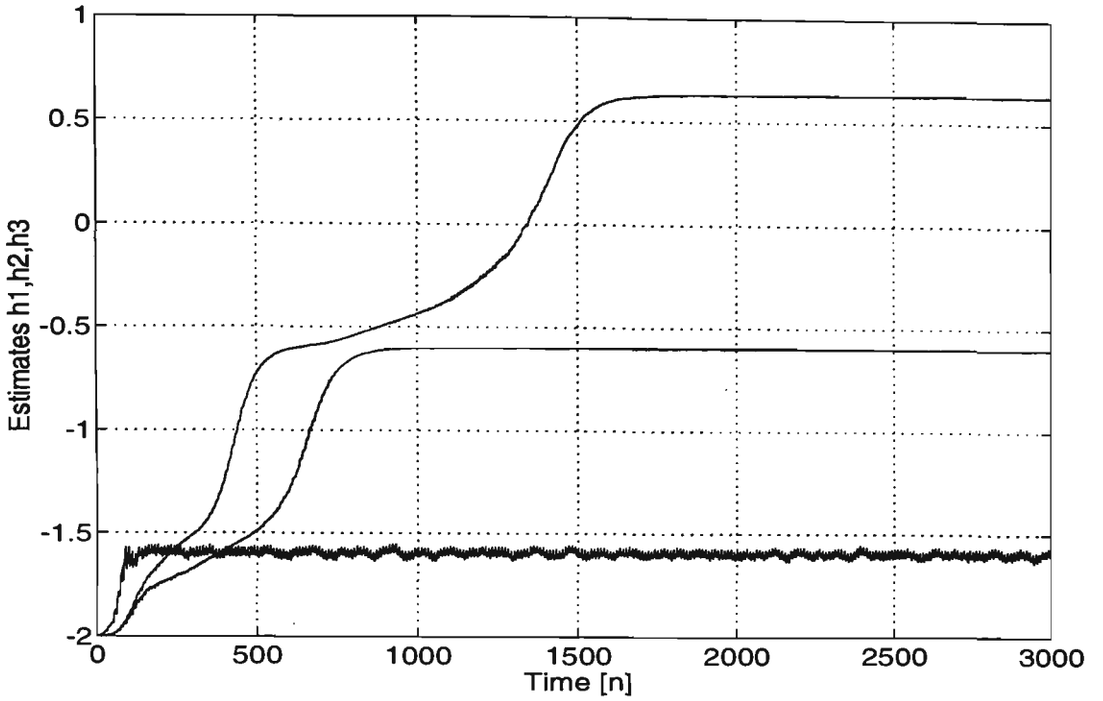

Figure 6.7: Parameter estimate trajectories for the proposed PALE using PLR algorithm, $C_1 = C_2 = C_3 = 5, \sigma_n = 1$, $m_1 = m_2 = m_3 = 0.008$, $g = 0.95$, $g = 0.95$, $h_1^* = -1.618$, $h_2^* = -0.618$, $h_3^* = 0.618$.

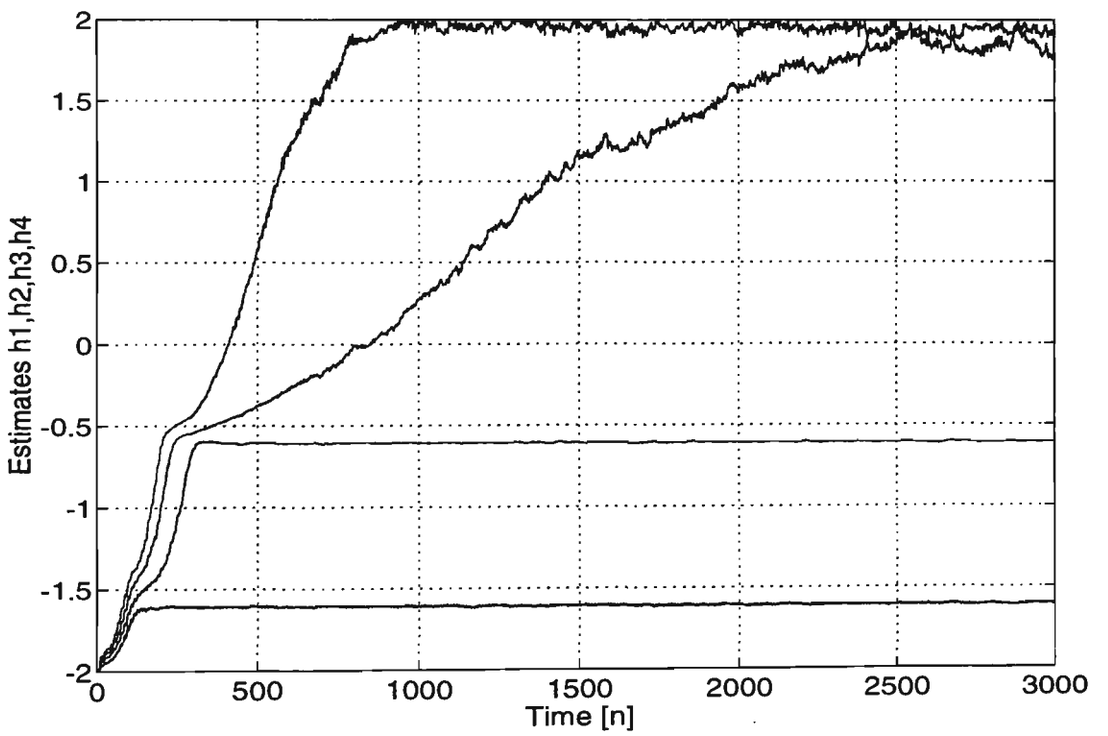

Figure 6.8: Parameter estimate trajectories when the input signal is composed of two components and four modules are used in the proposed PALE structure, $\mu_1 = \mu_2 = \mu_3 = \mu_4 = 0.003$, $C_1 = C_2 = 5$, $\sigma_n = 1$, $g = 0.95$, $\gamma = 0.95$, $h_1^* = -1.618$, $h_2^* = -0.618$.

Based on error surface analysis, it was shown that although the proposed structure is not unimodal, its convergence characteristics are predictable if all the parameters are properly initialised. Accordingly, a new scheme was developed which successfully detects the input frequencies even in situations where *a priori* information regarding the location of the input frequencies does not exist.

The convergence speed of the proposed structure is similar to that of the serial configuration. However, it is superior to the cascaded structures in the sense that we expect to obtain reduced phase and amplitude distortion of the enhanced sinusoidal components. Simulation tests were conducted to evaluate the proposed configuration and the results are compared with those of the conventional parallel and cascaded structures.

CHAPTER 7:

Conclusions and Suggestions for Further Research

7.1 Conclusions

This thesis deals with the enhancement of noise-corrupted sinusoidal components as well as the estimation of amplitude, phase and frequency of each constituent sinusoid. Several new techniques were developed to accurately estimate the parameters of the sinusoids. Chapters 2, 3 and 4 consider the problem of sinusoidal estimation when the frequency locations are known in advance while Chapter 5 and 6 deal with the situations where sinusoidal frequencies are unknown.

Chapter 2 assumed *a priori* knowledge of the input frequency locations and presented a new sliding algorithm for estimating the amplitude and phase of the Fourier coefficients of noise corrupted harmonic signals. The proposed method was similar in principle to the Notch Fourier Transform (NFT) technique suggested by Tadokoro and Abe (1987) except that it employs an Infinite Impulse Response (IIR) rather than a Finite Impulse Response (FIR) notch filter parametisation. This modification provides a bandwidth controlled filter bank whose resonant frequencies are equally spaced in the frequency spectrum. In this sense the proposed technique can be regarded as a Constrained Notch Fourier Transform (CNFT). This structure is most suitable for the enhancement and characterisation of harmonic signals. The filter bank was designed such that

phase characteristics of each bandpass filter become equal to zero at the resonant frequency. Therefore, the retrieved signal can be obtained in the time domain with the same phase and amplitude as the input signal. The bandwidth control parameter offers an efficient means for obtaining the required enhancement without necessarily increasing the order of the filter as it is in the NFT filter bank structure. Therefore a substantial saving in memory storage is achieved. The NFT filter bank was found to be equivalent to the real valued Frequency Sampling (FS) structure which has an FIR parametisation.

Chapter 2 also proposed a similar technique to the CNFT for the signals containing sinusoids at arbitrarily (i.e., nonequally spaced) known frequencies. The main feature of the modified CNFT is that it uses a second order IIR bandpass filter whose bandwidth and centre frequency can be adjusted independently. In this approach, the bandwidth control facility provides the user with an effective means of achieving the required resolution as well as reducing spectral leakage.

New sliding computational algorithms were derived for both the NFT [Tadokoro and Abe (1987)] and CNFT filter banks for the purpose of estimating the Fourier coefficients of the sinusoidal components. The sliding NFT algorithm has similar parametisation to the real valued conventional Goertzel algorithm except that it is presented in a sliding form. The given algorithms estimate the parameters (phase and amplitude) of individual components at every sample update.

The proposed approach provides an interesting interpretation for the relationship between the frequency resolution and the required acquisition time. Both methods provide accurate estimates once the transient of the filter has elapsed. The transient time itself depends on the bandwidth; that is, as the bandwidth

reduces, the transient time of the filter increases (or *vice versa*). The required acquisition time in both methods (i.e., NFT and CNFT) is determined by the bandwidth of the corresponding bandpass filter parametisation. When the input frequencies are closely spaced, high resolution is required to resolve the input sinusoids. This resolution is achieved by using narrower bandwidth bandpass filters which also results in increased acquisition time. Based on this approach, there is a trade off between the frequency resolution and the acquisition time.

In the NFT method the bandwidth depends on the order of the filter while in the CNFT method it depends to a large extent on the contraction pole factor. It was observed that the same acquisition time is obtained if both methods have same bandwidth (as expected). However, in situations where the input frequencies are mutually prime factor the proposed second order IIR bandpass filter together with the CNFT sliding algorithm yields faster acquisition time than the NFT method. This is due to the fact that the IIR bandpass filter can be tuned arbitrarily while the resonant frequencies of the NFT are constrained to be equally spaced. The NFT yields accurate estimates provided that the spectral lines fall exactly at the resonant frequencies. In order to obtain a bandpass filter at the desired frequency location, the NFT requires a higher order bandpass filter thus resulting in increased acquisition time. Simulation tests were conducted to evaluate the relative performances of both the NFT and the CNFT methods.

In Chapter 3, the Generalised Frequency Sampling (GFS) filter bank together with the CNFT algorithm was proposed for the sliding coefficient estimation of sinusoidal components given *a priori* information of the input frequencies. The GFS structure was derived based on the Least Mean Square (LMS) spectrum analyser. First, it was shown that the LMS spectrum analyser is equivalent to an IIR filter bank which has similar parametisation as the resonator based filter bank

proposed by Padmanabhan and Martin (1990). Unlike the NFT or conventional FS filter bank whose resonant frequencies and nulls are distributed uniformly, the GFS filter bank possesses a useful feature where the resonant frequencies and nulls are set arbitrarily at any desired frequency location. The resonant frequency can be tuned at the desired spectral line while the nulls are placed at other input sinusoids. As a result, leakage can be effectively minimised.

Since the gain and phase characteristics of the GFS filter bank are equal to unity and zero at the resonant frequencies, the output sinusoids have exactly the same phase and amplitude as the input sinusoids. It was shown that the GFS filter bank together with the CNFT algorithm provide faster acquisition time when compared with the conventional frequency sampling structure. It is also computationally more efficient than the direct LMS technique under similar acquisition times and accuracy conditions. Simulation tests were carried out to demonstrate the performance of the given technique and the results were compared with those of the LMS method.

In Chapter 4, the required acquisition time associated with the Discrete Fourier Transform (DFT) for estimating the sinusoidal coefficients was discussed. It was shown that the DFT requires a large number of samples when the input frequencies have a small common factor. The same problem exists for the sliding Goertzel algorithm based on the FS structure, since it is in fact equivalent to the DFT computation. In order to achieve fast detection and accurate estimation of sinusoidal parameters, a new sliding Goertzel algorithm was developed based on a second order digital resonator. The proposed technique exhibits good performance in low signal to noise ratio (SNR) conditions. This was verified by extensive simulation tests which were carried out under different SNR conditions. Further, the algorithm provides the following advantages when

compared with the conventional and modified Goertzel algorithms. Firstly, it computes Fourier coefficients in less than one signal period. Therefore, faster detection time is achieved particularly when the mutual common factor of the input frequencies is small. Secondly, the algorithm is quite suitable for the situations where the sinusoidal parameters (phase and amplitude) are time varying. Finally, it is less prone to numerical overflow problems in fixed-point arithmetic implementation. Simulation tests were carried out to demonstrate the performance of the proposed algorithm and the results were compared with those obtained by the conventional and modified Goertzel algorithms.

A new modular IIR FS filter bank was presented in Chapter 5, for adaptive line enhancement applications. The technique can be used for the situations where the input frequencies are not known *a priori*. The proposed filter bank is composed of a constrained IIR comb filter followed by a bank of digital resonators. The characteristics of the filter bank in terms of the transition band and the amount of ripple in the passband were given. A design procedure using characteristic graphs was presented which can be used for selection of appropriate comb filter parameters. The structure preserves the modularity of the FS filter bank while providing reduced spectral overlap as well as minimal spectral hole between adjacent channels.

By using the proposed IIR FS filter bank together with a self-orthogonalising LMS algorithm, faster convergence was achieved when compared with conventional adaptive FS methods. This is expected since the amount of overlap among the bandpass filters is significantly reduced. Analysis was given to provide insight into the minimum Mean-Squared-Error (MSE), steady-state excess MSE and convergence conditions of the adaptive FS filter bank technique. The minimum and excess MSE of the FS filter bank approach were obtained and

compared with those of the conventional and normalised LMS algorithms. The analysis showed that under the same excess MSE the convergence rate of the adaptive FS method is faster than that of the TDL method. It is well known that the convergence speed associated with the TDL is slow when the eigenvalues of the input autocorrelation matrix are widely spread. The eigenvalue disparity is due to large spectral dynamic range of the input signals. If the signal at the output of each bin of the filter bank is normalised, the eigenvalues of the resulting signals approach unity thus resulting in faster convergence rate. The normalisation is performed by the self-orthogonalising LMS algorithm which utilises a time varying step size factor for the adaptive weights. The step size factor is inversely proportional to the signal at the output of each bin thus resulting in faster convergence. Computer simulations were carried out to illustrate the performance of the proposed structure and the results were compared with those of the TDL and conventional FS methods.

In an attempt to reduce the computational complexity associated with TDL and FS ALE, Chapter 6 proposed a new Parallel IIR Adaptive Line Enhancer (PALE). The proposed structure can be viewed as a modification of the conventional IIR PALE scheme introduced in [David (1984), Hush and Ahmed (1984)]. One of the difficulties associated with the conventional PALE is that it has a multimodal error surface. Therefore, the adaptive parameters may converge to local minima or saddle points if gradient-based algorithm is used. The conventional IIR PALE was modified such that convergence is always achieved. The structure is comprised of parallel bandpass filter modules whose resonant frequencies are adjusted by using a gradient-based algorithm. Once convergence takes place, the input frequencies are determined by the resonant frequencies of the bandpass filter. The Recursive Prediction Error (RPE) and Pseudolinear Regression (PLR) algorithms were used together with the proposed PALE structure. Error surface

analysis was employed to obtain the convergence characteristics of the given approach. It was shown that although the error surface is not unimodal, its dynamic characteristics behave in a particular pattern as each successive module converges to the input sinusoids. Based on the error surface analysis, a new heuristic scheme was developed which prevents the adaptive parameters from converging to local minima or saddle points. Extensive simulation tests were conducted to illustrate the performance of the given technique and the results are compared with those of the conventional parallel and serial structures. From the simulation results, it was evident that the convergence speed of the given structure is approximately the same as the serial configuration. However, the proposed structure is superior since the individual enhanced sinusoids are expected to have reduced phase and amplitude distortion.

7.2 Suggestions For Further Research

Some aspects of the research presented in this thesis need further investigation. This section outlines some of the important issues which need to be addressed.

7.2.1 Phase and Amplitude Estimate Accuracy

Throughout Chapter 2, 3 and 4, the accuracy of the estimates were evaluated based on Monte Carlo simulations. It would be interesting to obtain analytical values for the bias and noise variance of the estimates. For example, when using IIR bandpass filters (Chapter 2 and 3), the contribution of noise on the amplitude estimate can be obtained by approximating the output noise as a sinusoid whose frequency is equal to the resonant frequency of the bandpass filter. The amplitude of the sinusoid is determined by using equivalent noise bandwidth as discussed in [Harris (1978)].

The z-transform technique was applied, in Chapter 4, to derive the output signal of the resonator when the input signal was composed of single sinusoid. For the multiple sinusoid case, the same technique may be used to obtain the output components associated with each input frequency. From the results, it is possible to establish a relationship between the accuracy of the estimate and the acquisition time.

7.2.2 Transient Effect Reduction

It was shown that the acquisition time depends on the transient behaviour of the filter for the case of the CNFT algorithm. The amplitude and phase estimates were obtained after the transient of the filter has elapsed and the output filter has settled. It is possible to improve the proposed method by reducing the effect of the transient thus resulting in faster acquisition time. This may be accomplished by obtaining the transient characteristics of the filter and using these to provide an earlier estimates of the various parameters.

7.2.3 Finite Word Implementation

All the simulations in this thesis are carried out by using simulated data and double precision floating point arithmetic. From a practical point of view, the signals and the filter coefficients must be quantised with finite precision. The sample values of the input signal or the coefficients of the filter must rounded to the nearest quantisation level. Roundoff error resulting from arithmetic manipulation and the possibility of overflow should also be considered when using fixed-point arithmetic. All these issues may cause numerical problems and need to be examined when implementing the various algorithms developed in this thesis.

7.2.4 Comparison Between the CNFT and the RLS Algorithms

The Recursive Least Square (RLS) algorithm has also been used for estimating the parameters of sinusoidal signals [Nehorai and Porat (1986), Chicharo and Ng (1990c)]. It is known that the RLS algorithm yields faster convergence than the LMS algorithm at the cost of increased complexity. In Chapter 2, an equivalent filter bank for the LMS spectrum analyser was obtained. The resulting filter bank together with the sliding CNFT algorithm were used for the task of sinusoidal signal characterisation. This approach provided a suitable means for comparing the proposed CNFT algorithm with the LMS technique. The comparison between the proposed sliding CNFT and the RLS algorithms can be made by using the same procedure but with the RLS algorithm.

7.2.5 Other Potential Applications For the IIR FS Filter Bank

The IIR FS filter bank developed in Chapter 5 was particularly useful for the task of enhancement of spectral lines buried in noise. The adaptive IIR FS filter bank technique can also be employed for those applications in which the frequency domain information is of primary interest. Examples of such applications may be found in channel equalisation [Picchi and Prati (1984)] and system identifications [Bitmead and Anderson (1981)]. The structure is also worth applying to the frequency domain realisation of parallel IIR filtering [Shynk (1989a)]. This approach employs a zero-pole filter rather than a first order FIR filter at the output of each bandpass filter.

7.2.6 Some Open Issues of the IIR Adaptive Line Enhancer

Chapter 6 discussed the important issue of the existence of local minima and saddle points in the error surface of a PALE structure. Based on the error surface analysis, the convergence behaviour of the given PALE structure using gradient based algorithms was studied. The proposed structure was evaluated under the

assumption that the input noise is white. The application of the proposed technique for the estimation of sinusoids in the presence of coloured noise would be an interesting issue. Assuming that the noise model is known, it is feasible to extend the error surface analysis to obtain the convergence characteristics of the proposed PALE structure.

The bias of the estimates was only analysed for the single sinusoid case. Further, it was presumed that the input frequencies are constant during the adaptation process. All these imply that the instantaneous frequency estimation and analysis of the bias for multiple sinusoid case have not been examined.

In summary, the research presented in this thesis like all other research raises more questions than it answers. The outstanding problems listed above are limited to those which are most relevant to this work.

References

Ahmed N., Hush D., Elliot G. R. and Fogler R. J., "Detection of multiple sinusoids using an adaptive cascaded structure," in Proc. IEEE Int. Conf. Acoustic., Speech, Sig. Proc., pp. 21.3.1-21.3.4, March 1984.

Astrom K. J., Jury E. I. and Angiel R. G., "A numerical method for the evaluation of complex integrals," IEEE Trans. Automatic Control, pp. 468-471, August 1970.

Beraldin J. A. and Steenaart W., "Overflow analysis of a fixed-point implementation of the Goertzel algorithm," IEEE Trans. Circuits Systems, Vol. CAS-36, No. 2, pp. 322-324, February 1989.

Bitmead R. R., Anderson B. D. O., "Adaptive frequency sampling filters," IEEE Trans. Circuits Systems, Vol. CAS-28, No. 6, pp. 524-634, June 1981.

Bitmead R. R., Anderson B. D. O. and Ng T. S., "Convergence rate determination of gradient based adaptive estimators," Automatica, Vol. 22, pp. 185-191, 1986.

Braun F. G., "Nonrecursive digital filters for detecting multifrequency code signals," IEEE Trans. Acoust., Speech, Sig. Proc., Vol. ASSP-23, No. 3, pp. 250-256, June 1975.

Chicharo J. F., "High resolution spectral estimation using a specially constrained adaptive notch filter," Int. J. Electronics, Vol. 72, No. 1, pp. 57-66, 1992.

Chicharo J. F., *Theory and Application of (IIR) Adaptive Notch Filtering*, PhD thesis, university of Wollongong, 1990.

Chicharo J. F. and Ng T. S., (1990a) "Gradient-based adaptive IIR notch filtering for frequency estimation," IEEE Trans. Acoust., Speech, Sig. Proc., Vol. ASSP-38, No. 5, pp. 769-777, May 1990.

Chicharo J. F. and Ng T. S., (1990b) "Tuneable/adaptive second-order IIR notch filter," Int. J. Electronics, Vol. 68, No. 5, pp. 779-792, 1990.

Chicharo J. F. and Ng T. S., (1990c) "A Roll eccentricity sensor for steel-strip rolling mills," IEEE Trans. Industry Applications, Vol. 26, No. 6, pp. 1063-1069, December 1990.

Chicharo J. F. and Ng T. S., "A comparative study of various algorithms suitable for adaptive notch filtering applications," Journal of Electrical and Electronic Engineering, Australia-IE Aust. & IREE Aust., Vol. 12, No. 4, pp. 378-386, December 1992.

Clark G. A., Parker S. R. and Mitra S. K., "A unified approach to time- and frequency-domain realisation of FIR adaptive digital filters," IEEE Trans. Acoust., Speech, Sig. Proc., Vol. ASSP-31, No. 5, pp. 1073-1083, October 1983.

Clark G. A., Soderstrand M. A. and Johnson T. G., "Transform domain adaptive filtering using a recursive DFT," in Proc. IEEE Int. Symp. Circuits Systems, Kyoto, Japan, pp. 1113-1116, June 1985.

David R., "An extended algorithm for the second order ALE," in Proc. 19th Asilomar Conf. Signals, Systems & Computers, Pacific Grove, CA, USA, pp. 304-308, November 1985.

David R. A., "Detection of multiple sinusoids using a parallel ALE," in Proc. IEEE Int. Conf. Acoustic., Speech, Sig. Proc., pp. 21.2.1-21.2.4, March 1984.

David R. A., Stearns S. D. and Elliot G. R., "IIR algorithms for adaptive line enhancement," in Proc. IEEE Int. Conf. Acoustic., Speech, Sig. Proc., pp. 17-20, 1983.

Dentino M., McCool J. and Widrow B., "Adaptive filtering in the frequency domain," in Proc. IEEE, Vol. 66, No. 12, pp. 1658-1659, December 1978.

Farhang-Boroujeny B. and Gazor S., "Selection of orthonormal transforms for improving the performance domain normalised LMS algorithm," in Proc. IEE, Vol. 139, No. 5, pp. 327-335, October 1992.

Ferrara E. R., "Fast implementation of LMS adaptive filters," IEEE Trans. Acoust., Speech, Sig. Proc., Vol. ASSP-28, No. 4, pp. 474-475, August 1980.

Friedlander B. and Smith J. O., "Analysis and performance evaluation of an adaptive notch filter," IEEE Trans. Information Theory, Vol. IT-30, pp. 283-295, March 1984.

Friedlander B., "A recursive maximum likelihood algorithm for ARMA line enhancement," IEEE Trans. Acoust., Speech, Sig. Proc., Vol. ASSP-30, No. 4, pp. 651-657, August 1982.

Gay S. L., Hartung J. and Smith G. L., "Algorithms for multi-channel DTMF detection for the WE DSP32 family," in Proc. IEEE Int. Conf. Acoustic., Speech, Sig. Proc., pp. 1134-1137, 1989.

Glover Jr, J. R., "Adaptive noise cancelling applied to sinusoidal interferences," IEEE Trans. Acoust., Speech, Sig. Proc., Vol. ASSP-25, No. 6, pp. 484-491, December 1977.

Goertzel G., "An algorithm for the evaluation of finite trigonometric series," Amer. Math. Monthly, Vol. 65, pp. 34-35, January 1958.

Griffiths L. J., "Rapid measurement of digital instantaneous frequency," IEEE Trans. Acoust., Speech, Sig. Proc., Vol. ASSP-23, No. 2, pp. 1024-1026, April 1975.

Gupta A. K., "On suppression of a sinusoid signal in broadband noise," IEEE Trans. Acoust., Speech, Sig. Proc., Vol. ASSP-33, No. 3, pp. 1024-1026, August 1985.

Harris F. J., "On the use of windows for harmonic analysis with discrete Fourier transform", in Proc. IEEE, Vol. 66, No. 1, pp. 51-83 January 1973.

Hostetter G. H., "Recursive discrete Fourier transform," IEEE Trans. Acoust., Speech, Sig. Proc., Vol. ASSP-28, No. 2, pp. 184-190, April 1980.

Hush D. R., Ahmed N., David R. and Stearns S. D., "An adaptive IIR structure for sinusoidal enhancement, frequency estimation and detection," IEEE Trans. Acoust., Speech, Sig. Proc., Vol. ASSP-34, No. 6, pp. 1380-1390, December 1986.

Hush D. R. and Ahmed N., "Detection and identification of sinusoids in broadband noise via a parallel recursive ALE," in Proc. IEEE Int. Conf. Acoustic., Speech, Sig. Proc., pp. 1193-1196, 1984.

Jain V. K., Collins W. and Davis D. C., "High accuracy analogue measurements via interpolated FFT," IEEE Trans. Instrumentation and Measurement, Vol. IM-28, No. 2, pp. 113-122, June 1979.

Jury E. I., *Theory and application of the z-transform method*, New York: John Wiley & sons, 1964.

Koval I. and Gara G., "Digital MF receiver using discrete Fourier transform," IEEE Trans. Communications, Vol. COM-21, No. 12, pp. 1331-1335, December 1973.

Kuo S. M. and Rodrigues M. A., "An adaptive frequency-sampling line enhancer," in Proc. IEEE Int. Conf. Acoustic., Speech, Sig. Proc., pp. 317-321, 1985.

Kuo S. M. and Rodriguez M. A., "Implementation of an adaptive frequency sampling line enhancer," in Proc. IEEE Int. Conf. Acoustic., Speech, Sig. Proc., pp. 896-899, 1986.

Kwan T. and Martin K., "Adaptive detection and enhancement of multiple sinusoids using a cascade IIR filter," IEEE Trans. Circuits and Systems, Vol. CAS-36, No. 7, pp. 937-947, July 1989.

Lee J. C. and Un Kwan C., "Performance of transform-domain LMS adaptive digital filters," IEEE Trans. Circuits & Systems, Vol. CAS-34, No. 7, pp. 499-510, June 1986.

Liu B. and Kaneko T., "Error analysis of digital filters with floating point arithmetic," in Proc. IEEE, Vol. 57, No. 10, pp. 1735-1747, Oct. 1969.

Liu J. C. and Lin T. P., "A note on notch Fourier transform," IEEE Trans. Signal Proc., Vol. 40, NO. 3, pp. 690-692, March 1992.

Ljung L., "Analysis of a general recursive prediction error identification algorithm," Automatica, Vol. 17, No. 1, pp. 89-99, 1981.

Makhoul J., "Linear prediction: A tutorial review," in Proc. IEEE, Vol. 63, pp. 561-580, April 1975.

Marshall D. F., Jenkins W. K. and Murphy J. J., "The use of orthogonal transforms for improving performance of adaptive filters," IEEE Trans. Circuits, Systems, Vol. 36, No. 4, pp. 474-484, April 1989.

Martin K. W., "The isolation of undistorted sinusoids in real time," IEEE Trans. Acoust., Speech, Sig. Proc., Vol. ASSP-38, No. 2, pp. 360-363, February 1990.

McGee W. F., (1989a) "Fundamental relations between LMS spectrum analyser and recursive least squares estimation," IEEE Trans. Circuits Systems, Vol. CAS-36, No. 1, pp. 151-153, January 1989.

McGee W. F., (1989b) "Frequency interpolation filter bank," in Proc. IEEE Int. Symp. Circuits Systems, pp. 1563-1566, 1989.

Narayan S. S., Peterson A. M. and Narashima M. J., "Transform domain LMS algorithm," IEEE Trans. Acoust., Speech, Sig. Proc., Vol. ASSP-31, No. 3, pp. 609-614, June 1983.

Narayan S. S. and Peterson A. M., "Frequency domain least-mean-square algorithm," in Proc. IEEE, Vol. 69, No. 1, pp. 124-126, January 1981.

Nehorai A., "A minimal parameter adaptive notch filter with constrained poles and zeros," IEEE Trans. Acoust., Speech, Sig. Proc., Vol. ASSP-33, No. 4, pp. 938-996, August 1985.

Nehorai A. and Porat B., "Adaptive comb filtering for harmonic signal enhancement," IEEE Trans. Acoust., Speech, Sig. Proc., Vol. ASSP-34, No. 5, pp. 1124-1136, October 1986.

Ng T. S., "Some aspects of an adaptive digital notch filter with constrained poles and zeros," IEEE Trans. Acoust., Speech, Sig. Proc., Vol. ASSP-35, No. 2, pp. 158-161, February 1987.

Ogunfunmi A. and Peterson A., "Adaptive methods for estimating amplitudes and frequencies of narrowband signals," in Proc. IEEE Int. Symp. Circuits Systems, pp. 2124-2127, 1989.

Oppenheim A. V., Schafer R. W., *Discrete-Time Signal Processing.* Englewood Cliffs, NJ: Prentice-Hall, 1989.

Padmanabhan M. and Martin K., "Resonator-based filter-banks for frequency-domain applications," IEEE Trans. Circuits Systems, Vol. CAS-38, No. 10, pp. 1145-1159, October 1987.

Picchi G. and Prati G., "Self-orthogonalising adaptive equalisation in the discrete frequency domain," IEEE Trans. Communications, Vol. COM-32, No. 4, pp. 371-379, April 1984.

Peceli G., "Resonator-based digital filters," IEEE Trans. Circuits Systems, Vol. CAS-36, No. 1, pp. 156-159, January 1989.

Petraglia M. R. and Mitra S. K., "On the use of filter banks in adaptive filtering," in Proc. 22nd Asilomar Conf. Signals, Systems & Computers, Pacific Grove, CA, USA, pp. 821-833, October 1988.

Rabiner L. R., and Gold B., Rader, C. M., *Theory and Application of Digital Signal Processing*. Englewood Cliffs. NJ: Prentice-Hall, 1975.

Rao D. V. B. and Kung S. Y., "Adaptive notch filtering for the retrieval of sinusoids in noise," IEEE Trans. Acoust., Speech, Sig. Proc., Vol. ASSP-32, No. 4, pp. 791-802, August 1984.

Reddy V. U., Edgardt B. and Kailath T., "Optimised lattice-form adaptive line enhancer for a sinusoidal signal in broadband noise," IEEE Trans. Acoust., Speech, Sig. Proc., Vol. ASSP-29, No. 3, pp. 702-710, June 1981.

Rickard J. T. and Zeidler J. R., "Second-order output statistics of the adaptive line enhancer," IEEE Trans. Acoust., Speech, Sig. Proc., Vol. ASSP-27, No. 1, pp. 31-39, February 1979.

Rife C. D. and Vincent G. A., "Use of the discrete Fourier transform in the measurement of frequencies and levels of tones," Bell Syst. Tech. Journal, Vol. 49, No. 2, pp. 197-228, February 1970.

Rodrigues M. A. and Kuo S. M., "Optimised adaptive frequency-sampling line enhancer," in Proc. 19th Asilomar Conf. Signals, Systems & Computers, Pacific Grove, CA, USA, pp. 320-324, November 1985.

Shynk J. J., (1989a) "Adaptive IIR filtering using parallel-form realisations," IEEE Trans. Acoust., Speech, Sig. Proc., Vol. ASSP-37, No. 4, pp. 519-533, April 1989.

Shynk J. J., "Frequency-domain and multirate adaptive filtering," IEEE Signal Processing Magazine, pp. 14-37, January 1992.

Shynk J. J., (1989b) "Adaptive IIR filtering," IEEE Signal Processing Magazine, pp. 4-21, April 1989.

Simington R. A. Z. and Percival T. M. P., "New frequency domain techniques for DSP based VSAT modems," in Proc. IREE, pp. 428-431, 1991.

Soderstrom T., Ljung L. and Gustausson I., "A theoretical analysis of recursive identification methods," Automatica, Vol. 14, pp. 231-244, 1978.

Sommen P. C. W., Gerwen P. J. V., Kotmans H. J. and Janssen A. J. E. M., "Convergence analysis of a frequency-domain adaptive filter with exponential power averaging and generalised window function," IEEE Trans. Circuits Systems, Vol. CAS-34, No. 7, July 1987.

Stearns S. D., "Error surface of recursive adaptive filters," IEEE Trans. Circuits and Systems, Vol. CAS-28, No. 6, pp. 603-606, June 1981.

Stevenson T. and Yates K. W., "A new multiple access technique for packet satellite communications," in Proc. Int. Symp. Signals, Systems and Electronics, Erlanger 1989.

Stoica P. and Nehorai A., "Performance analysis of an adaptive notch filter with constrained poles and zeros," IEEE Trans. Acoust., Speech, Sig. Proc., Vol. ASSP-36, No. 6, pp. 911-919, June 1988.

Tadokoro Y. and Abe K., "Notch Fourier transform," IEEE Trans. Acoust., Speech, Sig. Proc., Vol. ASSP-35, No. 9, pp. 1282-1288, September 1987.

Treichler J. R., "Transient convergence behaviour of the adaptive line enhancer," IEEE Trans. Acoust., Speech, Sig. Proc., Vol. ASSP-27, No. 1, pp. 53-62, February 1979.

Werter M. J., "FSK demodulation with an adaptive direct form II filter," in Proc. IEEE Int. Conf. Acoustic., Speech, Sig. Proc., pp. III: 328-III:331, 1993.

Widrow B., Glover J. R. Jr., McCool J. M., Kaunitz J., Williams C. S., Hearn R. H., Zeidler J. R., Dong E. Jr. and Goodlin R. C., "Adaptive noise cancelling: principle and applications," in Proc. IEEE, Vol. 63, No. 12, pp. 1692-1716, December 1975.

Widrow B., Baudrenghien P., Vetterli M. and Titchener P. F., "Fundamental relations between the LMS algorithm and the DFT," IEEE Trans. Circuits Systems, Vol. CAS-34, No. 7, pp. 814-820, July 1987.

Widrow B., McCool J. and Ball M., "The complex LMS algorithm," in Proc. IEEE, Vol. 63, NO. 4, pp. 719-720, June 1981.

Widrow B., McCool J. M., Larimore M. G. and Johnson C. R., Jr., "Stationary and nonstationary learning characteristics of the LMS adaptive filter," in Proc. IEEE, Vol. 64, No. 4, pp. 1151-1162, August 1976.

Widrow B. and Stearns S., *Adaptive Signal Processing*. Englewood Cliffs, NJ: Prentice-Hall, 1985.

Wong E. M. C. and Seng Y. P., "Communications signal processing for a PCM junction analyser," ISSPA, Int. Symp. Signal Processing. and Its Applications, Gold Coast, Australia, pp. 939-942, August 1990.

Yoganandam Y., Reddy V. U. and Kailath T., "Performance analysis of the adaptive line enhancer for sinusoidal signals in broadband noise," IEEE Trans. Acoust., Speech, Sig. Proc., Vol. ASSP-36, No. 11, pp. 1749-1757, November 1988.

Zeidler J. R., Satorius E. H., Chabries D. M. and Wexler H. T., "Adaptive enhancement of multiple sinusoids in uncorrelated noise," IEEE Trans. Acoust., Speech, Sig. Proc., Vol. ASSP-26, No. 3, pp. 240-254, June 1978.

Appendix A:

Derivation of the Second Order IIR Bandpass Filter Parameters

A bilinear transformed second order bandpass filter is given by [Padmanabhan and Martin (1987)]:

$$H_{BP}(z^{-1}) = (\frac{1-\alpha^2}{2})\frac{1-z^{-2}}{1+a\alpha z^{-1}+\alpha^2 z^{-2}} \qquad \text{(A-1)}$$

where $-2 < a < 2$ and α is the parameter which controls the bandwidth. In order to obtain guaranteed stability it is necessary to satisfy the inequality; $0 \leq \alpha < 1$. Subtracting the output of the above bandpass filter from the input signal results in the following notch filter transfer function:

$$H_N(z^{-1}) = (\frac{1+\alpha^2}{2})\frac{1+\frac{2a\alpha}{1+\alpha^2}z^{-1}+z^{-2}}{1+a\alpha z^{-1}+\alpha^2 z^{-2}} \qquad \text{(A-2)}$$

It can be easily shown that the bandpass filter given by Equation (A-1) has gain and phase characteristics which are unity and zero respectively at the peak frequency. The peak frequency occurs at the zero transmission of the resulting notch filter and is given by:

$$f_p = \frac{1}{2\pi}\cos^{-1}(\frac{-a\alpha}{1+\alpha^2}) \qquad \text{(A-3)}$$

Note also that this notch filter has unity gain at dc and at half the sampling frequency. The peak frequency also depends on the bandwidth control parameter. Applying the following changes in variable to Equation (A-1), the proposed bandpass filter parametisation given by Equation (2.8) is obtained:

$$g = \frac{1+\alpha^2}{2} \quad ; \quad h = \frac{2a\alpha}{1+\alpha^2} \qquad \text{(A-4)}$$

Appendix B:

Derivation of the Sliding Computation for $a_{N/2}$

We first derive the sliding algorithm for $\omega = \pi$ in the NFT case. The transfer function of the bandpass filter is given by (see Figure 2.1):

$$G_{1N/2}(z) = \frac{1 - z^{-N}}{1 - z^{-1}} \tag{B-1}$$

Evaluating Equation (B-1) at $\omega = \pi$ results in [Liu and Lin (1992)]:

$$H_{bN/2}(e^{j\pi}) = e^{-j(\frac{N}{2}-1)\pi}(-N\cos\frac{\pi N}{2}) \tag{B-2}$$

The $(N/2)$th component of the input signal is expressed as (Equation (2.2)):

$$x_{N/2}(n) = a_{N/2}\cos(\pi n) \tag{B-3}$$

Using Equation (B-2), the output is given by:

$$y_{N/2}(n) = N\cos\frac{\pi N}{2}\, a_{N/2}\cos(\pi n - \frac{\pi N}{2}) \tag{B-4}$$

Note that $N = 2m$, then two cases when m is an odd or even number are possible. In both cases it can be easily shown that:

$$y_{N/2}(n) = Na_{N/2}\cos(\pi n) \tag{B-5}$$

$A_{N/2}(n)$ is computed by:

$$A_{N/2}(n) = \frac{1}{N}(-1)^n y_{N/2}(n) \tag{B-6}$$

For the CNFT case , the filter transfer function is given by (see Figure 2.2):

$$H_{bN/2}(z^{-1}) = \frac{1 - z^{-N}}{1 + z^{-1}}\frac{1 - z^{-1}}{1 - \beta z^{-N}} \tag{B-7}$$

The first term is the same as the NFT case and the value of the second term at $\omega = \pi$ is:

$$\frac{1 - e^{-j\pi}}{1 - \beta e^{-jN\pi}} = \frac{2}{1 - \beta} = 2\rho \tag{B-8}$$

Using Equations (B-8) and (B-5), $A_{N/2}(n)$ is computed as follows:

$$A_{N/2}(n) = \frac{1}{2\rho N}(-1)^n y_{N/2}(n) \qquad \text{(B-9)}$$

Appendix C:

Derivation of the Resonator Output Signal

When the input frequency is the same as the resonance frequency of the resonator, the z-Transform of the output is given by:

$$y_k(z^{-1}) = \frac{a_k(1-\cos\omega_k z^{-1}) + b_k \sin\omega_k z^{-1}}{(1-2\cos\omega_k z^{-1}+z^{-2})^2} \qquad \text{(C-1)}$$

Considering the following z-Transform pairs [Jury (1964)]:

$$p_1(n) = n\sin\omega_k n \Leftrightarrow P_1(z^{-1}) = \sin\omega_k z^{-1}\frac{1-z^{-2}}{(1-2\cos\omega_k z^{-1}+z^{-2})^2} \qquad \text{(C-2)}$$

$$q_1(n) = n\cos\omega_k n \Leftrightarrow Q_1(z^{-1}) = \frac{\cos\omega_k z^{-1} - 2z^{-2} + \cos\omega_k z^{-3}}{(1-2\cos\omega_k z^{-1}+z^{-2})^2} \qquad \text{(C-3)}$$

together with the following equalities:

$$\cos\omega_k p_1(n) - \sin\omega_k q_1(n) = n\sin[\omega_k(n-1)] \qquad \text{(C-4)}$$

$$\sin\omega_k q_1(n) + \cos\omega_k p_1(n) = n\sin[\omega_k(n+1)] \qquad \text{(C-5)}$$

Using straight forward manipulations the following z-Transform pair will be obtained:

$$p_2(n) = (n+2)\sin[\omega_k(n+1)] \Leftrightarrow P_2(z^{-1}) = 2\sin\omega_k \frac{1-\cos\omega_k z^{-1}}{(1-2\cos\omega_k z^{-1}+z^{-2})^2} \qquad \text{(C-6)}$$

$$q_2(n) = n\sin[\omega_k(n+1)] \Leftrightarrow Q_2(z^{-1}) = 2\sin\omega_k z^{-1}\frac{\cos\omega_k - z^{-1}}{(1-2\cos\omega_k z^{-1}+z^{-2})^2} \qquad \text{(C-7)}$$

From Equations (C-6) and (C-7), it can be found that:

$$\frac{1}{2\sin^2\omega_k}(P_2(z^{-1})\cos\omega_k - Q_2(z^{-1})z) = \frac{\sin\omega_k z^{-1}}{(1-2\cos\omega_k z^{-1}+z^{-2})^2} \qquad \text{(C-8)}$$

Using Equations (C-8) and (C-6), the output of the resonator in time domain, $y_k(n)$, can be obtained. Now let us consider the case when the input frequency (ω_k) is different from the resonant frequency of the resonator (ω_r). Without loss

of generality consider the following input sinusoid which is only composed of a sine term:

$$x(n) = b_k \sin \omega_k n \tag{C-9}$$

For the input signal given by Equation (C-9), the resonator output in z-domain is given by:

$$Y(z) = \frac{b_k \sin \omega_k z^{-1}}{(1 - 2\cos\omega_k z^{-1} + z^{-2})(1 - 2\cos\omega_k z^{-1} + z^{-2})} \tag{C-10}$$

Using partial-fraction expansion, we have:

$$Y(z) = \frac{1}{-2(\cos\omega_r - \cos\omega_r)}\left(\frac{-b_k \sin \omega_k}{1 - 2\cos\omega_r z^{-1} + z^{-2}} + \frac{b_k \sin \omega_k}{1 - 2\cos\omega_k z^{-1} + z^{-2}}\right) \tag{C-11}$$

From Equation (C-11), the output in time domain is easily obtained and given by Equation (4.29).

Appendix D:

General Analytical Solution for Complex Integral

An analytic solution of the integral of the form:

$$I_n = \frac{1}{2\pi j} \oint_{\substack{unit \\ circle}} \frac{B(z)}{A(z)} \frac{B(z^{-1})}{A(z^{-1})} z^{-1} dz \tag{D-1}$$

where the transfer function $\frac{B(z)}{A(z)}$ is defined as:

$$\frac{B(z)}{A(z)} = \frac{b_0 z^2 + b_1 z + b_2}{a_0 z^2 + a_1 z + a_2} \tag{D-2}$$

is given by [Jury (1964)]:

$$I_2 = \frac{B_0 a_0 e_1 - B_1 a_0 a_1 + B_2 (a_1^2 - a_2 e_1)}{a_0 [(a_0^2 - a_2^2) e_1 - (a_0 a_1 - a_1 a_2) a_1]} \tag{D-3}$$

where

$$\begin{aligned} B_1 &= b_0^2 + b_1^2 + b_2^2 \\ B_1 &= 2(b_0 b_1 + b_1 b_2) \\ B_2 &= 2 b_0 b_2 \\ e_1 &= a_0 + a_2 \end{aligned} \tag{D-4}$$

Appendix E:

Bias Analysis of the Frequency Estimate

For an input signal which consists of single sinusoid buried in white noise ($x(t)$), we will show that the frequency estimate is asymptotically unbiased (i.e. for $N \to \infty$, where N denotes the number of data points). Consider the error signal as follows:

$$e(t,h) = H_N(q^{-1})x(t) \tag{E-1}$$

where q^{-1} denotes the unit delay operator and $H_N(q^{-1})$ is given by:

$$H_N(q^{-1}) = 1 - H_{BP}(q^{-1}) = g\frac{1 + hq^{-1} + q^{-2}}{1 + ghq^{-1} + (2g-1)q^{-2}} \tag{E-2}$$

We are looking for an appropriate h to minimise the mean squared error. In other words, the desired h should satisfy the following equation:

$$\hat{h} = \arg \min_{h} \frac{1}{N}\sum_{t=1}^{N} e^2(t,h) \tag{E-3}$$

Since the stochastic processes $e(t,h)$, $\frac{\partial e(t,h)}{\partial h}$ are ergodic, for $N \to \infty$ the stationary points of the loss function (Equation (E-3)) are the solutions of the following equation [Stoica and Nehorai (1988)]:

$$\frac{\partial E[e^2(t,h)]}{\partial h} = 2E[\frac{\partial e(t,h)}{\partial h} e(t,h)] = 0 \tag{E-4}$$

where E indicates the expectation operator for random processes. From Equation (E-1), the derivative of the error signal with respect to h is given by:

$$\frac{\partial e(t,h)}{\partial h} = \frac{\partial H_N(q^{-1})}{\partial h} x(t) \tag{E-5}$$

Substituting Equations (E-1) and (E-5) into Equation (E-4) we obtain:

$$E[H_N(q^{-1})x(t)(\frac{\partial H_N(q^{-1})}{\partial h} x(t)] = 0 \tag{E-6}$$

or equivalently:

$$\frac{1}{2\pi}\int_0^{2\pi} H_N^*(\omega)\frac{\partial H_N(\omega)}{\partial h}\Phi_{xx}(\omega)d\omega = 0 \qquad \text{(E-7)}$$

Using the following equality:

$$\frac{1}{2\pi}\int_0^{2\pi}\frac{\partial}{\partial h}|H(\omega)|^2 d\omega = \frac{1}{\pi}\int_0^{2\pi} H^*(\omega)\frac{\partial H(\omega)}{\partial h}d\omega \qquad \text{(E-8)}$$

Equation (E-7) is further simplified:

$$\frac{1}{2\pi}\frac{\partial}{\partial h}\int_0^{2\pi}|H_N(\omega)|^2\Phi_{xx}(\omega)d\omega = 0 \qquad \text{(E-9)}$$

It is worth noting that the above result can be directly derived from the error surface analysis as well. Assuming that the input signal is composed of a single sinusoid with frequency ω_1 and amplitude C_1 corrupted by noise of power σ_n^2, Equation (E-9) becomes:

$$\frac{C_1^2}{2}H_N^*(\omega_1)\frac{\partial H_N(\omega_1)}{\partial h} + \frac{\sigma_n^2}{2}\frac{\partial}{\partial h}\int_0^{2\pi}|H_N(\omega)|^2 d\omega = 0 \qquad \text{(E-10)}$$

From Equation (6.15), it is evident that the second term in the left hand side of Equation (E-10) is equal to zero. The first term is zero only when $h = -2\cos(\omega_1)$ and this verifies that the minimum occurs exactly at the frequency of the input component.